

Diploma Thesis

The Effects of Passive Path Spring Implementation Parallel to Weakened M. Rectus Femoris during Walking: An OpenSim Simulation Study

carried out for the purpose of obtaining the degree of Diplom-Ingenieur (DI), submitted at TU
Wien, Faculty of Mechanical and Industrial Engineering, by

Pia Stefanek

Mat.Nr.: 0808550

under the supervision of

Univ. Prof. Dipl.-Ing. Dr. Margit Gföhler
Institute of Engineering Design and Product Development

Reviewed by

Univ. Prof. Dipl.-Ing. Dr. Margit Gföhler

Institute of Engineering Design and Product Development

Getreidemarkt 9

A-1060 Vienna, Austria

Univ. Prof. Dipl.-Ing. Dr. Philipp Thurner

Institute of Lightweight Design and Structural Biomechanics

Getreidemarkt 9

A-1060 Vienna, Austria

Abstract

Muscle weakness can cause devastating impacts on the gait pattern. Thus, research on devices and elements, capable to assist walking movement is of high importance. This thesis intends to investigate the effects of passive path spring implementation parallel to m. rectus femoris for persons suffering from m. rectus femoris weakness. The study is limited to the pre-swing, initial and mid-swing phases of gait and focusses on the three muscles m. rectus femoris, m. vastus intermedius and m. biceps femoris caput longum. Five main muscle parameters are selected for investigation: force, power, normalized fiber length, normalized fiber velocity and induced femur acceleration. Results show that the spring exhibits a positive effect on force and power of m. vastus intermedius but shows a comparable negative effect in force and power of m. biceps femoris caput longum. Furthermore, the spring affects the induced femur accelerations of all considered muscles in a negative way. The study is performed using the simulation software OpenSim

Table of Contents

1. Introduction.....	1
1.1. Motivation.....	1
1.2. Focus of Thesis	2
2. Literature study	4
2.1. Human Gait.....	4
2.1.1. The Gait Cycle	4
2.1.2. The Gait Phases.....	4
2.1.3. Quantitative Gait Analysis	9
2.2. Muscles	14
2.2.1. M. quadriceps femoris.....	15
2.2.2. M. biceps femoris.....	15
2.2.3. Muscle Roles.....	16
2.3. OpenSim.....	16
2.3.1. Musculoskeletal model.....	17
2.3.2. Dynamic simulation	22
2.3.3. Springs.....	29
3. Methods.....	31
3.1. Model and Data	31
3.2. Preliminary determinations	31
3.2.1. Gait cycle	31
3.2.2. Path Spring	32
3.3. Preliminary simulations.....	33
3.3.1. Muscle replacement.....	34
3.3.2. Force Takeover.....	34
3.3.3. Muscle weakening.....	35
3.4. Simulation	37
4. Results.....	41
4.1. Actuation Force.....	41
4.1.1. M. rectus femoris.....	41
4.1.2. M. vastus intermedius	43
4.1.3. M. biceps femoris caput longum	44
4.2. Actuation Power.....	45

4.2.1. M. rectus femoris.....	45
4.2.2. M. vastus intermedius.....	46
4.2.3. M. biceps femoris caput longum	48
4.3. Normalized fiber length.....	49
4.3.1. M. rectus femoris.....	49
4.3.2. M. vastus intermedius.....	50
4.3.3. M. biceps femoris caput longum	50
4.4. Normalized Fiber Velocity	50
4.4.1. M. rectus femoris.....	51
4.4.2. M. vastus intermedius.....	51
4.4.3. M. biceps femoris caput longum	52
4.5. Induced Accelerations of the Femur.....	52
4.5.1. M. rectus femoris.....	52
4.5.2. M. vastus intermedius.....	56
4.5.3. M. biceps femoris caput longum	60
4.6. Induced Accelerations of the Femur – Illustrations using Resultant Vectors	64
5. Discussion	68
5.1. Validation	68
5.1.1. CMC Validation	68
5.1.2. IAA Validation.....	74
5.2. Usability	75
5.3. Comparison to other studies	76
5.4. Limitations	76
5.5. Simulation results	76
5.5.1. Comparison of activation deficits.....	77
5.5.2. Force and Power	78
5.5.3. Normalized Fiber Length and Normalized Fiber Velocity.....	81
5.5.4. Induced Accelerations	81
6. Summary	85
7. Bibliography.....	87
7.1. List of References.....	87
7.2. List of Figures	91
7.3. List of Tables.....	92

1. Introduction

1.1. Motivation

The ability to walk upright is the characteristic trait that separated the first hominids from apes. It opened the opportunity to free the hands for carrying tools and food and made long-distance walks possible (Gray, 2016). Starting from the point where evolution enabled them to do it, humans instinctively use this form of bipedal locomotion from primal childhood on (Hazen, 2015). In a lifetime, humans take hundreds of millions of steps. Although walking appears as an automatic and simple process, it is actually a highly complex motor function. Every step requires an accurate interaction of the musculoskeletal and the nervous systems (Mansfield and Neumann, 2014). Only then, balance maintenance and smooth forward progression is possible. In case of a healthy body, walking is a very energy-efficient process (Hislop et al., 2014).

Muscle weakness, arising from a combination of disease, trauma, lack of use and nerve inhibition (Fritz et al., 2008), can have devastating impacts on gait (Hislop et al., 2014). It leads to diminution of muscle strength, resulting in inability to use the whole function of a given muscle (Horak, 2012). In consequence, the ease and efficiency of walking decreases, leading to a laboured and inefficient gait pattern (Mansfield and Neumann, 2014). Therefore, research on exoskeletons, devices capable to assist, restore or enhance the motor skills of the wearer are of high importance (Nacy et al., 2016).

Especially in the recent years, the progress in the development of exoskeletons has been increasing. Many different exoskeleton systems have been designed and tested. Depending on the supported body part, upper extremity exoskeletons, lower extremity exoskeletons, full body exoskeletons or joint-specific exoskeletons exist (Chen et al., 2016). Furthermore, one can distinguish between active (powered) and passive (unpowered) devices. Active exoskeletons are powered through actuators, as for example electric motors or hydraulics. Passive exoskeletons on the other side do not contain any actuators. Human movement solely produces the energy that powers the device. Beside the reduction of musculoskeletal disorders, exoskeleton research focuses on the improvement of human performance (McGowan, 2018).

Regarding the design of the exoskeletons, the high weight of the powered actuators represents a major challenge (Farris et al., 2013). Furthermore, energy efficiency is a big problem. The acceleration and deceleration of the limbs and the body mass support against gravity require a lot of energy. Power supply for several hours is hardly possible with current battery technology (Van den Bogert, 2003). To minimize the mass and improve energy efficiency, research is conducted in the field of passive exoskeletons. They replace actuators with light springs, which are able to store and return energy similar to tendons. The usage of this energy storage mechanism helps to power locomotion (Farris et al., 2013).

In the year 2009, Grabowski and Herr developed an exoskeleton consisting of fiberglass springs that were spanned over all three joints of the leg. The device enabled a reduction of the metabolic cost of two-legged hopping in place. Farris and Sawicki (2012) tested a spring-loaded ankle exoskeleton during hopping and reported similar effects. In the year 2015, a passive exoskeleton acting in parallel to the calf muscles was

developed and tested during gait movement. Similar to hopping movement, improvements in walking efficiency were documented (Collins et al., 2015).

All these studies are concerned with the augmentation of locomotor function in case of healthy persons. In this thesis, we focus on the assistance of locomotor function in case of impaired persons suffering from muscle weakness.

1.2. Focus of Thesis

The purpose of this thesis is to investigate the changes in muscle performance resulting from weakness of m. rectus femoris during walking. Furthermore, this thesis aims at answering the following research question:

What are the effects of a passive path spring implementation parallel to weakened m. rectus femoris on the main muscle parameters during walking?

As main muscle parameters we consider force, power, normalized fiber length, normalized fiber velocity and induced femur acceleration. The investigation is limited to three muscles of the thigh, namely m. rectus femoris, m. vastus intermedius and m. biceps femoris caput longum, whose performance is examined during the pre-swing, initial swing and mid-swing phases of gait.

Four hypotheses are proposed:

H1: Weakness of m. rectus femoris reduces force, power and induced femur acceleration of m. rectus femoris, increases these muscle parameters for m. vastus intermedius and does not change m. biceps femoris caput longum performance.

H2: The passive path spring has no effect on the performance of the muscle parameters of weakened m. rectus femoris.

H3: The passive path spring has a positive effect on the performance of the muscle parameters of m. vastus intermedius in case of weakened m. rectus femoris.

H4: The passive path spring has a negative effect on the performance of the muscle parameters of m. biceps femoris caput longum in case of weakened m. rectus femoris.

The passive path spring has a positive effect on the performance of the muscle parameters, if the muscle parameter curves representing spring implementation show better approximation to the reference curve describing the healthy case than the curve describing the weakened m. rectus femoris case.

The passive path spring has a negative effect on the performance of the muscle parameters, if the muscle parameter curves representing spring implementation show worse approximation to the reference curve describing the healthy case than the curve describing the weakened m. rectus femoris case.

1.3. Structure of this thesis

This thesis contains six subsequent chapters. Chapter two is a literature report, providing basic knowledge important for further proceedings. In chapter three the applied methods are described. Chapter four is divided with respect to the main muscle parameters and illustrates and describes the study results. Chapter five first validates the applied OpenSim tools and discusses the usability of the OpenSim software. Furthermore, the results are compared to other studies, study limitations are considered and the simulation results are discussed. In chapter six the key findings are summarized and future research is considered. The last chapter serves as bibliography.

2. Literature study

2.1. Human Gait

Human gait is highly individual. It adapts to existing conditions like age, height, body weight, soil properties, footwear, environment and many more. Due to this high variability, the term *normal gait* is controversial. Nevertheless, it makes sense to classify basic parameters of gait as normal or typical for an average human. Only then, a pathological gait can be discriminated from a healthy one. In this thesis, all declared gait characteristics follow the examination results of Dr. Jaquelin Perry and her team of the Rancho Los Amigos National Rehabilitation Centre. They analysed the gait pattern of 420 healthy persons and determined normal ranges for basic parameters (Götz-Neumann, 2003).

2.1.1. The Gait Cycle

During walking, repeated, rhythmic and alternating movements of body segments lead to a forward translation of the centre of gravity of the human body. One leg always has contact to the ground and acts as mobile support. Meanwhile the other leg swings to a new location in the front. Then the legs swap their roles. When the body weight is transferred from one leg to the other, both legs have contact to the ground. The legs repeat this process with a time shift until the walking person has reached its target location. A single sequence of the repeated process is referred to as gait cycle. Generally the gait cycle is defined to start with initial contact of one foot (Perry, 2003).

2.1.2. The Gait Phases

The gait cycle can be divided into two phases: the stance phase and the swing phase. The stance phase describes the period of the gait cycle when the foot is in contact with the ground. In this phase double-leg and single-leg stance occur. Double-leg stance (double support) is characterized by ground contact of both feet. The body weight is split up on both legs. In single-leg stance (single support) phases, one leg has to bear the whole body weight. During swing phase the foot has no contact to the ground and is swinging in the air. Stance phase constitutes about 60% and swing phase about 40% of gait cycle (Disselhorst-Klug et al., 2015).

Eight gait sub-phases exist, five during stance phase and three during swing phase. The stance phase events are called: Initial Contact, Loading Response, Mid Stance, Terminal Stance and Pre-Swing. The swing phase is consists of three events: Initial Swing, Mid-Swing and Terminal Swing (Götz-Neumann, 2003).

In the following figure 1, the stance and the swing phase, as well as the eight gait sub-phases are illustrated. Their starting and end times are specified as per cent of the entire gait cycle interval. Additionally, the division of the stance phase into double-leg and single-leg stance (double support and single support phase) is shown.

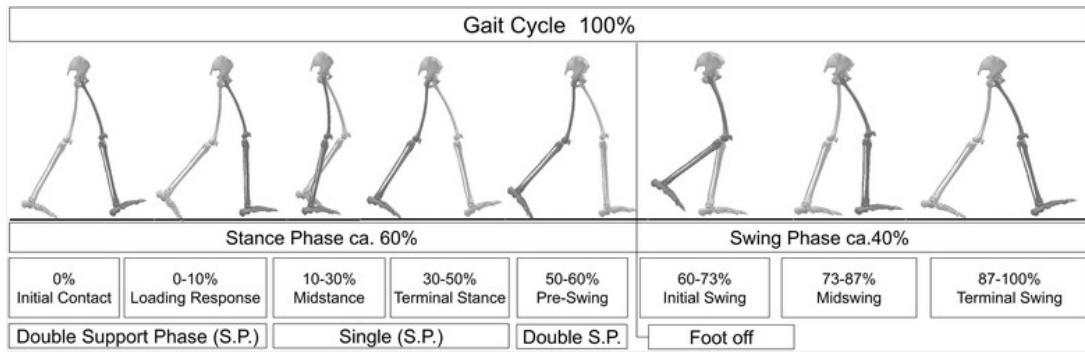


Figure 1: Illustration of the gait cycle (Perry, 2003).

There are three fundamental tasks the stance and swing phases have to perform (Perry, 2003):

a) Weight acceptance:

Three functional patterns have to be realized simultaneously: shock absorption, initial stabilization and perpetuation of locomotion. The transfer of body weight on the limb that has just finished forward swing represents a difficult challenge. The procedure of weight acceptance lasts for the two sub-phases initial contact and loading response.

b) Single-limb support:

The entire body weight is supported by one limb, which also has to preserve forward movement of the body. Body transfer beyond the reference foot has to be performed. Single-limb support comprises the two sub-phases mid- and terminal stance. The beginning of the pre-swing phase is included as well.

c) Limb advancement:

The positioning of the leg in stance guarantees optimal progression of forward swing. Afterwards the leg swings through the three sub-phases performing leg lift, forward swing and preparation for the following stance phase. Limb advancement extends over the four phases pre-swing, initial swing, mid-swing and terminal swing.

Table 1 describes the eight gait sub-phases in detail. It lists their starting and terminating events, fundamental and special tasks, ratio of the gait cycle interval and associated phases.

Table 1: Overview of the gait sub-phases.

Sub-phase	Starting event	Terminating Event	Fundamental task	Special task	Ratio of gait cycle interval in per cent	Phase
Initial Contact	reference foot contacts ground			✓ positioning of the leg to initiate stance phase	0%	stance
Loading Response	initial contact of reference foot	toe-off of contralateral foot	weight acceptance	✓ shock absorption ✓ stability preservation of the weight bearing leg ✓ perpetuation of locomotion	0% - 10%	double-leg stance
Mid Stance	toe-off of contralateral foot	body weight transfer on the forefoot		✓ body weight transfer on the forefoot ✓ stability preservation of leg and torso	10% - 30%	single-leg stance
Terminal Stance	heel rise of reference foot	initial contact of contralateral foot	single-limb support	✓ body weight progress beyond the reference leg	30% - 50%	single-leg stance
Pre-Swing	initial contact of contralateral foot	toe-off of reference foot	single-limb support & limb advancement	✓ preparation for swing phase	50% - 60%	double-leg stance
Initial Swing	toe-off of reference foot	maximum knee flexion of reference leg		✓ lift reference leg from ground ✓ forward movement of the reference leg	60% - 73%	single-leg stance
Mid-Swing	maximum knee flexion of reference leg	tibia of reference foot perpendicular to ground	limb advancement	✓ forward movement of the reference leg ✓ assure distance between ground and reference leg	73% - 87%	single-leg stance
Terminal Swing	tibia of reference foot perpendicular to ground	initial contact of reference foot		✓ termination of forward movement of the reference leg ✓ preparation for initial contact	87% - 100%	single-leg stance

(Götz-Neumann, 2003, Disselhorst-Klug et al., 2015 and Bassile and Hayes, 2016)

In the electromyography part of this chapter m. rectus femoris activation during pre-swing and initial swing is revealed. In mid-swing m. rectus femoris is not activated but its counter muscle, m. biceps femoris caput longum, starts to activate. To include activation and deactivation phases of m. rectus femoris, further steps of this thesis are concentrated on the three phases pre-swing, initial swing and mid-swing. Furthermore, the methods section will show that springs which are implemented parallel to m. rectus femoris exhibit their peak force during these phases. The three phases are described in detail in the following section. Only the proceedings in the lower body are explained.

Pre-Swing

The pre-swing phase represents the last sub-phase that is part of the stance phase. It is responsible for generating the major part of knee flexion for the following initial swing phase. Therefore, one can assume that the flexion of the knee is the most critical event in this phase of the gait cycle (Perry, 2003). Figure 2 illustrates the start and end positions of the pre-swing phase.

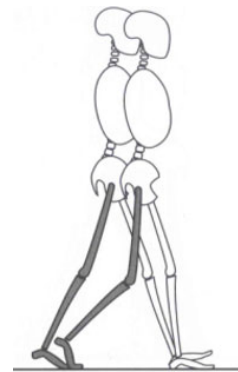


Figure 2: Start and end positions of pre-swing (Therani and Vermeire, 2007).

Range of movement (Götz-Neumann, 2003):

- Ankle joint moves from 10° dorsal extension to 15° plantar flexion
- The metatarsophalangeal joints (MTP joints) move from 30° dorsal extension to 60° dorsal extension
- Knee joint moves from 5° flexion to 40° flexion
- Hip joint moves from 20° hyperextension to 10° hyperextension

At the beginning of the pre-swing phase, the body weight is transferred from the reference leg to the contralateral leg. Due to this relief of the reference leg, the necessity for a powerful stabilisation by the plantarflexors m. soleus and m. gastrocnemius decreases. As a result, they reduce their activation level. This decreasing activation is enough to perform plantar flexion on the relieved foot and lift the heel from the ground. Moreover, the centre of pressure has moved forward to the MTP joints already in terminal stance. Thus, the force that pressed the midfoot to the ground is reduced. The interaction of all these events allows the tibia of the reference foot to roll forward. The ground reaction force vector moves behind the knee, thereby inducing a knee flexion torque and encouraging further passive knee flexion. This movement is supported by m. popliteus, which shows high activation during pre-swing. The knee flexion movement is limited by m. rectus femoris, which is able to slow down excessive knee flexion and hip hyperextension, thereby supporting hip flexion. Further, the mechanical processes occurring at the ankle joint lead to a forward movement of the femur resulting in hip flexion. Hip flexion is also initiated by the adductor muscles, which have to slow down passive abduction induced by body weight transfer to the contralateral leg. At the end of the pre-swing phase, the dorsal extensors prevent the foot from performing too much plantar flexion (Perry, 2003).

Initial Swing

During the initial swing phase, knee and hip flexion represent the most critical events. Knee flexion is important to lift the reference foot from the ground. Hip flexion, resulting from fast forward movement of the femur, induces forward propulsion (Perry, 2003). Figure 3 shows the start and end positions of the initial swing phase.

Range of movement (Götz-Neumann, 2003):

- Ankle joint moves from 15° plantar flexion to 5° plantar flexion
- The MTP joints move from 60° dorsal extension to neutral position
- Knee joint moves from 40° flexion to 60° flexion
- Hip joint moves from 10° hyperextension to 15° flexion



Figure 3: Start and end positions of initial swing (Tehrani and Vermeire, 2007).

The toe-off of the reference foot represents the starting event of the initial swing phase. At this time, the ankle joint shows a plantar flexion of about 15°. Since the tibia is placed in a position behind the body, the plantarflexed position of the foot does not disturb forward movement of the leg. But in the following mid-swing phase the dorsal extension of the ankle joint is required to keep the toes above the ground. Therefore, the dorsal extensors increase their activation level to the maximum. To lift the foot from the ground and perform forward movement of the leg, sole dorsal extension of the foot is not enough. The compulsory precondition is knee flexion. Three crucial factors enable the knee to reach a flexion movement up to 60°. First, the pre-swing phase has to ensure sufficient knee flexion up to 40°. Second, the hip has to produce a fast flexion movement, resulting in a forward movement of the femur. This movement of the femur generates a moment of inertia at the tibia, leading to knee flexion. Third, knee flexion is induced by activation of the m. biceps femoris caput breve. If necessary, m. rectus femoris is activated to prevent excessive knee flexion. Its contraction brings the tibia more forward and supports hip flexion. As during pre-swing, hip flexion in initial swing is generated due to knee flexion movement. As a result of all the above described events, the leg is able to swing passively forward (Perry, 2003).

Mid-Swing

In mid-swing phase, dorsal extension of the ankle joint and hip flexion are the main challenges. Dorsal extension in the ankle joint ensures that the foot stays in a position above the ground. Continued hip flexion movement ensures forward movement of the leg (Perry, 2003). The start and end positions are illustrated by figure 4.

Range of movement (Götz-Neumann, 2003):

- Ankle joint moves from 5° plantar flexion to neutral position
- The MTP joints do not change their angle in this phase.
- Knee joint moves from 60° flexion to 25° flexion
- Hip joint moves from 15° flexion to 25° flexion

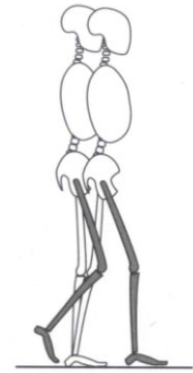


Figure 4: Start and end positions of mid-swing (Tehrani and Vermeire, 2007).

In mid-swing, the tibia reaches a position perpendicular to the ground. This occurs due to processes in the previous gait phase. As a reaction to this forward movement of the tibia, the dorsal extensors of the ankle joint are activated. The reason for these activations is that the muscles have to work against a plantar flexion torque induced by the weight of the foot. When the foot reaches a position in front of the hip joint, strong knee flexion as during initial swing is not needed anymore. The knee performs an extension movement, thereby terminating the forward swing of the leg and preparing for imminent ground contact. The extension movement is not initiated by muscle activation. When the knee flexors relax, gravitation and hip flexion induce the required knee extension. The occurring hip flexion is also passively induced and continues from the previous gait phase. At the end of mid-swing the ischiocrural muscles contract to decelerate the femur (Perry, 2003).

Since further work of this thesis is concentrated on m. rectus femoris, m. vastus intermedius and m. biceps femoris caput longum, the following table 2 summarizes their performance during pre-swing, mid-swing and initial swing.

Table 2: Overview of muscle activity and tasks of m. biceps femoris caput longum, m. rectus femoris and m. vastus intermedius during pre-swing, mid-swing and initial swing.

Muscle	Pre-Swing		Initial Swing		Mid-Swing	
	Active	Task	Active	Task	Active	Task
M. biceps fem. c. l.	☞	-	☞	-	☞	femur deceleration
M. rectus fem.	☞	hip flexion restrains excessive knee flexion	☞	hip flexion restrains excessive knee flexion	☞	-
M. vastus intermedius	☞	-	☞	-	☞	-

2.1.3. Quantitative Gait Analysis

Quantitative gait analysis is consists of three primary components (Lisa and Shalala, 1998):

1. Kinematics (analysis of motion)
2. Kinetics (analysis of the forces that generate the motion)
3. Electromyography (analysis of muscle activity)

Kinematics

Kinematic variables describe human motion without regard to the forces that initiate it. They consist of linear and angular displacements, velocities and accelerations (Winter, 2009). To derive kinematic motion data, the use of a 3D motion analysis system, which illustrates the individual's body as a multisegment system, is necessary. Using markers and cameras, the system is able to determine coordinates and orientations of the rigid body segments. In consequence, joint angles, angular velocities and angular accelerations can be calculated at every time in each plane of motion (Dicharry, 2010).

The presented kinematics are reduced to sagittal plane. The reason for this restriction is that walking motion is mainly determined by the proceedings in this plane. Further, hip, knee and ankle are focussed because the proceedings in the other body parts are not subject in this thesis.

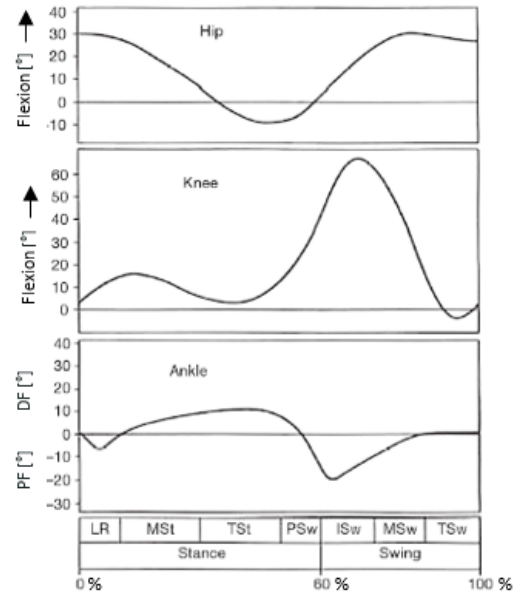


Figure 5: Gait kinematics (Lovegreen et al., 2015).

Figure 5 shows the change of joint angle in hip, knee and ankle in degrees during a gait cycle. The y-axis indicates the joint angle in degrees and the x-axis represents the gait cycle in per cent and divided into the gait sub-phases.

The hip shows an extension movement from the beginning of the gait cycle until it reaches peak extension at the end of terminal stance. Peak flexion is then achieved at mid- or terminal swing. During loading response, the knee first exhibits a flexion movement. At mid stance, the flexion movement is followed by an extension movement. Then, the knee exhibits a rapid flexion movement, starting at the end of stance phase and continuing until mid-swing, where a peak flexion of about 60° is reached. After the peak flexion, the knee moves into a period of knee extension. Just before initial contact, another flexion movement can be considered. The gait cycle starts with the ankle joint in nearly neutral position. During loading response, plantar flexion is initiated, followed by a dorsiflexion motion. Just before pre-swing, peak dorsiflexion is reached. During pre-swing the ankle plantar flexes until initial swing. The ankle then moves back into the neutral position (Lovegreen et al., 2015).

Kinetics

Kinetics deal with the forces that generate a motion (Winter, 2009). A force applied to a body shows two effects. External forces, arising for example due to gravity, lead to body acceleration. Internal forces arise due to muscle contractions and passive anatomical structures. They lead to a deformation or state of mechanical strain inside the body. Newton's second law describes the relationship of force and motion (Bach and Hasan, 1999):

$$F = m \cdot a \quad (1)$$

$$T = I \cdot \alpha = F \cdot d \quad (2)$$

with

F	...	force
m	...	mass
a	...	linear acceleration
T	...	torque, rotational equivalent to force
I	...	mass moment of inertia
α	...	angular acceleration
d	...	moment arm

All segment motion during walking is generated by the moment of force acting at the joints and by the segment's inertial effects. The inertial effects are usually small in comparison to the total moment around the joint and can therefore be omitted (Koca and Verim, 2016).

Important kinetic variables are muscle force, ground reaction force, joint moments, work and power (Beardsley, n. d.). Just as with kinematics, the following section focuses on kinetics of the hip, knee and ankle.

a) Ground Reaction Force

During walking, when the foot contacts the ground, it applies force to the ground. In reaction, an equal and opposite force is exerted from the ground to the foot. This force is called ground reaction force (Sisto, 1998).

Figure 6 shows the progress of the ground reaction forces in the three different planes during a gait cycle. The y-axis indicates the ground reaction force in Newton. The x-axis represents the gait cycle in per cent.

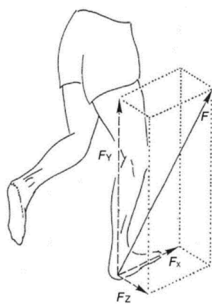


Figure 7: Coordinate system of the ground reaction forces (Watkins, 2018).

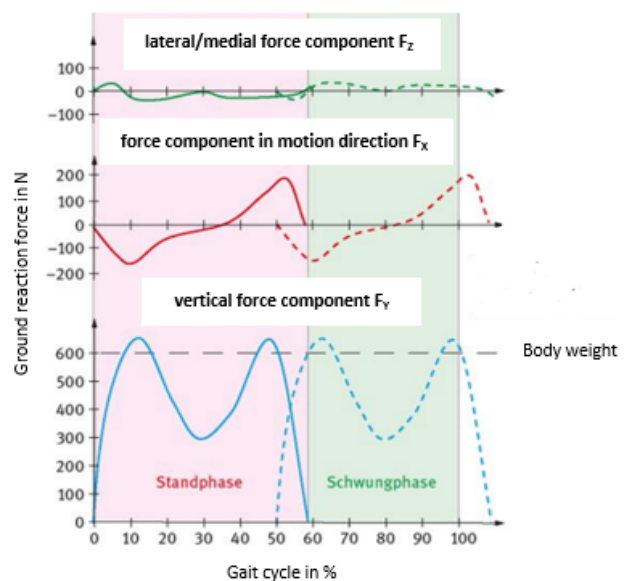


Figure 6: Ground reaction forces (Disselhorst-Klug et al., 2015).

The continuous line

illustrates the ground reaction force of the reference leg, while the dotted line marks the ground reaction force of the contralateral leg. When the foot has no ground contact, the ground reaction forces are all zero (Disselhorst-Klug et al., 2015). Figure 6 is based on the coordinate system shown in figure 7.

It is easy to see that the principal component of the ground reaction force vector is represented by the vertical force component F_Y . During stance phase, two peaks can be identified. The first peak occurs due to weight-acceptance and corresponds to 110% of body weight. This peak is followed by a force minimum. The minimum occurs because the centre of mass moves upwards during mid stance. The second peak appears in terminal stance and is explained by the upwards acceleration of the centre of mass for the following swing phase. The horizontal forces correspond to shear forces. The negative phase of the shear force in direction of movement F_X indicates for a slowing down of the body, while the positive is caused by a forward acceleration of the body. The lateral/medial shear force F_Z is produced by weight acceptance from one leg to the other, which shifts the centre of mass slightly to the side (Disselhorst-Klug et al., 2015).

b) Muscle Force

As described above, muscle forces, F , produce internal torques, T , acting at joints:

$$T = F \cdot d \quad (3)$$

The moment arm d describes the perpendicular distance between the rotation axis and the muscle force (Disselhorst-Klug et al., 2015).

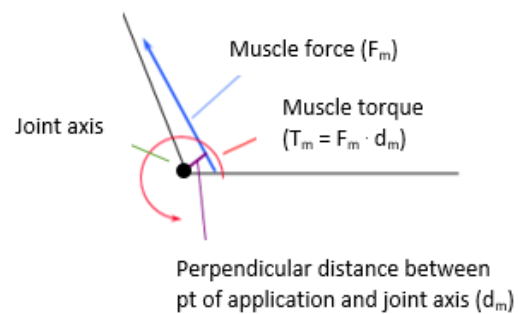


Figure 8: Illustration of muscle force and moment arm (Fleming, n. d.).

Figure 8 illustrates muscle force and moment arm.

c) Muscle Power

Muscle power P is defined as work W per unit of time t .

$$P = \frac{dW}{dt} \quad (4)$$

Further, work is the product of muscle force \vec{F} and the distance \vec{s} covered by the body segment.

$$W = \vec{F} \cdot \vec{s} \quad (5)$$

Insertion equation 5 in 4 of in results in equation 6, where \vec{v} corresponds to the muscle lengthening/shortening velocity (Disselhorst-Klug et al., 2015).

$$P = \frac{dW}{dt} = \vec{F} \cdot \frac{d\vec{s}}{dt} = \vec{F} \cdot \vec{v} \quad (6)$$

A muscle that is able to produce high power has the capability to exert force quickly (Plowman and Smith, 2014).

Electromyography

Electromyographic recordings reveal information about the final control signal of each muscle. Knowledge about the input to the muscular system helps for example to identify which muscle is responsible for a specific muscle moment (Winter, 2009).

Due to the cyclic form of the gait pattern, the activation of muscles relevant for walking can be assigned to the gait phases. Since this thesis focuses on m. rectus femoris, m. vastus intermedius and m. biceps femoris caput longum, the following section deals with the activation of those muscles during gait (Perry, 2003).

Muscle activity was measured using dynamic electromyography. The EMG data were normalized using a manual muscle test (%MMT) (Perry, 2003). This test measures the EMG values during maximal voluntary isometric contractions (MVIC) of the muscles of interest. The recorded EMG values are then used as reference values (Halaki and Gi, 2012).

a) M. rectus femoris

M. rectus femoris is active during late pre-swing and early initial swing. The intensity always stays below 20% MMT. M. rectus femoris contracts to prevent excessive knee flexion and to support hip flexion (Perry, 2003).

For the sake of completeness, it has to be mentioned that there are studies showing rectus femoris activity additionally during loading response (Annaswamy et al., 1999). These measurements can be explained by cross-talk from vastus intermedius (Nene et al., 2003).

Figure 9 illustrates the activation pattern of m. rectus femoris in %MMT for the whole gait cycle. The parameter N indicates the number of usable recordings.

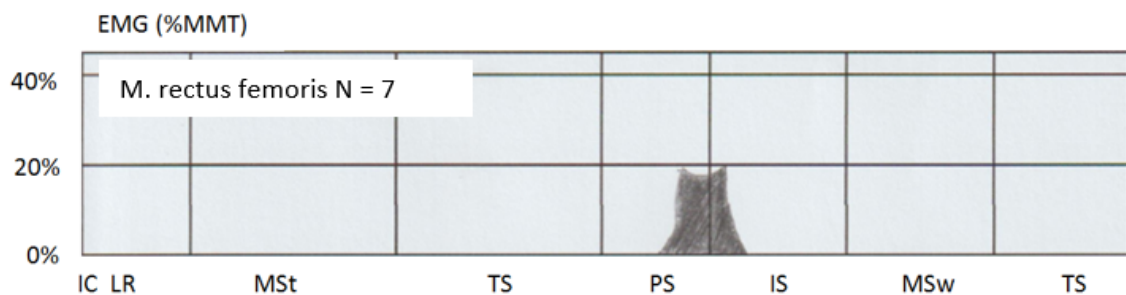


Figure 9: Activation pattern of m. rectus femoris during gait (Perry, 2003).

b) M. vastus intermedius

In contrast to biarticular m. rectus femoris, m. vastus intermedius only spans the knee. Therefore, the activation patterns of these two muscles are not similar at all. Together with the other Mm. vasti (M. vastus lateralis and M. vastus medialis), the m. vastus intermedius is activated during the terminal swing phase (Perry, 2003). The muscle extends the knee and prepares it for initial contact. After initial contact, hip extension and knee flexion occur (Nene et al., 2003). To control the occurring knee flexion, the activation of the Mm. vastii increases until a level of 25% MMT is reached in loading response (Perry, 2003).

Figure 10 illustrates the activation pattern of m. rectus femoris in %MMT for the whole gait cycle. The parameter N indicates the number of usable recordings.

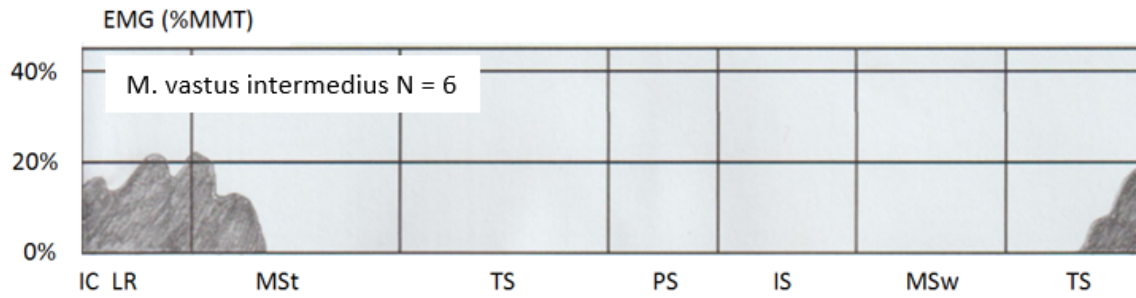


Figure 10: Activation pattern of *m. vastus intermedius* during gait (Perry, 2003).

c) *M. biceps femoris caput longum*

M. biceps femoris caput longum is activated during mid-swing and reaches its peak activation of about 21% MMT during terminal swing. The activation continues until loading response (Perry, 2003). During terminal swing, the muscle acts eccentrically thereby decelerating knee extension. From initial contact on, the muscle acts concentrically to extend the hip (Cianca and Mimbella, 2018).

Figure 11 illustrates the activation pattern of *m. rectus femoris* in %MMT for the whole gait cycle. The parameter N indicates the number of usable recordings.

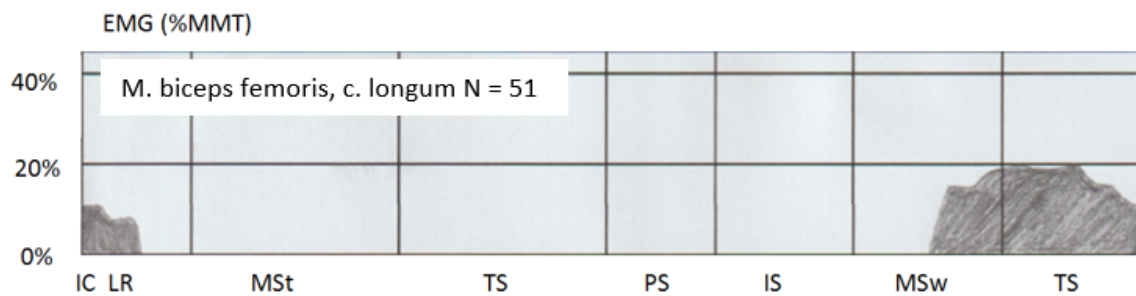


Figure 11: Activation pattern of *m. biceps femoris caput longum* during gait (Perry, 2003).

2.2. Muscles

The muscles of the human body can be divided into three types: skeletal muscles, smooth muscles and cardiac muscles. All of these muscle types possess the following characteristics: contractibility, excitability, extensibility and elasticity. Skeletal muscles are attached to bones and their main function is to move the skeletal components. Furthermore, they are under voluntary nerve control. Its structural units are elongated, cylindrical and multinucleated cells known as muscle fibers (Sreekumar, 2010). Different skeletal muscles exhibit different physiological features, depending on their designated tasks in the body. As a result, muscles vary in size, force, velocity and endurance (Mason, 2017).

Since further work in this thesis is concentrated on *m. rectus femoris*, *m. vastus intermedius* and *m. biceps femoris caput longum*, these three muscles are described in detail.

2.2.1. M. quadriceps femoris

The quadriceps femoris muscle is composed of four part-muscles: m. rectus femoris, m. vastus lateralis, m. vastus intermedius and m. vastus medialis. M. quadriceps femoris extends over the anterior surface of the thigh. M. rectus femoris is the only part-muscle that originates above the hip joint. The other three part-muscles originate from the femur. At the patella, the four part-muscles unite and form the ligamentum patellae. This string tendon inserts into to the tuberosity of the tibia. The main function of the quadriceps femoris is knee extension (Palastanga and Soames, 2012).

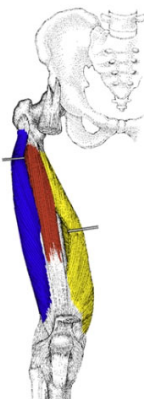
M. rectus femoris

M. rectus femoris is a spindle-shaped bipennate muscle. Additionally to the knee extension function, m. rectus femoris works as a hip flexor. During knee extension, m. rectus femoris particularly acts when the straight leg is raised and when knee extension and hip flexion occur simultaneously (Palastanga and Soames, 2012). Figure 12 shows the position of m. rectus femoris in relation to the other quadriceps muscles.



Figure 12: Red marked m. rectus femoris (King of the Gym, 2012).

Vastus Intermedius
Vastus Lateralis
Vastus Medialis



M. vastus intermedius

M. vastus intermedius is a fusiform muscle. It sits under the rectus femoris muscle, thereby forming the deepest part of the quadriceps femoris muscle. M. vastus intermedius only performs knee extension movement (Hansen, 2014). Figure 13 illustrates the location of m. vastus intermedius in relation to the other quadriceps muscles.

Figure 13: Red marked m. vastus intermedius (King of the Gym, 2012).

2.2.2. M. biceps femoris

The biceps femoris muscle is a fusiform, double-headed muscle comprises a long head (caput longum) and a short head (caput breve) (Strickland et al., 2017). It is situated on the rear of the thigh. The biceps femoris long head arises from the ischial tuberosity. The short head originates at the linea aspera of the femur (Palastanga and Soames, 2012). The two heads unite and form a common tendon. This tendon inserts on the lateral side of the fibula's head, the fibular collateral ligament, and the lateral tibial condyle (Cramer and Darby, 2014).

M. biceps femoris caput longum

Together with m. semimembranosus and m. semitendinosus, the m. biceps femoris caput longum constitutes the ischiocrural musculature or the hamstrings. A so called true hamstring must originate from the ischial tuberosity, operate on the hip and knee joint and be innervated by the tibial branch of the sciatic nerve. The short head of the double-headed biceps femoris muscle does not belong to the hamstrings group. Neither does it arise from the ischial tuberosity nor does the tibial branch of sciatic nerve innervate it. Further, it only crosses the knee joint and therefore does not act on

Biceps Femoris Long Head
Biceps Femoris Short Head
Semimembranosus
Semitendinosus



Figure 14: Red marked m. biceps femoris long head (King of the Gym, 2012).

the hip joint (Chaitow and DeLany, 2011). Just as the other hamstring muscles, the biceps femoris' caput longum function is concentrated on hip extension, particularly when the torso is bent forwards and should be raised to the erect position. Further, all three hamstring muscles control the forward bending of the torso. In this case, they are acting in an eccentric manner. Flexion of the knee joint is another function of the hamstrings (Palastanga and Soames, 2012). In figure 14, m. biceps femoris caput longum is depicted in relation to the other hamstring muscles and in relation to m. biceps femoris caput breve.

2.2.3. Muscle Roles

Depending on a given movement, a muscle can play various roles such as agonist, antagonist or synergist.

Agonist – Antagonist relationship

Agonist-antagonist relationships are found between opposing muscles. Agonists cause a particular motion, while the antagonists induce the opposite motion. The antagonist is usually located at the other side of the joint that the agonist is acting on. The very fine balanced relationship between agonist and antagonist proceeds in the following way: When the agonist contracts, the antagonist has to relax to some degree. Only then, the agonist can carry out the desired motion. Sometimes agonist and antagonist perform so called co-contractions. In this case, the antagonist contracts eccentrically at the end of the motion. For example, co-contractions are utilized to decelerate body parts. During the swing phase of walking, the thigh is moved forward by contraction of the hip flexors, in this case representing the agonists. The hip extensors, representing the antagonists, first relax, but contract eccentrically at the end of the motion to decelerate the thigh (MacLester and St. Pierre, 2008).

Synergists

Synergists are muscles that contract at the same time as the agonists and support them to achieve their movement goal. Furthermore, they prohibit undesired secondary motion from the agonists. (Clippinger, 2016) When the agonist spans two joints, the synergist has to stabilize one joint, while the agonist is acting on the other one (Bonewit-West et al., 2016).

Concerning hip flexion and extension, m. rectus femoris and m. biceps femoris caput longum represent an agonist - antagonist relationship. In case of knee flexion and extension, m. biceps femoris caput longum and m. vastus intermedius are connected in the same manner, while m. rectus femoris and m. vastus intermedius act as synergists (Chaitow and DeLany, 2011).

2.3. OpenSim

In the years 2004 and 2005, the National Institutes of Health (NIH), the medical research agency of the U.S., established seven National Centres for Biomedical Computing (NCBC) to take increased advantage of computation in biomedical research. They were charged with acting as hubs to improve the computational infrastructure for biomedical computing in the nation. Therefore, each centre aims at generating innovative software tools to process and share data on human health and disease. Simbios, the National Centre for Physics-

Based Simulation of Biological Structures, is one of the NCBCs. Its head seat is located at Stanford University. Simbios focuses on the understanding of biological form and function at several scales with the goal of uniting them in multiscale simulations (National Institutes of Health, n. d.).

Beside research aims, Simbios provides a framework for information and software dissemination by establishing the platform simtk.org. Simtk.org contains the SimTK simulation toolkit, which includes tools essential for physics-based simulations. (Schmidt et al., 2008) The tools consist of algorithms performing for example complex linear algebra, integration and optimization calculations. The SimTK applications, which are also available on the website simtk.org, are built from these SimTK tools (Delp et al., 2012).

OpenSim, representing one of the SimTK applications, focuses on biomechanical simulations of the human body. It is an open-source simulation platform, that is freely available at Simtk.org and enables researchers to model, simulate and analyse the neuromusculoskeletal system (Schmidt et al. 2008). The software is written in C++, while the graphical user interface is written in Java. Figure 15 shows the graphical user interface of the OpenSim application. It allows users to view and modify models, perform simulations and plot results.

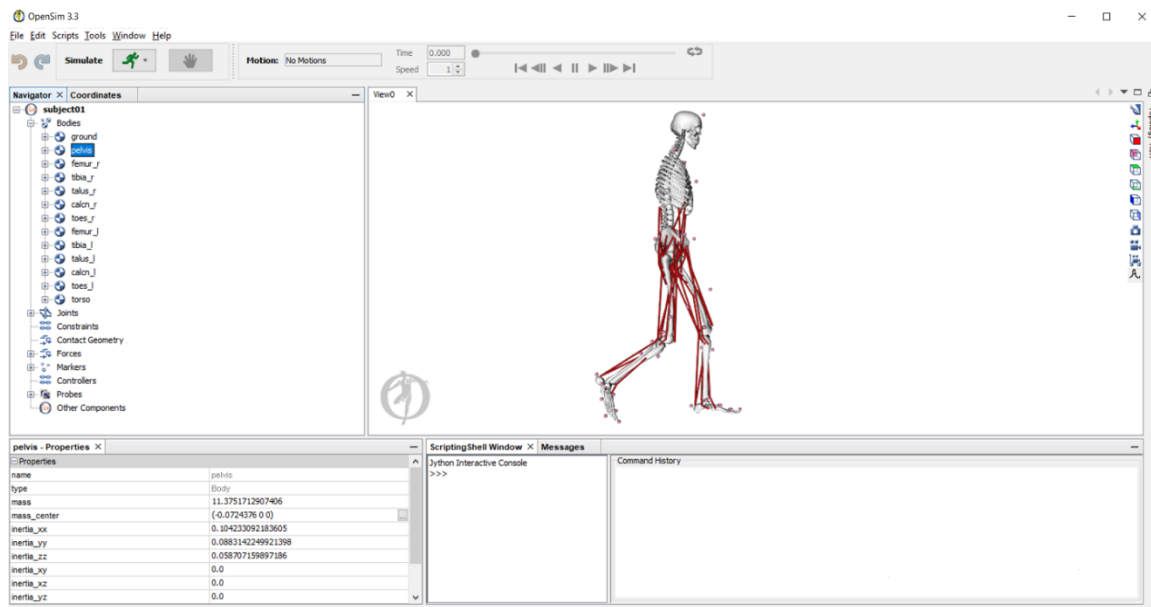


Figure 15: Graphical User Interface of OpenSim.

2.3.1. Musculoskeletal model

The OpenSim library contains many different musculoskeletal models with different musculoskeletal structures. Depending on research needs, one can choose models for the lower and upper extremities, all differing in the amount of muscle-tendon actuators and degrees of freedom. In this thesis, the so called *Gait2354* model is used. In the following section, information about the model are listed and explained. A complete description is provided in the OpenSim documentation on <https://simtk-confluence.stanford.edu> (National Center for Simulation in Rehabilitation Research, n. d. 1).

The model Gait2354 represents a three-dimensional lower extremity computer model of the human musculoskeletal system. It includes 23 degrees of freedom, 54 muscle-tendon actuators and comprises two legs and a lumped torso segment. Since the model is intended to simulate and analyse human movement that is focussed on the lower extremities, walking data are included in the model package (National Center for Simulation in Rehabilitation Research, n. d. 1).

Kinematics

The lower extremity of the Gait2354 model consists of seven body segments: pelvis, femur, patella, tibia/fibula, talus, foot and toes. Relative motions of these body segments are dependent on the definitions of the hip, knee, ankle, subtalar, and metatarsophalangeal joints. The hip joint is modelled as ball-and-socket joint, while the ankle, subtalar, and metatarsophalangeal joints are represented via frictionless revolute joints. Since the structure of the knee joint is highly complicated, the Gait2354 provides a simplified version, containing one degree of freedom. The paths of the muscle-tendon actuators are represented by line segments. Origin and insertion points are determined via anatomical landmarks on the bone surfaces. If required, intermediate via points are applied to describe the muscle path more accurately, for example when the muscle is wrapping over the bone (National Center for Simulation in Rehabilitation Research, n. d. 1).

Actuators

The Gait2354 model contains 54 muscle-tendon actuators. For many muscles, the peak isometric force value is based on healthy, living subjects derived from the studies of Anderson and Pandy (1999). In some cases, the muscle strengths are acquired from the lower limb model created by Delp et al. (1990). Then, strength scaling is added because the data from Delp et al. are obtained from cadavers and not from living subjects. The values for the optimal fiber length and pennation angle are based on the studies of Wieckiewicz et al. (1983) and Friedrich et al. (1990). Each muscle is defined by the following five constants: maximum isometric force (F_0^M), optimal muscle fiber length (L_0^M), tendon slack length (L_S^T), maximum contraction velocity (V_{max}^M) and pennation angle (α_0^M) at optimal fiber length. The pennation angle α^M defines the angle between the muscle fibers and the tendon. Tendon slack length L_S^T expresses the length when the tendon begins to resist lengthening and transmits force (National Center for Simulation in Rehabilitation Research, n. d. 1).

Muscle Mechanics

The muscle mechanics used in Gait2354 is derived from Thelen (2003). The Thelen2003Muscle model is based on the Hill-type muscle model (National Center for Simulation in Rehabilitation Research, n. d. 2).

The Hill model was developed by the physiologist A.V. Hill in the late 1930s and illustrates the concept of muscle contraction. (Abernethy et al., 2013) The model considers both active and passive components of muscle tension. It consists of three elements, comprising a musculotendon actuator: a contractile element (CE) representing active muscle tension and two non-linear spring elements, one in series (SE) and one in parallel (PE) with CE, representing passive muscle tension. (Knudson, 2003) The contractile element (CE) is fully extensible when inactive but is able to shorten when

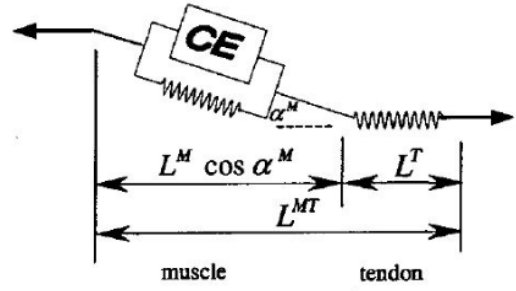


Figure 16: Hill-type muscle model (National Center for Simulation in Rehabilitation Research, n. d. 2).

activated. It accounts for the force-length and force-velocity properties of the muscle. The serial-elastic element (SE) represents the tendon and the cross-bridges formed by actomyosin binding, inducing elasticity during isometric contractions (active stiffness). The parallel-elastic element (PE) represents the intermuscular connective tissue (fascia, epimysium, perimysium and endomysium) that surrounds the muscle fibers inducing elasticity in resting state (passive stiffness) (Van den Berg and Cabri, 2003 and Abernethy et al., 2013).

Figure 16 illustrates the musculotendon actuator used in Gait2354. It is based on the hill-type muscle model and estimates muscle contractile dynamics in the musculoskeletal model. L^{MT} represents the instantaneous length of the muscle-tendon actuator. It depends on the instantaneous length of the muscle L^M , the instantaneous length of the tendon L^T , and the muscle's pennation angle α^M (National Center for Simulation in Rehabilitation Research, n. d. 2).

Mathematical description of muscle mechanics

The dynamic behaviour of the contractile element in a hill-type muscle model is described using two major types of dynamics: Activation Dynamics and Contraction Dynamics (Romero and Alonso, 2016).

The former explains the transformation relationship between the muscular excitation signal, u , and the activation signal, a . The latter relates the activation state, a , with muscle force development (Romero and Alonso, 2016).

Activation Dynamics

Activation dynamics expresses the time lag between the firing of motor units and the formation of actin-myosin cross-bridges (Romero and Alonso, 2016). The following non-linear first order differential equation shows the relation of the muscular excitation signal, u , describing the muscle input signal, and the activation signal, a , describing the muscle fibers recruitment state. Both variables, u and a , are dimensionless quantities between 0 and 1 (Thelen, 2003).

$$\frac{da}{dt} = \frac{u(t) - a(t)}{\tau_a(a(t), u(t))} \quad (7)$$

The term $\tau_a(a, u)$ expresses the time constant, which Thelen defines in the following way (Thelen, 2003):

$$\tau_a(a(t), u(t)) = \begin{cases} \tau_{act}(0,5 + 1,5a(t)); & u(t) > a(t) \\ \frac{\tau_{deact}}{0,5+1,5a(t)}; & u(t) \leq a(t) \end{cases} \quad (8)$$

The term τ_{act} represents the activation time constant, while τ_{deact} expresses the deactivation time constant. Analysis of the equation 7 and 8 shows that when activation level increases ($u < a \rightarrow u - a < 0$), the activation slows, since $\frac{da}{dt}$ is negative. This happens because calcium ions are released and diffused less efficiently. When the activation level decreases ($u > a \rightarrow u - a > 0$), the deactivation slows, because $\frac{da}{dt}$ is positive. There is only a low amount of calcium ions left for uptake by the sarcoplasmic reticulum (Thelen, 2003).

Contraction Dynamics

Contraction dynamics shows the relationship between the activation signal, a , and the force, F^{MT} , produced by the musculotendon actuator (John, n. d.).

According to the distribution of the elements in the musculotendon actuator, it follows:

$$F^{CE}(t) = \frac{F^T(t)}{\cos \alpha^M(t)} - F^{PE}(t) \quad (9)$$

$$\text{and } F^T(t) = F^{MT}(t) \quad (10)$$

with $F^{CE} = F^M$, F^T and F^{PE} describing the force of the contractile element (CE), of the tendon (T) and of the parallel-elastic element (PE) (John, n. d.).

The pennation angle of the muscle depends on the width of a muscle ($w = L_0^M * \sin \alpha_0^M$) and on the current fiber length, $L^M(t)$ (Romero and Alonso, 2016).

The force exerted by the muscle is described by the following equation:

$$F^{CE}(t) = F_0^M \cdot a(t) \cdot f_L(\tilde{L}^M(t)) \cdot f_V(\tilde{V}^M(t)) \quad (11)$$

The term $f_L(\tilde{L}^M)$ represents the force-length relationship depending on the normalized muscle length $\tilde{L}^M = L^M(t)/L_0^M$. Similarly, the force-velocity relationship is described by the term $f_V(\tilde{V}^M)$ depending on the normalized contraction velocity $\tilde{V}^M = V^M(t)/V_{max}^M$, where V^M describes the instantaneous muscle contraction velocity (Romero and Alonso, 2016).

The force of PE is expressed by:

$$F^{PE}(t) = F_0^M \cdot f_{PE}(\tilde{L}^M(t)) \quad (12)$$

where f_{PE} describes the normalized passive force-length relationship.

Tendon force is calculated by:

$$F^T(t) = F_0^M \cdot f_T(\varepsilon^T(t)) \quad (13)$$

where f_T represents the normalized tendon force-strain relationship also known as tendon stiffness. ε^T expresses the tendon strain, which is calculated by $\varepsilon^T(t) = (L^T(t) - L_s^T)/L_s^T$ (John, n. d. and Romero and Alonso, 2016).

Insertion of the equations 11, 12 and 13 in 9 results in:

$$F_0^M \left(a(t) \cdot f_L(\tilde{L}^M(t)) * f_V(\tilde{V}^M(t)) + f_{PE}(\tilde{L}^M(t)) \right) \cdot \cos \alpha^M(t) - F_0^M \cdot f_T(\varepsilon^T(t)) = 0 \quad (14)$$

Solving this equation for $f_V(\tilde{V}^M(t))$ yields:

$$f_V(\tilde{V}^M(t)) = \left(\frac{f_T(\varepsilon^T(t))}{\cos(\alpha^M(t))} - f_{PE}(\tilde{L}^M(t)) \right) / \left(\alpha^M(t) \cdot f_L(\tilde{L}^M(t)) \right) \quad (15)$$

Inversion of the force-velocity curve leads to:

$$\tilde{L}^M(t) = \tilde{V}^M(t) = f_V^{-1} \left\{ \left(\frac{f_T(\varepsilon^T(t))}{\cos(\alpha^M(t))} - f_{PE}(\tilde{L}^M(t)) \right) / \left(\alpha^M(t) \cdot f_L(\tilde{L}^M(t)) \right) \right\} \quad (16)$$

Equation 16 can be written in a simplified version, since it only depends on three states, namely activation value, muscle fiber length and muscle-tendon actuator length:

$$\frac{dL^M}{dt} = f_V^{-1}(L^M, L^{MT}, a) \quad (17)$$

The differential equations 16 and 17 represent how musculotendon contraction dynamics are modelled in the OpenSim software. (National Center for Simulation in Rehabilitation Research, n. d. 2).

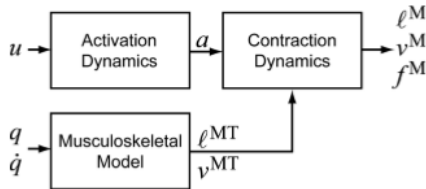


Figure 17: Illustration of musculotendon mechanics modeling (Millard et al., 2013).

Figure 17 illustrates the process of modeling musculotendon mechanics in muscle-driven simulations. Muscle activations, a , are calculated from neural excitations, u , using activation dynamics. Musculotendon lengths, L^{MT} , and velocities, V^{MT} , are determined from the generalized coordinates, q , and velocities, \dot{q} , of the musculoskeletal model. These results are then used by contraction dynamics to produce a forward simulation of muscle length, L^M , velocity, V^M , and force, F^M .

Thelen Muscle Model

Each element in the hill-type muscle model (CE, PE and SE) can be described using different mathematical models (Romero and Alonso, 2016). Thelen adjusts the Hill model in a way that it reflects nominal aging effects on muscle mechanics that arise between the ages 30 and 70. The adaption is achieved by different parameter settings depending on age. The isometric muscle forces, the deactivation time constant and the maximum contraction velocity are reduced in older adults. On the other side, maximum normalized force during lengthening and the relative passive stiffness value (in proportion to total tension) are increased (Thelen, 2003).

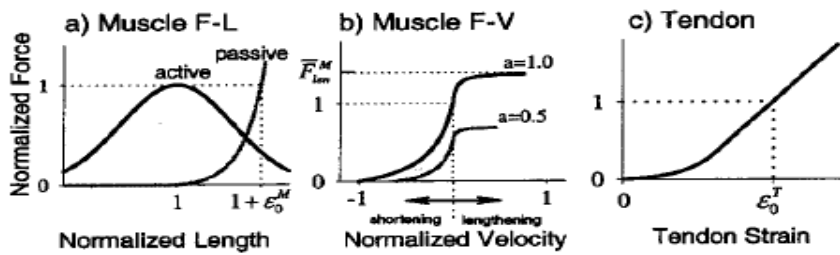


Figure 18: Thelen muscle model – muscle properties (National Center for Simulation in Rehabilitation Research, n. d. 2).

The curves of figure 18 show the intrinsic muscle properties of the Thelen muscle model. All curves are normalized. Normalized Force is expressed by $\tilde{F}^M = \frac{F^M(t)}{F_0^M}$, normalized length by $\tilde{L}^M = \frac{L^M(t)}{L_0^M}$ and normalized velocity by $\tilde{V}^M = \frac{V^M(t)}{V_{max}^M}$. The muscle force-length relationship is represented by a Gaussian curve. The curve showing the force-velocity relationship is scaled with activation, leading to lower unloaded contraction velocities during sub-maximal activations. Tendon force is modelled to rise exponentially with strain (Thelen, 2003).

2.3.2. Dynamic simulation

A muscle-driven simulation of movement in OpenSim includes four steps: Scaling, inverse kinematics (IK), refinement of model kinematics by the residual reduction algorithm (RRA) and generation of a forward dynamic simulation using the computed muscle control (CMC) algorithm. In the following section, the steps are described in detail in the context of performing gait simulations (Delp et al., 2007).

Figure 19 illustrates the steps of a dynamic simulation in OpenSim. First, a generic model is scaled based on experimental marker positions. With the scaled model, inverse kinematics is performed, using experimental marker trajectories of motion. The calculated joint angles are filled in RRA together with experimental reaction forces and moments. Thereby, dynamically consistent joint angles are achieved. Together with the experimental reaction forces and moments, they are used to compute muscle activations and forces with CMC.

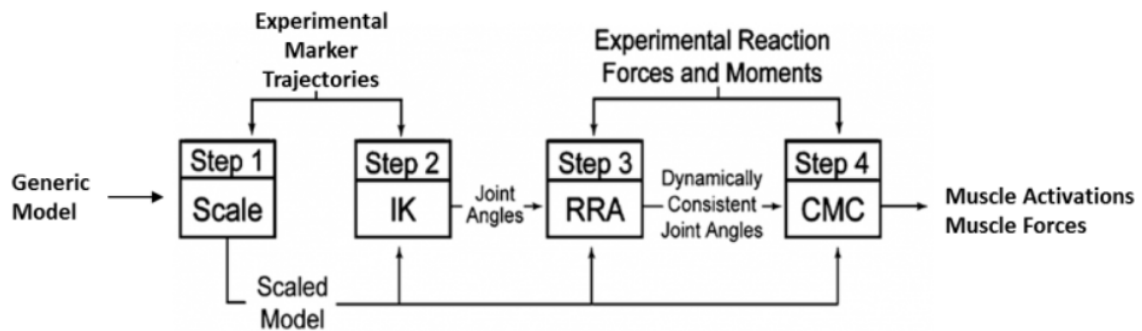


Figure 19: Schematic of a muscle-driven simulation in OpenSim (The Ohio State University, 2018).

Scaling

The Scale Tool adapts the anthropometry of a dynamic musculoskeletal model so that it matches an individual subject as good as possible. The scaling step includes the adaption of (National Center for Simulation in Rehabilitation Research, n. d. 3):

- the model's mass properties (mass and inertia tensor), by proportional distribution to reproduce the subject's total mass.
- the body segments' dimensions, by computation of scale factors. These factors depend on the relative distances between pairs of experimental marker positions and the corresponding virtual marker positions.
- the muscle fiber length and tendon slack length of the musculotendon actuator and other length-dependent components. A scale factor is calculated as the ratio of the length before and after scaling, and this scale factor is used to scale the length-dependent properties.

Inverse Kinematics (IK)

This step includes the calculation of the model's generalized coordinate values (joint angles and translations) for each time frame by positioning the model in a pose that the coordinate values reproduce the experimental marker data as precisely as possible. The inverse kinematics tool is implemented as a weighted least squares problem whose solution aims at minimization of the difference between the measured and virtual marker locations of model and subject, thereby complying with joint constraints (National Center for Simulation in Rehabilitation Research, n. d. 4).

For each time frame in the experimental kinematics, the IK tool solves the following least squares problem (Delp et al., 2007):

$$\min_q \left[\sum_{i=1}^{\text{markers}} w_i \|x_i^{\text{exp}} - x_i(q)\|^2 + \sum_{j=1}^{\text{unprescribed coordinates}} \omega_j \|q_j^{\text{exp}} - q_j\|^2 \right] \quad (18)$$

$$q_j = q_j^{\text{exp}} \text{ for all prescribed coordinates } j$$

with

q	...	vector of generalized coordinates, which is aimed to be calculated
x_i^{exp}	...	three-dimensional position of the i-th experimental marker
$x_i(q)$...	three-dimensional position of the i-th model marker, dependent on the coordinate values
q_j^{exp}	...	value of the j-th joint angle of the subject
q_j	...	value of the j-th joint angle of the model
w_i and ω_j	...	factors for different weighting of markers and joint angles

The first term deals with marker errors describing the distance between the experimental marker data and the corresponding virtual marker data when the model is in the position that the generalized coordinates computed by the IK solver induce. The second term concentrates on coordinate errors defined by the difference between an experimental coordinate value and the coordinate value calculated by the IK solver. There is a distinction between prescribed and unprescribed coordinates. Prescribed coordinates are locked coordinates with a known trajectory value. They are just set to their experimental values and not computed by the IK solver (National Center for Simulation in Rehabilitation Research, n. d. 4).

Residual Reduction Algorithm (RRA)

RRA application minimizes nonphysical compensatory forces, called residuals, which occur due to modelling assumptions (for example having a model without arms) and marker data processing (experimental) errors. In other words, RRA helps to make the generalized coordinates calculated with IK more dynamically consistent with the experimental ground reaction force data. This is achieved by small alterations of the model mass parameters and slight perturbations to motion trajectory (Delp et al., 2007).

RRA is generally intended to be used for movements where the model changes position relative to the ground as for example walking and running. Six generalized coordinates calculated with IK, specifying the six degrees of freedom (three translational and three rotational), indicate the local relationship between the model's pelvis and the ground. These six degrees of freedom are regarded as joint between pelvis and ground. Exactly one actuator, called residual actuator, exists for all of the six generalized coordinates in the model. The actuators of the three translational degrees of freedom are called residual forces (F_x, F_y, F_z), while the actuators of the three rotational degrees of freedom are called residual torques (M_x, M_y, M_z) (National Center for Simulation in Rehabilitation Research, n. d. 5). According to Newton's second law, the following equation 19 relates the experimental ground reaction force to the model kinematics and the residual force. There is an analogous equation describing the relationship between the experimental ground reaction moment, model kinematics and

the residual moment (Delp et al., 2007). Equation 19 describes the same relation as equation 1, thereby using different variables.

$$\vec{F}_{external} = \sum_{i=1}^{segments} m_i \vec{a}_i - \vec{F}_{residual} \quad (19)$$

with

$\vec{F}_{external}$...	experimental ground reaction force minus the body weight vector
\vec{a}_i	...	translational acceleration of the center of mass of the i-th body segment
m_i	...	mass of the i-th body segment
$\vec{F}_{residual}$...	residual force

The residual force is only zero when the model contains no modelling or experimental errors, which is practically never the case. Non-zero residual force accounts for the dynamic inconsistency of the model. The application of the RRA tool leads to a minimization of the residual forces and moments (Delp et al., 2007).

RRA starts with the performance of a tracking simulation. First, the model is placed in its starting configuration, which is based on the generalized coordinates computed by IK. The movement of the model from its current configuration to the following configuration, indicated by the generalized coordinates of the next time step, requires force generation from the model's actuators. For the whole duration of the motion, RRA calculates the force values for all of the model's actuators (not only for the residuals) by minimization of an objective function. After finishing the simulation, the residuals are averaged for the duration of the motion. Depending on the results, the algorithm adjusts the torso mass center and recommends mass changes to body segments (National Center for Simulation in Rehabilitation Research, n. d. 5).

Then the tracking simulation is repeated with the adjusted torso mass center. Besides, special restrictions on the residuals are applied. Higher weights are assigned to the residuals in the objective function, resulting in the selection of smaller residual values by the optimizer during minimization of the objective function. Furthermore, minimum and maximum limits are chosen for the residuals. These restrictions help to keep the residual values at the absolute minimum required to follow the desired kinematics, and if possible generate the motion solely by internal forces. Due to maximum and minimum limitations of the residuals, the model's movement is slightly changed (National Center for Simulation in Rehabilitation Research, n. d. 5).

Computed Muscle Control (CMC)

The CMC tool is used to generate a set of actuator controls (muscle excitations) that drive the generalized coordinates of the musculoskeletal model to follow the desired kinematics. CMC is performed using proportional-derivative control, static optimization and forward dynamics (National Center for Simulation in Rehabilitation Research, n. d. 6).

Initial Values

Before the CMC algorithm starts, the initial states comprising the generalized coordinates and velocities (joint angles and angular velocities) and muscle states (muscle activations and fiber lengths) are computed (National Center for Simulation in Rehabilitation Research, n. d. 6).

Desired Accelerations

The CMC algorithm starts with the calculation of a set of desired accelerations. These accelerations enable the model coordinates to track the experimental coordinates. The computation is done using a proportional-derivative control law (National Center for Simulation in Rehabilitation Research, n. d. 6):

$$\ddot{\vec{q}}^{desired}(t + T) = \ddot{\vec{q}}^{exp}(t + T) + \vec{k}_v (\dot{\vec{q}}^{exp}(t) - \dot{\vec{q}}(t)) + \vec{k}_p (\vec{q}^{exp}(t) - \vec{q}(t)) \quad (20)$$

with

$\ddot{\vec{q}}^{desired}$...	desired accelerations of the generalized coordinates
$\ddot{\vec{q}}^{exp}, \dot{\vec{q}}^{exp}, \vec{q}^{exp}$...	experimental accelerations, velocities and positions corresponding to the generalized coordinates of the model
$\dot{\vec{q}}, \vec{q}$...	generalized velocities and coordinates of the model
\vec{k}_v, \vec{k}_p	...	feedback gains for velocity and position errors
T	...	small, user-defined time interval

The desired accelerations are calculated for minor time T in the future, since muscle forces cannot change instantaneously. Considering musculoskeletal models, T is generally selected to be about 0,01 seconds. After having achieved the desired accelerations, the velocity errors ($\vec{e}_v = \dot{\vec{q}}^{exp}(t) - \dot{\vec{q}}(t)$) and the position errors ($\vec{e}_p = \vec{q}^{exp}(t) - \vec{q}(t)$) are driven to zero. One can rewrite equation 20 as a second-order ordinary equation, where \vec{e}_a are the acceleration errors ($\ddot{\vec{q}}^{exp}(t) - \ddot{\vec{q}}^{desired}(t)$) (National Center for Simulation in Rehabilitation Research, n. d. 6).

$$\ddot{\vec{e}}_a - \vec{k}_v \dot{\vec{e}}_a - \vec{k}_p \vec{e}_a = 0 \quad (21)$$

For musculoskeletal models it is recommended to select the feedback gains in a way that they slowly drive errors to zero (National Center for Simulation in Rehabilitation Research, n. d. 6).

Static Optimization

Next to the computation of the desired accelerations, CMC calculates the actuator controls that induce the desired accelerations under steady-state conditions at time $t + T$. A static optimization criterion is applied to distribute forces across synergistic actuators. It is called static optimization because calculations are only performed at each time step without integration of the equations of motion between the time steps (Thelen et al., 2003).

It is possible to add reserve actuators to the model. Reserve actuators are able to provide extra actuation to the model, when the muscles cannot provide enough accelerations to the joint. They can be added to each degree-

of-freedom including the six residual actuators (National Center for Simulation in Rehabilitation Research, n. d. 7).

Forward Dynamics

Finally, CMC generates a forward dynamic simulation, thereby using the calculated muscle excitations as input. The forward dynamic simulation advances forward in time by user-defined time steps T (National Center for Simulation in Rehabilitation Research, n. d. 6).

A forward dynamic simulation is performed by the integration of first-order equations for activation dynamics, first-order equations for contraction dynamics and second-order equations of body movement. The states are advanced to the next step and the generalized coordinates and velocities are fed back to repeat the algorithm (Thelen et al., 2003).

The equation of body movement relates the accelerations of the generalized coordinates to applied forces (Thelen et al., 2003).

$$\ddot{q} = [M(q)]^{-1}\{G(q) + V(q, \dot{q}) + [R(q)] \cdot F + E(q, \dot{q})\} \quad (22)$$

with

- \ddot{q} ... generalized accelerations of the model
- $[M(q)]^{-1}$... inverse mass matrix
- G ... vector of generalized forces due to gravity
- V ... vector of generalized forces due to coriolis and centrifugal effects
- R ... force transmission matrix (muscle moment arms)
- F ... vector of muscle forces or any other applied forces, transformed to a generalized force using R
- E ... vector of generalized forces that represent interactions with the environment

The three stages – calculation of desired accelerations, static optimization and forward dynamic simulation – are repeated every T seconds for the whole motion duration (Thelen et al., 2003).

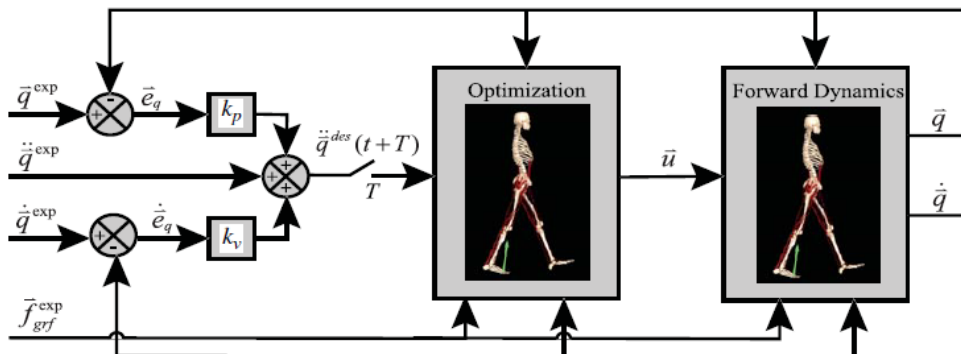


Figure 20: Schematic of CMC applied to gait (Thelen and Andersen, 2006).

Figure 20 illustrates the CMC process. The algorithm starts with the calculation of a set of desired accelerations ($\ddot{q}^{\text{desired}}$). They drive the generalized coordinates \bar{q} and velocities $\dot{\bar{q}}$ towards the experimental coordinates

\vec{q}^{exp} and velocities $\dot{\vec{q}}^{exp}$. Static optimization is applied to calculate a set of actuator controls at time $t + T$. Experimental forces, such as ground reaction forces \vec{f}_{grf}^{exp} , are also incorporated in the static optimization problem. The neural excitations \vec{u} are used as input to the forward dynamic simulation. Numerical integration is used to advance all states to $t + T$. The generalized coordinates and velocities are then fed back (Thelen et al., 2003).

Analysis

The Analyze tool is generally used to analyse a simulation, computed with CMC. Depending on the research interest, the user can choose different analysis types as for example: Muscle Analysis and induced acceleration analysis (National Center for Simulation in Rehabilitation Research, n. d. 8).

Muscle Analysis

The muscle analysis tool enables to record and compute muscle quantities during a simulation. The analysis comprises the calculation of many muscle parameters including muscle fiber length, shortening velocity and power (National Center for Simulation in Rehabilitation Research, n. d. 9).

Induced Acceleration Analysis

Individual forces cause the accelerations of generalized coordinates (e.g. knee angle), body segments (e.g. femur) or body locations (e.g. model's center of mass). The induced acceleration analysis tool enables the user to calculate these induced accelerations (National Center for Simulation in Rehabilitation Research, n. d. 9).

Generalized coordinates, body segments and body locations are generally not directly accelerated by internal forces but by external reaction forces including gravity, forces due to velocity effects (i.e., Coriolis and centripetal forces) and muscle forces. To compute system acceleration contribution of individual forces, it is necessary to decompose the external reaction forces. Only then, the partial contribution of each individual force to the external reaction force and to the system acceleration can be calculated (Hamner et al., 2013).

To decompose ground reaction forces and moments for examination of muscle force acceleration contribution, different constraint-based foot-ground contact models can be applied. They model contact between the foot and the ground. A rolling-on-surface constraint models the contact between a rolling body and a plane defined on another body (National Center for Simulation in Rehabilitation Research, n. d. 9). It produces a sagittal (F_x), vertical (F_y) and transverse (F_z) reaction force and a vertical reaction moment (M_y) about the center of pressure. The rolling-on-surface constraint comprises four individual constraints (Hamner et al., 2013).

$$\rho_y(q) \geq 0 \quad (23)$$

$$\dot{\rho}_x(q, \dot{q}) = 0 \quad (24)$$

$$\dot{\rho}_z(q, \dot{q}) = 0 \quad (25)$$

$$\omega_y(q, \dot{q}) = 0 \quad (26)$$

The term ρ_y expresses the vertical position of the foot, while $\dot{\rho}_x$ and $\dot{\rho}_z$ represent the sagittal and transverse velocities of the foot. The vertical angular velocity of the foot is given by ω_y . Equation 23 expresses the vertical, unilateral, non-penetrating constraint. Penetration of the ground is not possible, but the foot can be lifted. Equation 24 and 25 represent the sagittal and the transverse no-slip constraints, which limit foot translations in these directions. The last constraint restricts vertical rotations and is called vertical no-twist constraint. It is expressed by equation 26.

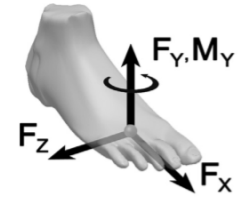


Figure 21: Illustration of the Rolling on surface constraint (Hamner et al., 2013).

Figure 21 illustrates the rolling on surface constraint. It produces a fore-aft (F_x), vertical (F_y) and mediolateral (F_z) reaction force and a vertical reaction moment (M_y) about the center of pressure (Hamner et al., 2013).

2.3.3. Springs

Springs are elastic devices, capable of mechanical energy storage. They consist of wound coils or spirals. When a pulling force is applied to the spring, it stretches. Thereby the pulling force uses energy. The tighter (higher stiffness) the spring, the more energy is required. This energy is stored by the spring in form of potential energy. After removing the force, the spring immediately recoils back to its original shape, thereby releasing the stored energy (Woodford, 2018).

One can distinguish between linear and variable rate springs. Linear springs satisfy Hooke's law

$$F = k \cdot x \quad (27)$$

where the force F required for spring extension or compression by distance x is proportional to this distance x . The term k represents the spring rate or spring stiffness, which stays constant. Variable rate springs show different behaviour. Their spring rate changes with spring deflection (Wu, 2013).

Due to their mechanical behaviour, springs are commonly used in passive and quasi-passive exoskeletons. In the year 2015, Collins et al. developed a passive ankle exoskeleton using a coil spring and examined its effect on walking performance of healthy subjects. The device was implemented in parallel to the calf muscles and the Achilles tendon. Grabowski and Herr (2009) implemented fiberglass leaf springs in parallel to the leg. They studied the effects on hopping in place of healthy subjects.



Figure 22: Unpowered exoskeleton design from Grabowski and Herr (2009).

The pictures 22 and 23 show different designs of unpowered exoskeletons.



Figure 23: Unpowered exoskeleton design from Collins et al. (2015).

Springs in OpenSim

OpenSim offers the possibility to include springs to the musculoskeletal model. Since this thesis is focussed only on path springs, the following section solely deals with this specific passive element.

Path Spring

A path spring refers to a massless force element. During implementation, the user has to determine the spring's path along which tension is applied. The tension of the spring is defined in the following way (National Center for Simulation in Rehabilitation Research, n. d. 10):

$$T = (K \cdot s) \cdot (1 + D \cdot \dot{L}) \quad (28)$$

$$\text{with } s = \begin{cases} L - L_0 & L > L_0 \\ 0 & L \leq L_0 \end{cases}$$

with

- L ... path length of the spring
- L_0 ... resting length of the spring
- K ... stiffness value
- D ... Dissipation factor

Since the equation does not fulfil Hooke's law, it is a nonlinear spring. The dissipation factor describes how tension is affected by the rate of stretch. When the spring's length equals or falls below the resting length, no tension is produced (National Center for Simulation in Rehabilitation Research, n. d. 10).

3. Methods

3.1. Model and Data

Model and data are all taken from the OpenSim library. The three-dimensional model 'Gait2354' is downloaded from the simtk.org page. The 'Gait2354' package includes experimental data (marker trajectories and ground reaction forces) for a healthy male walking on a treadmill with self-selected velocity. The data were collected as part of the study from John et al. in the year 2012. For all simulations, the tool-specific setup files included in the 'Gait2354' package are used. In these files, the scale factors and coordinate weights are chosen according to the study from John et al. (2012).

3.2. Preliminary determinations

3.2.1. Gait cycle

The study is constrained to pre-swing, initial swing and mid-swing. These three phases were chosen to examine both activation and deactivation phases of m. rectus femoris. Furthermore, this chapter will show that springs which are implemented parallel to m. rectus femoris exhibit their peak force during these phases. The data of the 'Gait2354' package report gait motion for 2,5 seconds, corresponding to approximately two gait cycles.

To determine the gait cycle to be analysed, the first initial contact (vertical force > 0) with the right leg is taken as start time, while the time step prior to the subsequent initial contact of the right leg is taken as end time. According to the ground reaction force file, the start time is selected at time 0,5983s and the end time at 1,8283s. As a next step, the start and end times of the pre-swing, initial swing and the mid-swing phases are determined. They are chosen depending on the starting and terminating events described in table 1.

Table 3: Start and end times of the relevant gait sub-phases.



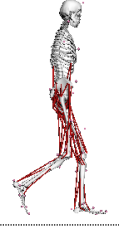



Gait sub-phase	Start pose	Start time	Per cent of gait cycle	End pose	End time	Per cent of gait cycle
Pre-swing		1,225s	~51%		1,43s	~68%
Initial swing		1,43s	~68%		1,533s	~76%
Mid-swing		1,533s	~76%		1,725s	~92%

Table 3 shows the start and end times in seconds and in per cent of the gait cycle of the three relevant gait phases pre-swing, initial swing and mid-swing. They depend on the experimental data of the ‘Gait2354’ package. Further, the start and end poses of the ‘Gait2354’ musculoskeletal model are represented.

3.2.2. Path Spring

The path spring is implemented at the path of the rectus femoris muscle on the right leg. The force element is constructed of three parameters, namely resting length, dissipation factor and stiffness.

Resting length

The resting length parameter marks the spring’s force production. When the path length of the spring exceeds the spring’s resting length, force is generated.

According to figure 24, illustrating the tendon-force length relationship, the tendon starts producing force at tendon slack length (L_s^T). Figure 25 shows the normalized active and passive force-length curves of muscles. The muscle fibers (active curve) start to generate force at 40% of their optimal length (L_0^M). (Delp and Arnold, 2011)

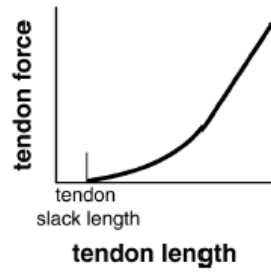


Figure 24: Tendon-force length relationship (Allison, n. d.).

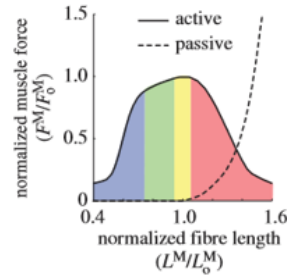


Figure 25: Normalized active and passive force-length curves (Delp and Arnold, 2011).

The spring's resting length, L_0 , is determined in the following way:

$$0,4 \cdot L_0^M + L_s^T = L_0 \quad (29)$$

Table 4 lists the sought values, optimal fiber length and tendon slack length, of m. rectus femoris in the 'Gait 2354' musculoskeletal model, to calculate the spring's resting length.

Table 4: Sought values from the 'Gait 2354' musculoskeletal model.

<i>M. rectus femoris</i>	
Optimal fiber length in m	0,13
Tendon slack length in m	0,355

Insertion of the values in equation 29 gives:

$$0,4 \cdot 0,13 + 0,355 \approx 0,41m$$

The result is rounded to two decimal figures.

Dissipation factor

The dissipation factor is selected to be 0,01 s/m, identical to the dissipation factor of m. gastrocnemius described in an OpenSim example. (National Center for Simulation in Rehabilitation Research, n. d. 11)

Stiffness

The stiffness level is selected dependent on the results of the preliminary studies.

3.3. Preliminary simulations

In this section, three preliminary studies are described. They ensure that spring implementation parallel to weakened m. rectus femoris is justified.

3.3.1. Muscle replacement

As a first step, m. rectus femoris is replaced by a passive path spring, to test whether the spring is able to replicate the function of m. rectus femoris. Therefore, m. rectus femoris is removed from the ‘Gait2354’ musculoskeletal model and replaced by a path spring.

The purpose of this preliminary study is to examine the forces produced by the passive spring and compare them to timing and magnitude of a healthy rectus femoris muscle (Willson, 2017).

To get a better understanding which stiffness level replicates healthy muscle function as good as possible, three different levels are chosen.

Results



Figure 26: Replacement of m. rectus femoris by a path spring.

Figure 26 illustrates the forces of m. rectus femoris and the springs for each condition. At the beginning of pre-swing, the spring's curves reach higher values than the m. rectus femoris curve. When rectus femoris' force goes up, the springs cannot produce the sharp peak. Thus, the springs are not able to replicate the shape of m. rectus femoris during the pre-swing phase (51%-68% of gait cycle). During the initial swing phase (68%-76%) and the mid-swing phase, the springs are able to follow the force curve of m. rectus femoris.

The spring with stiffness value 1.500N/m replicates the force curve of m. rectus femoris best.

3.3.2. Force Takeover

The second preliminary simulation aims at demonstrating the effects of the path spring on the force production of m. rectus femoris. Therefore, the spring is implemented in the ‘Gait2354’ musculoskeletal model including healthy m. rectus femoris. The spring parameters are chosen identically to the first preliminary simulation.

The purpose of the second preliminary study is to clarify if the spring is able to take over force from m. rectus femoris. If the spring is able to take over force, the force curve of m. rectus femoris is reduced. Further, the magnitude of the force takeover depending on the stiffness value is analysed.

Results

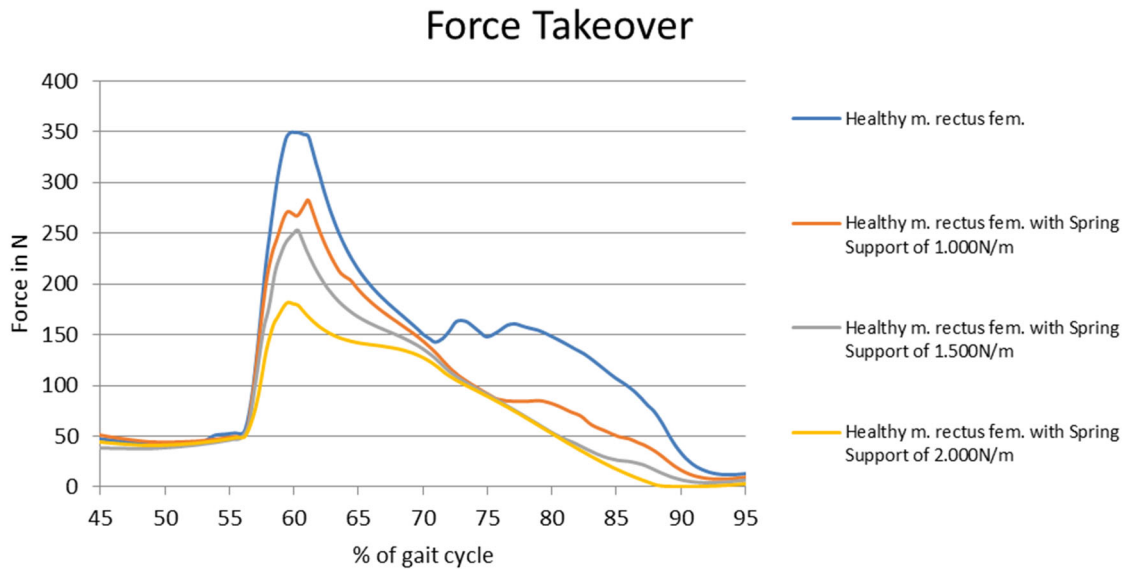


Figure 27: Effects on force production of m. rectus femoris, when a path spring is implemented in parallel to healthy m. rectus femoris.

The results show that the spring implementation leads to force reduction of m. rectus femoris at all stiffness values. The higher the stiffness value, the higher the force takeover. Especially the sharp peak is lowered. The curves then assimilate again until ~70% of the gait cycle. Afterwards the spring is again able to drop force production of m. rectus femoris until the end of mid-swing, when the curves assimilate again.

Although the stiffness values are chosen in intervals of 500N/m, the force takeover does not reflect this regularity. The force curves of rectus femoris with springs of stiffness values 1.000N/m and 1.500N/m are really close to each other during the pre-swing phase (51%-68% of the gait cycle). During initial swing and mid-swing the force curves of rectus femoris with springs of stiffness values 1.500N/m and 2.000N/m nearly show the same course.

3.3.3. Muscle weakening

In this thesis, muscle weakness of m. rectus femoris is supposed to arise from an inability to activate all muscle fibers. The activation deficit is implemented by modifications of the actuator constraints file included in the ‘Gait2354’ model. The control level is constrained to 50%, 25% and 10% of the maximum healthy control level regarding the whole gait cycle (Thompson et al., 2013).

The purpose of this study is to clarify if muscle weakness can be generated by reducing the m. rectus femoris maximum control level.

Muscle weakening - Controls

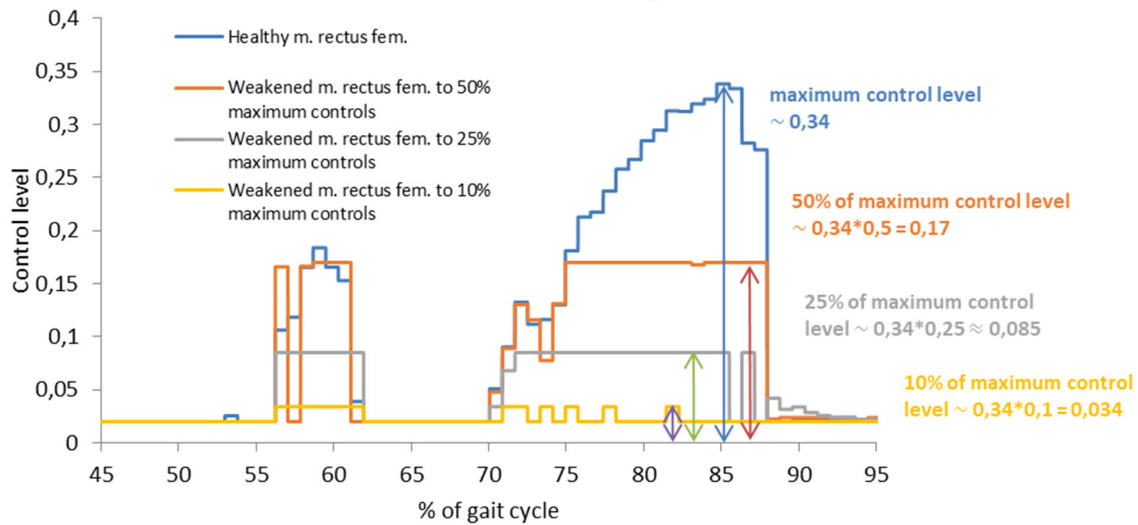


Figure 28: Controls (muscle excitations) of m. rectus femoris with different maximum limitations. A control level of zero expresses zero excitation, a control level of 1 expresses maximum excitation.

Muscle weakening - Forces

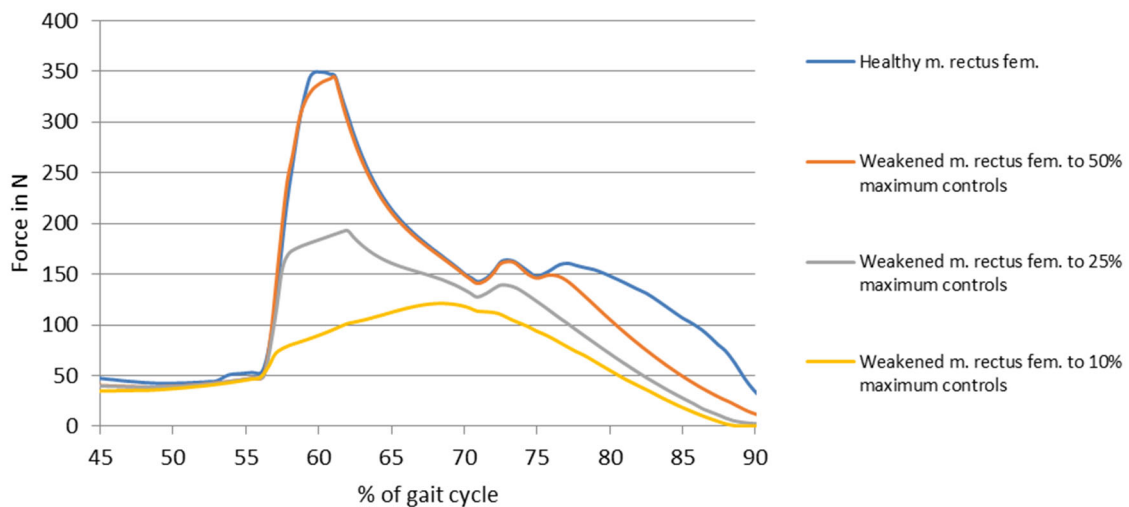


Figure 29: Force curves of healthy weakened m. rectus femoris. Muscle weakening is performed using control constraints.

Muscle weakening by decreasing the control level of m. rectus femoris (figure 28) influences the force of m. rectus femoris (figure 29). All arising force differences are based on the differences in control level.

Figure 29 shows that the reduction of controls to 50% of the maximum level does not have much effect on the force curve. This fact is explained by figure 28. The control levels of healthy m. rectus femoris and weakened m. rectus femoris to 50% of maximum controls start to differ at 75% of gait cycle. This behaviour is reflected

in the force curve. Therefore, the peak force value, which is achieved at $\sim 60\%$ of the gait cycle, cannot be reduced.

When m. rectus femoris controls are constrained to 25% and 10% of maximum level, the decrease in force production is clearly visible for the entire selected part of the gait cycle. From 45% to $\sim 57\%$ of the gait cycle the healthy and the weakened curves follow the same course. Then, the force curves differentiate and reach a peak difference at $\sim 60\%$. The curves assimilate again at $\sim 70\%$ of the gait cycle. Afterwards they differ again and reach another peak difference at approximately 81% of the gait cycle.

Conclusions

In summary, the following findings derived from preliminary simulations can be stated:

Figure 26 shows that the passive spring is not able to exactly reproduce the force of m. rectus femoris. Nevertheless, neglecting the small time period accounting for $\sim 5\%$ in the gait cycle where the m. rectus femoris produces its peak force ($\sim 60\%$ to $\sim 65\%$ of the gait cycle), enables a good replication of the general shape of the force curve.

Implementation of a passive spring reduces force production of m. rectus femoris. The stiffer the spring, the higher the force decrease. Furthermore, the controls of m. rectus femoris (figure 28) influence the spring's force takeover (figure 27). High healthy muscle activation leads to a high force takeover by the spring.

Muscle weakening by reduction of m. rectus femoris' control level represents a possible method to simulate muscle activation deficit.

3.4. Simulation

Generally, all simulations are performed with the OpenSim software version 3.3. Version 4.1 is only used because the required OutputReporter function, included in the Analyze tool, is not accessible with version 3.3.

Prior to simulation, degree of muscle weakening and spring stiffness values are selected according to the results of the preliminary simulations. Further, the muscles to be analysed, are chosen.

Selection of degree of muscle weakening

Following the results of the preliminary studies, the rectus femoris control level for further simulations are chosen to be 25% and 10% of maximum level.

Selection of stiffness value

Per degree of weakening, three different stiffness values are selected. Preliminary studies show that m. rectus femoris weakened to 10% maximum controls can produce a force curve similar to healthy m. rectus femoris supported by a passive spring with stiffness of 2.000N/m. To support the weakened muscle appropriately without risking insufficient muscle challenge, the additional stiffness values are set to a lower level. The stiffness value of 2.000N/m is reduced in steps of 500N/m. Weakening of m. rectus femoris to 25% of

maximum controls leads to a force curve similar to the force curve generated by healthy m. rectus femoris supported by a passive spring with stiffness of 1.500N/m. Further stiffness values are again selected by reduction of 1.500N/m in steps of 500N/m.

Selection of muscles

M. rectus femoris is a biarticular muscle of the thigh which extends from knee to hip. Therefore, implementation of the spring parallel to this muscle influences both hip and knee movement. To measure the effect of spring implementation, two muscles of the right leg beside m. rectus femoris are chosen for detailed examination: m. biceps femoris caput longum and m. vastus intermedius. M. biceps femoris caput longum is one of the counter muscles of m. rectus femoris and is responsible for hip extension and knee flexion. It is located on the rear of the thigh. M. vastus intermedius acts similar to m. rectus femoris as knee extensor. As m. rectus femoris, it is located at the front side of the thigh.

Figures 30 and 31 show the locations of the selected muscles in the musculoskeletal model 'Gait2354'. In figure 31 the path spring, implemented parallel to m. rectus femoris, is also represented.

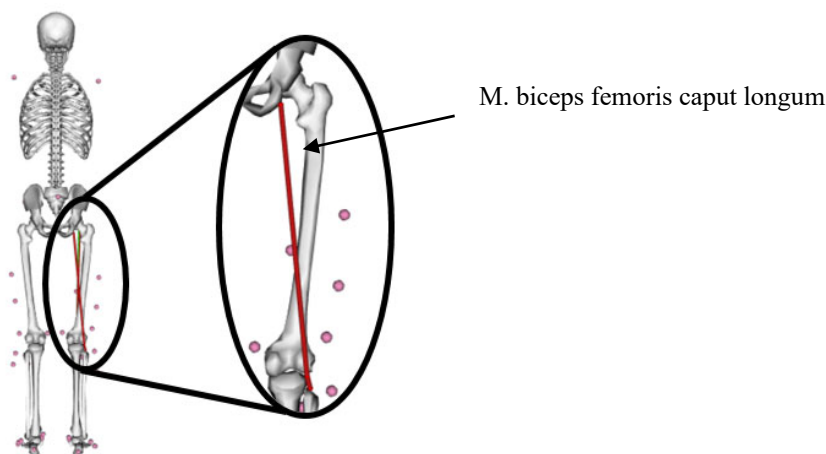


Figure 30: *M. biceps femoris caput longum*.

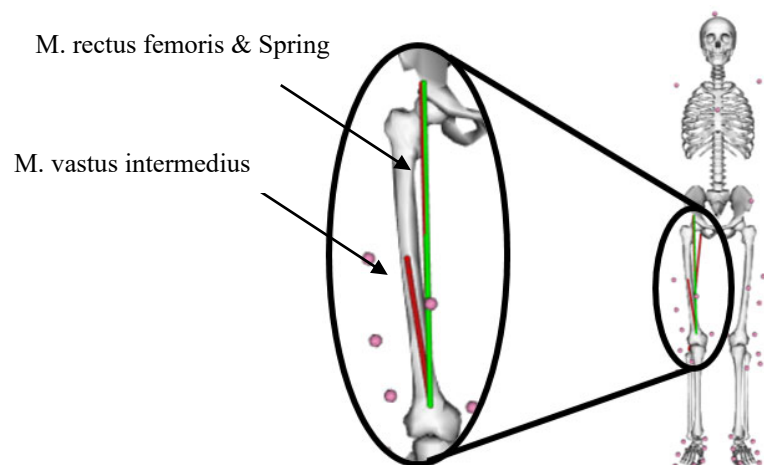


Figure 31: *M. vastus intermedius, M. rectus femoris & passive path spring*.

Selection of muscle parameters

For all selected muscles, the following parameters are documented:

- Actuation Force
- Actuation Power
- Normalized Fiber Length
- Normalized Fiber Velocity
- Induced Acceleration of the Femur

Simulation process

Using model and motion data from the ‘Gait2354’ package, five different OpenSim tools are used to simulate and analyse gait. The simulation process is illustrated in figure 32 on the next page. The picture shows all the simulation steps and the applied input and output files. OpenSim files are shown in red, experimental data in green, settings files in blue and files computed in the workflow are marked in purple. The desired outcomes are written in black.

The first simulation is based on healthy model conditions and aims at the achievement of reference data. No additional force elements are included. To compare healthy and weak muscle effects, the second simulation illustrates the effect of muscle weakening. Just before the performance of the CMC algorithm, the constraints file is modified and m. rectus femoris is weakened. In the third simulation the path spring is implemented. All simulations use experimental data of healthy persons to maintain normal gait. Table 5 represents an overview of all performed simulations. The colours of the cells refer to the colour of the corresponding curves in the results section. The reference curves are always coloured in blue while the curves showing muscle behaviour with weakened m. rectus femoris are yellow and red. Green curves represent muscle behaviour with weakened m. rectus femoris to 10% maximum controls, including spring implementation. Purple curves illustrate simulation 3 just like the green curves, but m. rectus femoris is weakened to 25% maximum controls.

Table 5: Overview of all performed simulations.

	Degree of weakening	Stiffness value of the spring
Simulation 1	-	-
Simulation 2	10%	-
	25%	-
Simulation 3		1.000N/m
	10%	1.500N/m
		2.000N/m
		500N/m
	25%	1.000N/m
		1.500N/m

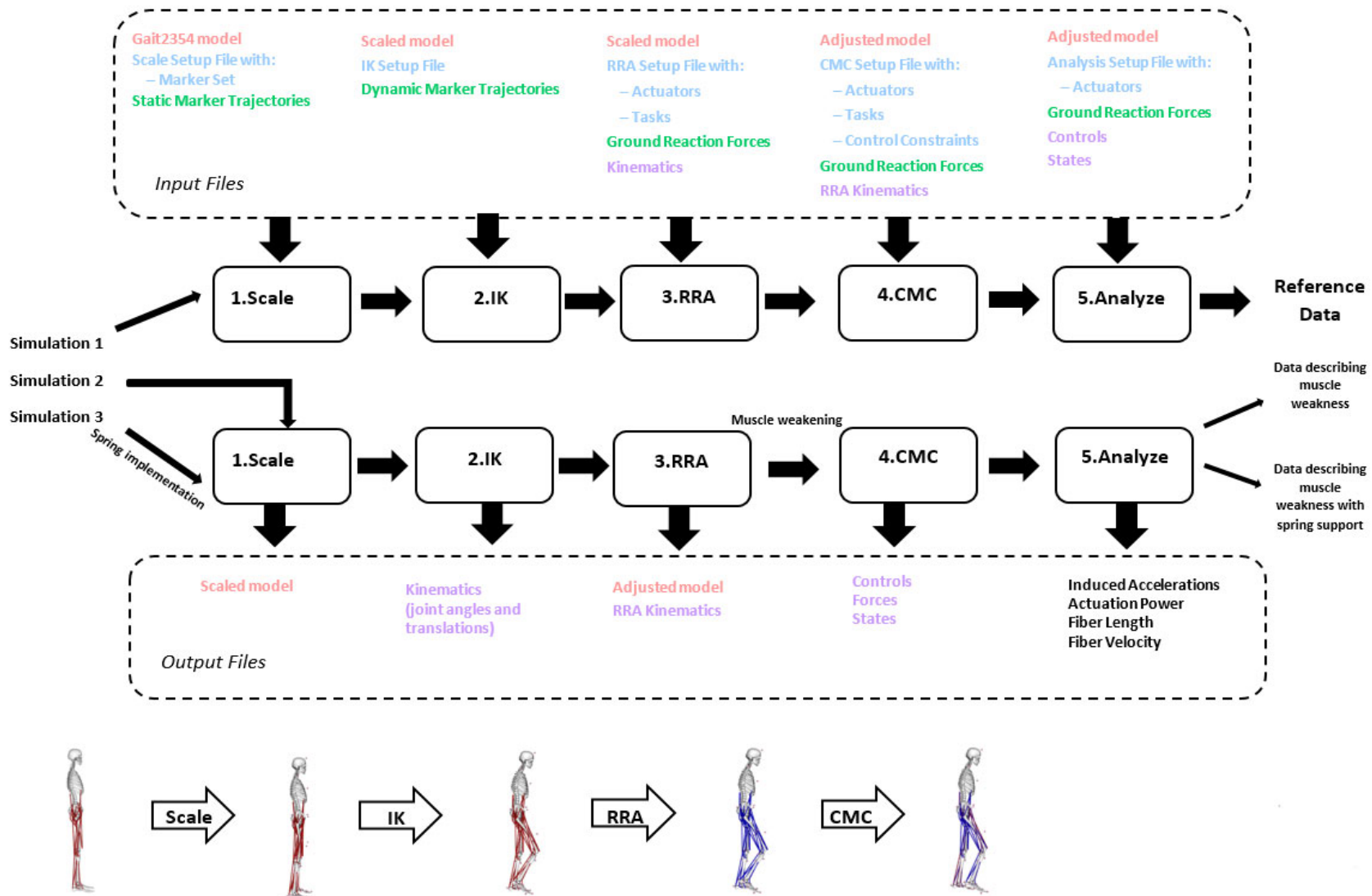


Figure 32: Simulation process.

4. Results

This chapter illustrates the results of the OpenSim simulations. Since the part of the gait cycle to be analysed starts at 51% (start of initial swing) and ends with 92% (end of mid-swing), the diagrams only picture an expansion of this specific gait cycle period. The included per cent before the start and after the end help to give an idea of prior and further curve progression. The first four sections deal with actuation force, actuation power, normalized fiber length and normalized fiber velocity of the selected muscles of the right femur. There are two diagrams for every muscle. One documents the behaviour of the selected muscle, when m. rectus femoris is weakened to 10% of maximum controls, while the other one describes the muscle performance when m. rectus femoris is weakened to 25% of maximum controls. Every diagram contains five curves. The blue curve is the reference curve. It shows the behaviour of the chosen muscle during healthy conditions. The yellow and the red curve illustrate muscle characteristics when m. rectus femoris is weakened. The three curves marked in green or purple colour steps, represent muscle behaviour during path spring support of weakened m. rectus femoris. The different green and purple colours illustrate the different stiffness values of the spring. The last section deals with induced femur accelerations. For all selected muscles, contributions to fore-aft and vertical acceleration of the right femur are measured. Additionally to the curves described above, the diagrams include a grey dotted curve describing the total fore-aft or total vertical acceleration during healthy conditions. Finally, the fore-aft and vertical muscle contributions to femur acceleration are integrated in one diagram for each muscle. A resultant vector describes the contributions to femur acceleration.

For each muscle, the result report starts with a description of the effects of muscle weakening, by comparison of the reference curve and the curve describing the weakened m. rectus femoris condition. This knowledge is important, since it shows the discrepancy between the healthy and the weakened case. Then, the effects of the spring on the weakened m. rectus femoris condition are considered. Further, it is described if the discrepancy between the healthy and weakened m. rectus femoris case increases or decreases with spring implementation.

In the following sections the unit specifications as for example statements about the per cent of gait cycle or about the force production in Newton are just estimated from the diagrams and do not refer to exact values.

4.1. Actuation Force

The following section shows actuation forces of the three selected muscles m. rectus femoris, m. vastus intermedius and m. biceps femoris long head, for different m. rectus femoris conditions during walking in pre-swing, initial swing and mid-swing.

4.1.1. M. rectus femoris

a) Effects of weakening - Healthy m. rectus fem. (blue) vs. weakened m. rectus fem. (yellow & red)

As already considered in the preliminary simulations, an activation deficit of m. rectus femoris leads to a decrease in muscle force. The higher the activation deficit, the higher the decrease. The force difference between healthy and weakened m. rectus femoris increases from 57% of the gait cycle and reaches maximum

difference at 61%. The difference reduces until 70% of the gait cycle and then increases again until a second peak is reached at 85%. The curves assimilate again at 95%.

b) Effects of the spring – Weakened m. rectus fem. (yellow & red) vs. weakened m. rectus fem. with spring (green & purple) & assimilation to reference curve (blue)

The spring implementation has no effect on the force curve, when m. rectus femoris is constrained to 10% maximum controls. When m. rectus femoris is constrained to 25% maximum controls, the spring implementation has little effect between 70% and 85% of the gait cycle. The force produced of weakened m. rectus femoris with spring support is lower than the force generated by weakened m. rectus femoris without support.

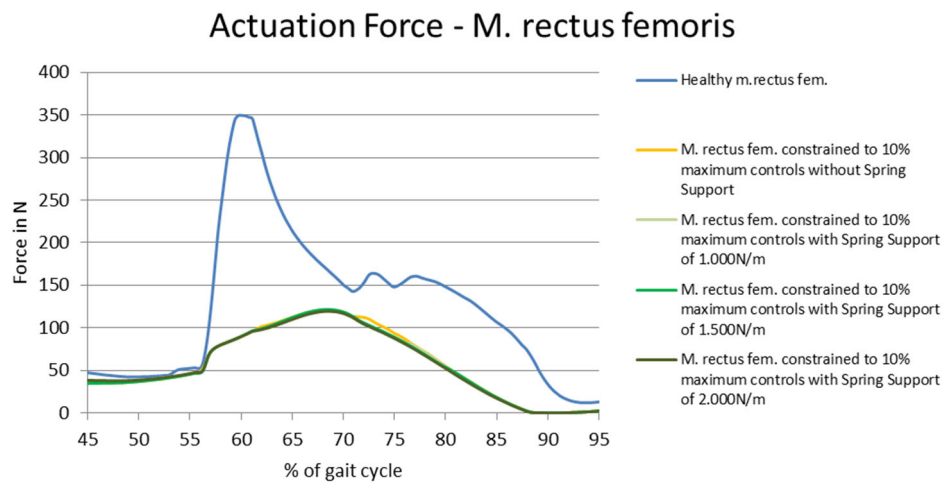


Figure 33: Actuation force of m. rectus femoris 1. The curves of healthy m. rectus femoris, weakened m. rectus femoris (10% maximum controls) and weakened m. rectus femoris with spring support are compared.

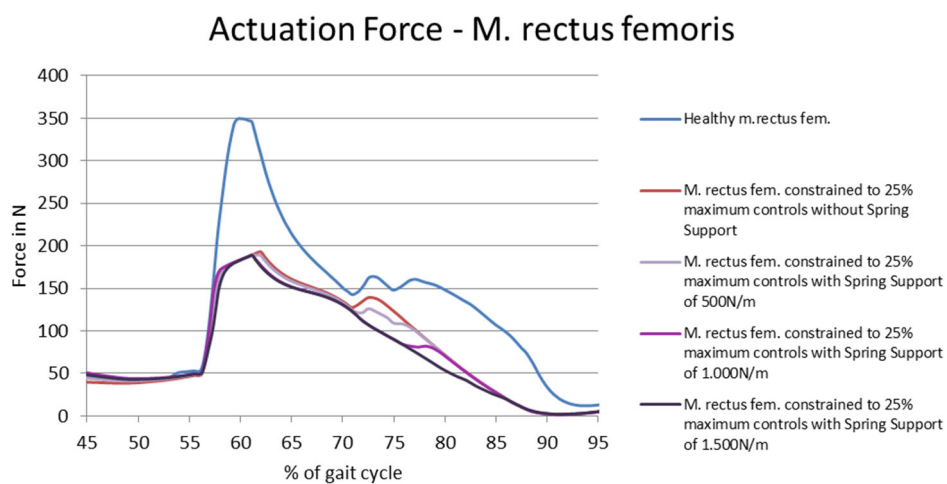


Figure 34: Actuation force of m. rectus femoris 2. The curves of healthy m. rectus femoris, weakened m. rectus femoris (25% maximum controls) and weakened m. rectus femoris with spring support are compared.

4.1.2. M. vastus intermedius

a) Effects of weakening - Healthy m. rectus fem. (blue) vs. weakened m. rectus fem. (yellow & red)

M. rectus femoris weakness leads to an increase of the m. vastus intermedius force curve during 57% and 91% of the gait cycle, whereby the maximum m. vastus intermedius force curve difference is reached at 61% of the gait cycle. At 70% the curves assimilate again before they show another peak difference at 85% of the gait cycle. The curves assimilate again at 95%.

b) Effects of the spring – Weakened m. rectus fem. (yellow & red) vs. weakened m. rectus fem. with spring (green & purple) & assimilation to reference curve (blue)

Spring implementation leads to a decrease in force production of m. vastus intermedius.

The higher the stiffness value, the more the force curve assimilates to the reference force curve of m. vastus intermedius. Most of the curves representing the spring support condition of weakened m. rectus femoris only show differences to the healthy m. rectus femoris condition from 57% to 70% of the gait cycle.

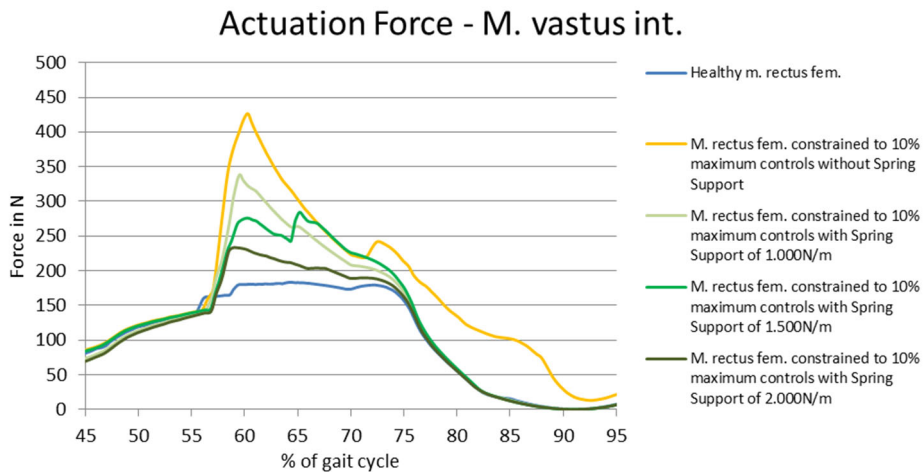


Figure 35: Actuation force of m. vastus intermedius 1. The curves of m. vastus intermedius in healthy conditions, m. vastus intermedius with weakened m. rectus femoris (10% maximum controls) and m. vastus intermedius with weakened m. rectus femoris and spring support are compared.

Actuation Force - M. vastus int.

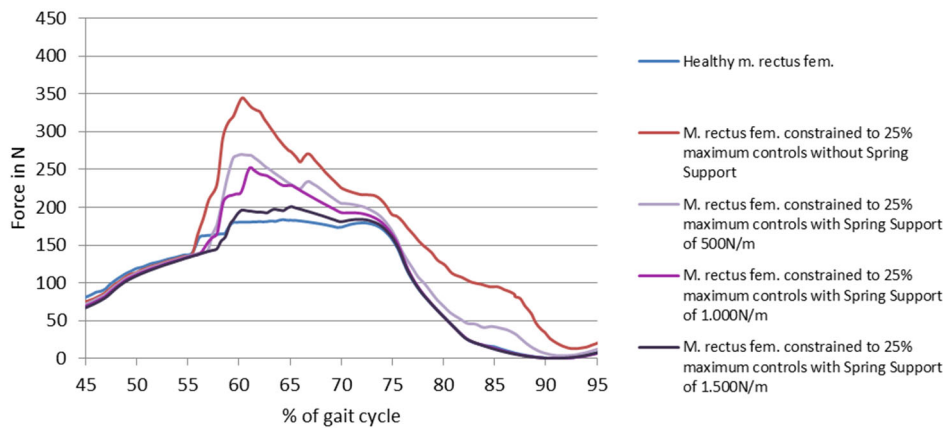


Figure 36: Actuation force of *m. vastus intermedius* 2. The curves of *m. vastus intermedius* in healthy conditions, *m. vastus intermedius* with weakened *m. rectus femoris* (25% maximum controls) and *m. vastus intermedius* with weakened *m. rectus femoris* and spring support are compared.

4.1.3. M. biceps femoris caput longum

a) Effects of weakening - Healthy *m. rectus fem.* (blue) vs. weakened *m. rectus fem.* (yellow & red)

The *m. biceps femoris caput longum* force curve does not show much reaction to *m. rectus femoris* weakness. Only between 45% and 57% of the gait cycle, the weakness of *m. rectus femoris* leads to a small decrease in force curve of *m. biceps femoris caput longum*. When *m. rectus femoris* is constrained to 25% maximum controls the force of *m. biceps femoris caput longum* increases a little bit between 65% and 75% of the gait cycle.

b) Effects of the spring – Weakened *m. rectus fem.* (yellow & red) vs. weakened *m. rectus fem.* with spring (green & purple) & assimilation to reference curve (blue)

Spring support of weakened *m. rectus femoris* increases the force curve of *m. biceps femoris caput longum* for the entire period of the considered gait cycle. The force increase reaches three peaks, namely at 50%, at 70% and at 95% of the considered gait cycle period. The higher the stiffness value of the spring, the higher the force increase.

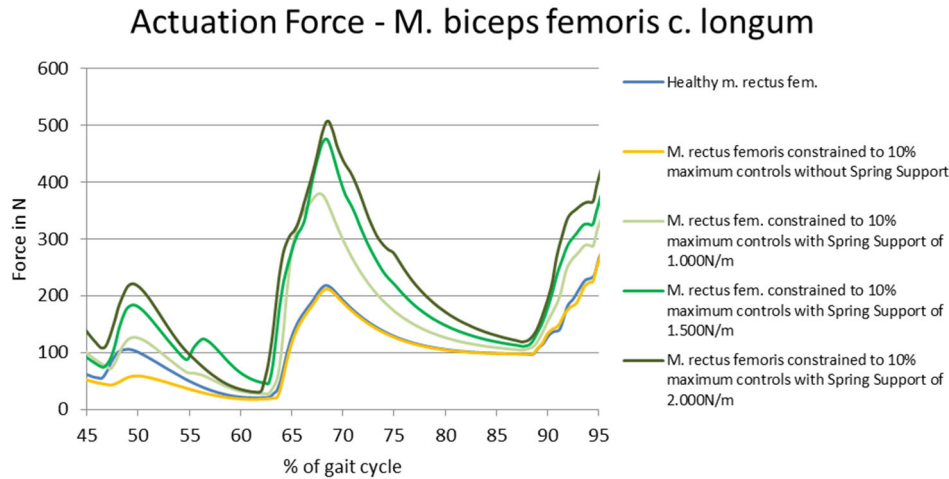


Figure 37: Actuation force of *m. biceps femoris c. longum* 1. The curves of *m. biceps femoris c. longum* in healthy conditions, *m. biceps femoris c. longum* with weakened *m. rectus femoris* (10% maximum controls) and *m. biceps femoris c. longum* with weakened *m. rectus femoris* and spring support are compared.

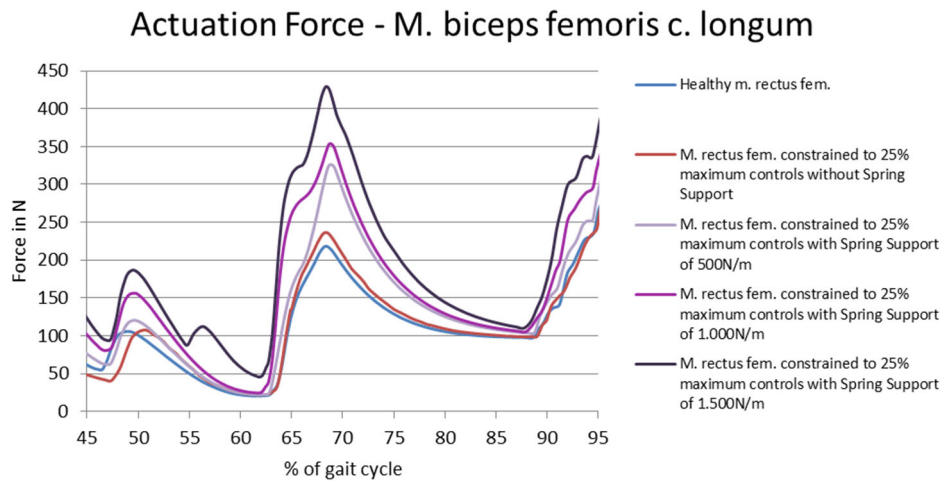


Figure 38: Actuation force of *m. biceps femoris caput longum* 2. The curves of *m. biceps femoris c. longum* in healthy conditions, *m. biceps femoris c. longum* with weakened *m. rectus femoris* (25% maximum controls) and *m. biceps femoris c. longum* with weakened *m. rectus femoris* and spring support are compared.

4.2. Actuation Power

The next section deals with actuation power of *m. rectus femoris*, *m. vastus intermedius* and *m. biceps femoris* long head, for different *m. rectus femoris* conditions during walking in pre-swing, initial swing and mid-swing.

4.2.1. *M. rectus femoris*

a) Effects of weakening - Healthy *m. rectus fem.* (blue) vs. weakened *m. rectus fem.* (yellow & red)

Healthy *m. rectus femoris* produces much more negative power from 57% to 70% of the gait cycle and much more positive power from 70% to 95% of the gait cycle. The peak power difference between healthy and weakened *m. rectus femoris* is reached at approximately 61% and 87% of the gait cycle. The higher the degree of weakening, the higher the power reduction.

b) Effects of the spring – Weakened *m. rectus fem.* (yellow & red) vs. weakened *m. rectus fem.* with spring (green & purple) & assimilation to reference curve (blue)

Spring support of weakened *m. rectus femoris* has no considerable effects on the power curves.

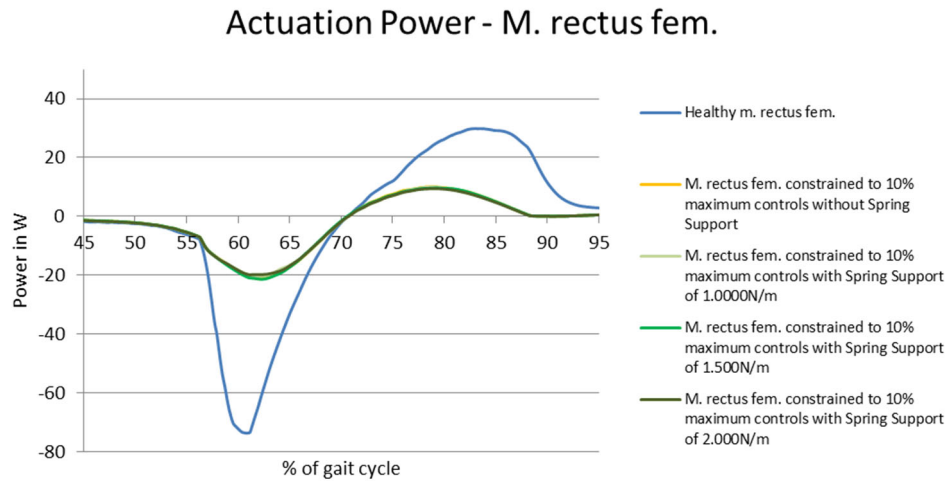


Figure 39: Actuation power of *m. rectus femoris* 1. The curves of healthy *m. rectus femoris*, weakened *m. rectus femoris* (10% maximum controls) and weakened *m. rectus femoris* with spring support are compared.

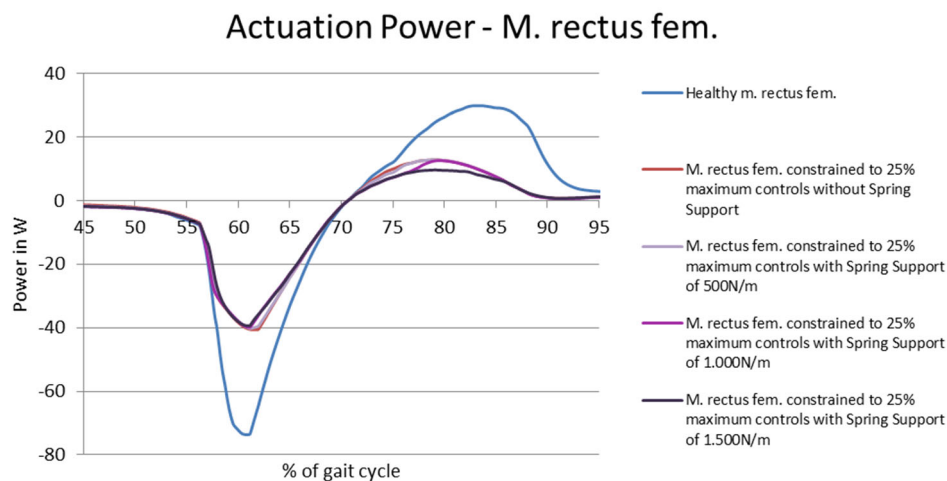


Figure 40: Actuation power of *m. rectus femoris* 2. The curves of healthy *m. rectus femoris*, weakened *m. rectus femoris* (25% maximum controls) and weakened *m. rectus femoris* with spring support are compared.

4.2.2. *M. vastus intermedius*

a) Effects of weakening - Healthy *m. rectus fem.* (blue) vs. weakened *m. rectus fem.* (yellow & red)

M. rectus femoris weakening leads to an increase of *m. vastus intermedius* negative power production from 57% to 70% of the gait cycle, whereby the peak difference between the power curves is reached at about 61%. From 70% to 95% the *m. vastus intermedius* positive power in case of weakened *m. rectus femoris* exceeds the positive power production in case of healthy *m. rectus femoris*. A peak difference is reached at 87% of the gait cycle before the curves assimilate again at 95%.

b) Effects of the spring – Weakened *m. rectus fem.* (yellow & red) vs. weakened *m. rectus fem.* with spring (green & purple) & assimilation to reference curve (blue)

Spring support increases the *m. vastus intermedius* power curve from 55% to 75% of the gait cycle and decreases it from 75% to 95% of the gait cycle.

Spring implementation helps the *m. vastus intermedius* power curve to assimilate to the power curve of healthy *m. rectus femoris*. The higher the stiffness value, the better the assimilation.

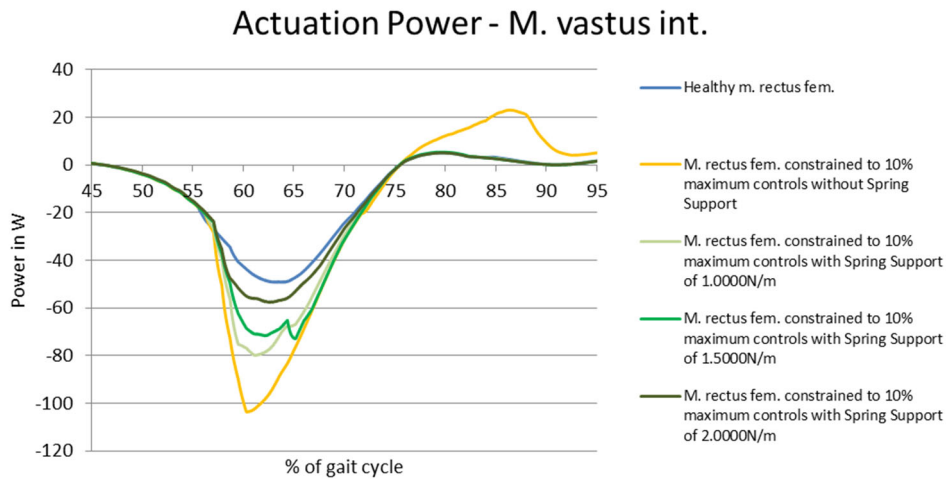


Figure 41: Actuation power of *m. vastus intermedius* 1. The curves of *m. vastus intermedius* in healthy conditions, *m. vastus intermedius* with weakened *m. rectus femoris* (10% maximum controls) and *m. vastus intermedius* with weakened *m. rectus femoris* and spring support are compared.

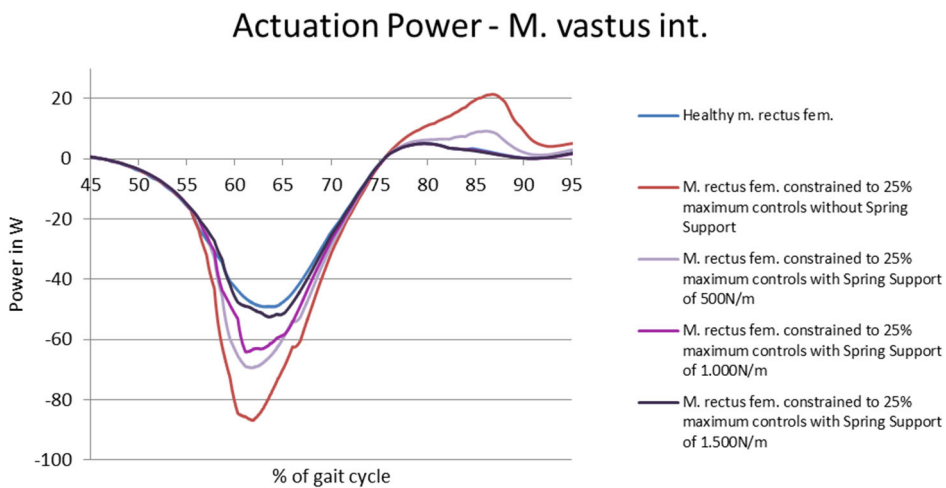


Figure 42: Actuation power of *m. vastus intermedius* 2. The curves of *m. vastus intermedius* in healthy conditions, *m. vastus intermedius* with weakened *m. rectus femoris* (25% maximum controls) and *m. vastus intermedius* with weakened *m. rectus femoris* and spring support are compared.

4.2.3. M. biceps femoris caput longum

a) Effects of weakening - Healthy m. rectus fem. (blue) vs. weakened m. rectus fem. (yellow & red)

The power curves of m. biceps femoris caput longum in case of healthy and weakened m. rectus femoris do not show much difference. At the beginning and at the end of the considered gait cycle period small differences are visible.

b) Effects of the spring – Weakened m. rectus fem. (yellow & red) vs. weakened m. rectus fem. with spring (green & purple) & assimilation to reference curve (blue)

The m. rectus femoris spring support leads to an increase of positive power from 45% to about 66% of the gait cycle and to an increase in negative power from 66% to 95% of the gait cycle. The higher the stiffness value, the higher the power production of m. biceps femoris caput longum. High difference between the power curves in case of healthy m. rectus femoris and weakened m. rectus is reached at 70% of the gait cycle.

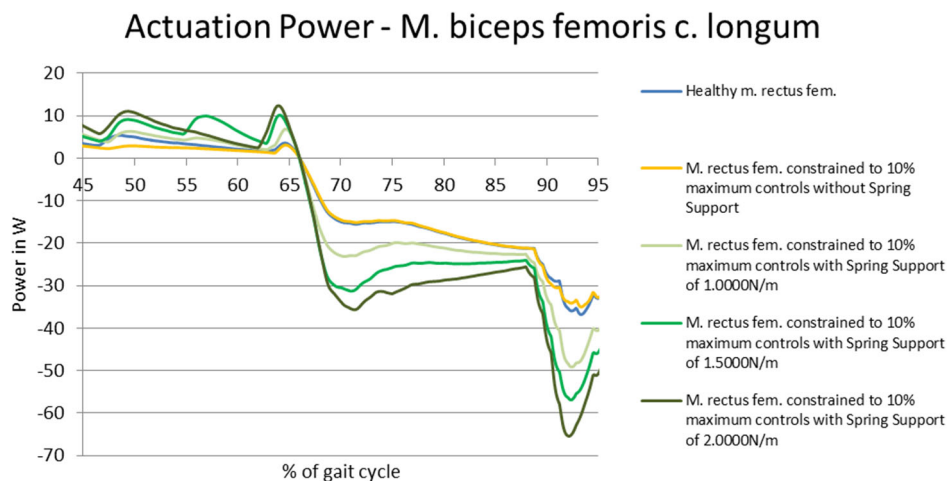


Figure 43: Actuation power of m. biceps femoris caput longum 1. The curves of m. biceps femoris c. longum in healthy conditions, m. biceps femoris c. longum with weakened m. rectus femoris (10% maximum controls) and m. biceps femoris c. longum with weakened m. rectus femoris and spring support are compared.

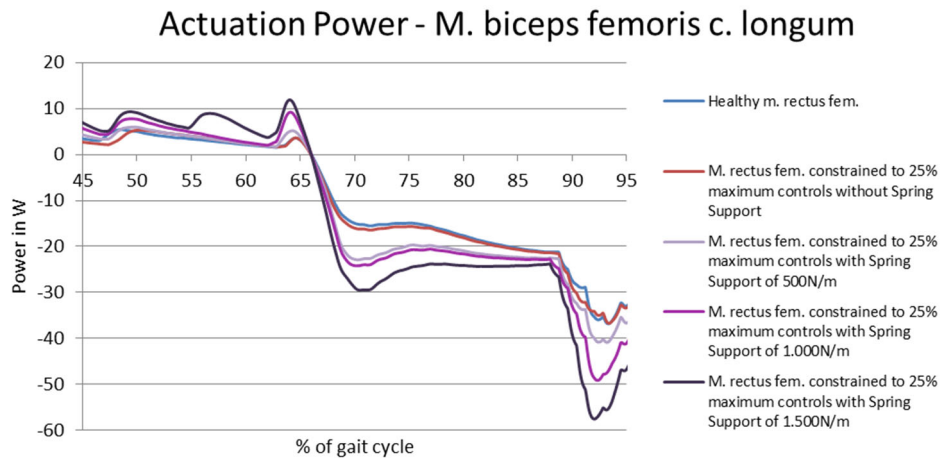


Figure 44: Actuation power of *m. biceps femoris caput longum 2*. The curves of *m. biceps femoris c. longum* in healthy conditions, *m. biceps femoris c. longum* with weakened *m. rectus femoris* (25% maximum controls) and *m. biceps femoris c. longum* with weakened *m. rectus femoris* and spring support are compared.

4.3. Normalized fiber length

The following figures represent the normalized fiber length of the three selected muscles rectus femoris, vastus intermedius and biceps femoris long head, for different *m. rectus femoris* conditions. Normalization is reached by scaling with optimal fiber length.

No considerable differences are noticed between the documented curves for all three reported muscles. Therefore, only one diagram, describing *m. rectus femoris* weakening to 10% maximum controls, is represented for each muscle.

4.3.1. *M. rectus femoris*

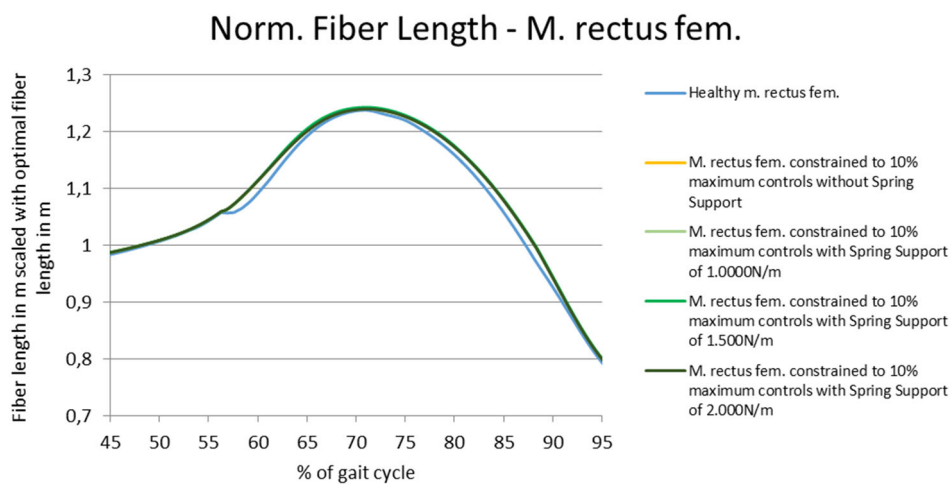


Figure 45: Normalized fiber length of *m. rectus femoris*. The curves of healthy *m. rectus femoris*, weakened *m. rectus femoris* (10% maximum controls) and weakened *m. rectus femoris* with spring support are compared.

4.3.2. M. vastus intermedius

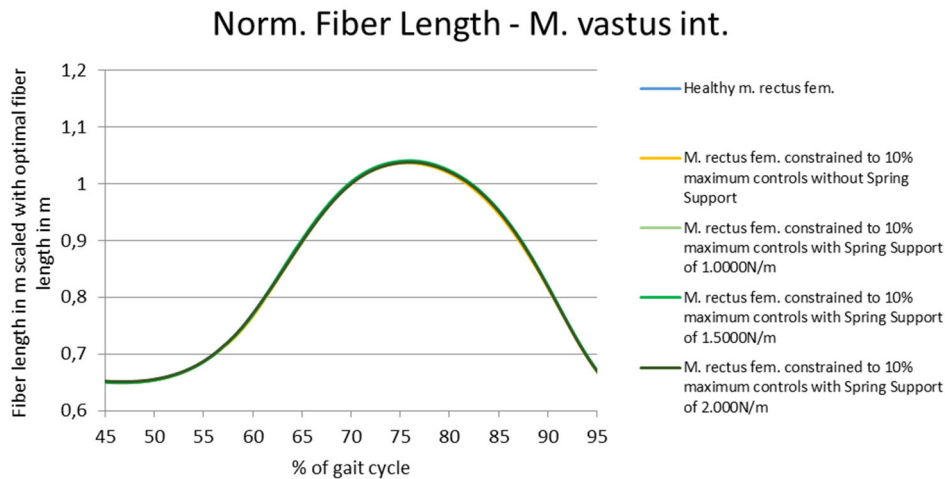


Figure 46: Normalized fiber length of *m. vastus intermedius*. The curves of *m. vastus intermedius* in healthy conditions, *m. vastus intermedius* with weakened *m. rectus femoris* (10% maximum controls) and *m. vastus intermedius* with weakened *m. rectus femoris* and spring support are compared.

4.3.3. M. biceps femoris caput longum

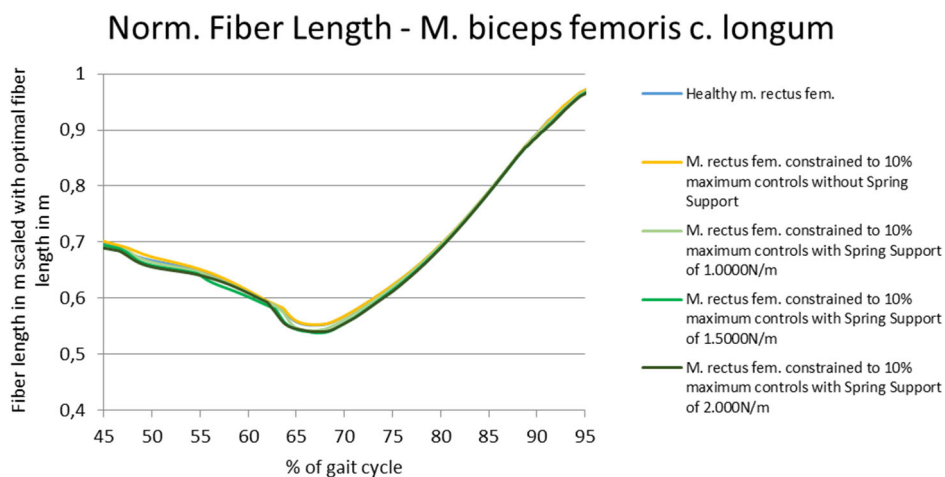


Figure 47: Normalized fiber length of *m. biceps femoris caput longum*. The curves of *m. biceps femoris c. longum* in healthy conditions, *m. biceps femoris c. longum* with weakened *m. rectus femoris* (10% maximum controls) and *m. biceps femoris c. longum* with weakened *m. rectus femoris* and spring support are compared.

4.4. Normalized Fiber Velocity

The next section illustrates the normalized fiber velocity of the selected muscles for different *m. rectus femoris* conditions. Normalization is reached by scaling with maximum fiber velocity.

As with normalized fiber length, no considerable differences are noticed between the documented curves for all three reported muscles. Therefore, only one diagram, describing *m. rectus femoris* weakening to 10% maximum controls, is represented for each muscle.

4.4.1. M. rectus femoris

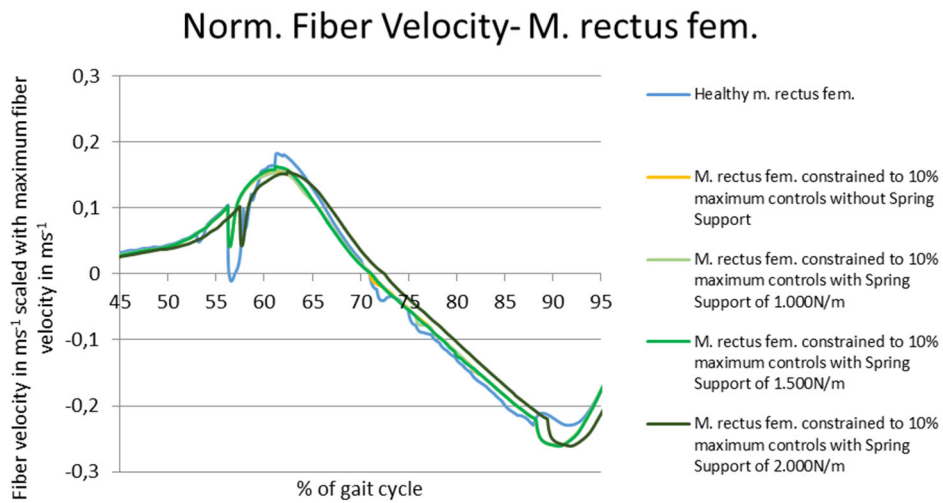


Figure 48: Normalized fiber velocity of *m. rectus femoris*. The curves of healthy *m. rectus femoris*, weakened *m. rectus femoris* (10% maximum controls) and weakened *m. rectus femoris* with spring support are compared.

4.4.2. M. vastus intermedius

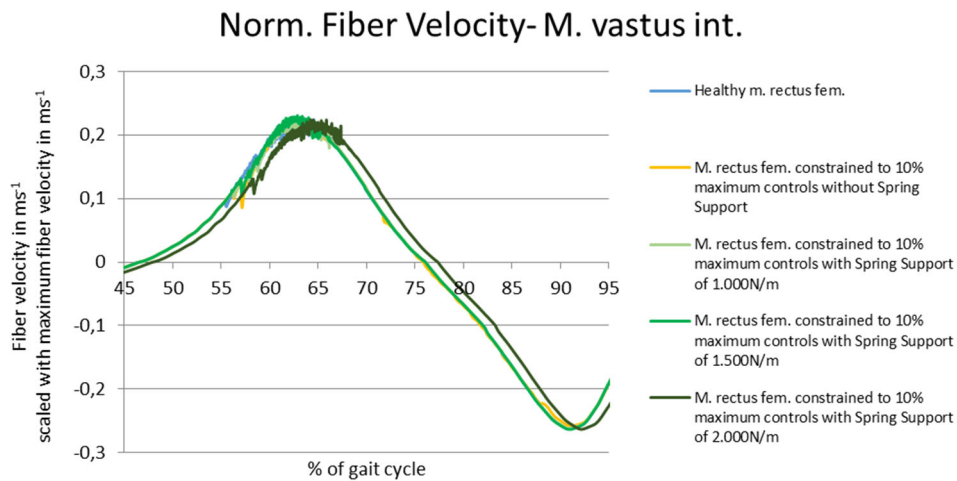


Figure 49: Normalized fiber velocity of *m. vastus intermedius*. The curves of *m. vastus intermedius* in healthy conditions, *m. vastus intermedius* with weakened *m. rectus femoris* (10% maximum controls) and *m. vastus intermedius* with weakened *m. rectus femoris* and spring support are compared.

4.4.3. M. biceps femoris caput longum

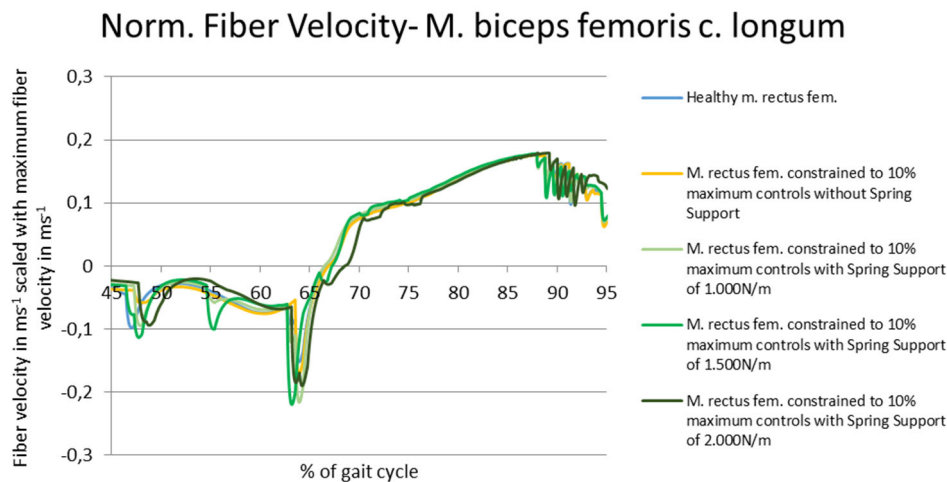


Figure 50: Normalized fiber velocity of *m. biceps femoris caput longum*. The curves of *m. biceps femoris c. longum* in healthy conditions, *m. biceps femoris c. longum* with weakened *m. rectus femoris* (10% maximum controls) and *m. biceps femoris c. longum* with weakened *m. rectus femoris* and spring support are compared.

4.5. Induced Accelerations of the Femur

The following section illustrates the contributions to fore-aft and vertical femur acceleration of the selected muscles. The lateral femur acceleration is not taken into account since femur movement in this direction is negligible.

All results refer to the global coordinate system shown in figure 51.

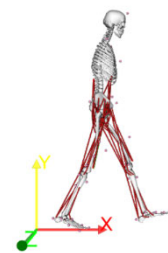


Figure 51: IAA – coordinate system.

4.5.1. M. rectus femoris

a) Effects of weakening - Healthy m. rectus fem. (blue) vs. weakened m. rectus fem. (yellow & red)

Weakened *m. rectus femoris* shows reduced contribution to acceleration in comparison to healthy muscle. Only at the beginning of the considered gait cycle period (from 45% to approximately 57%) healthy and weakened *m. rectus femoris* acceleration contribution curves follow the same course. The higher the activation deficit, the lower the acceleration contribution. Highest differences between the weakened and the healthy acceleration contribution occur at approximately at 59% and 87% of the gait cycle. These points of highest difference occur in the curve concerning the fore-aft acceleration contribution, as well as in the curve considering the vertical acceleration contribution.

b) Effects of the spring – Weakened m. rectus fem. (yellow & red) vs. weakened m. rectus fem. with spring (green & purple) & assimilation to reference curve (blue)

Spring support of weakened *m. rectus femoris* leads to increased contributions to fore-aft and vertical femur acceleration. The higher the spring support, the higher the contribution of *m. rectus femoris*.

One cannot say that spring implementation definitely leads to an assimilation to reference curve. In each of the two weakness cases, the lowest stiffness value shows better assimilation to the reference curve than the higher stiffness values.

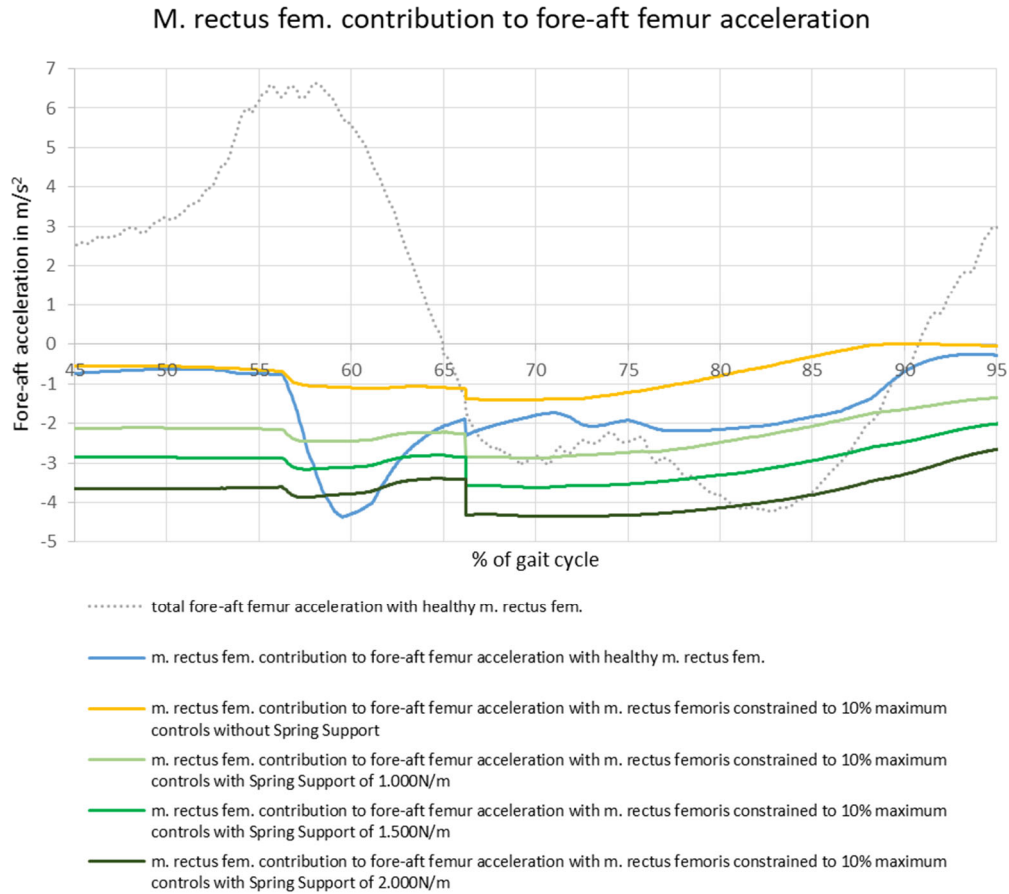


Figure 52: M. rectus femoris contribution to fore-aft femur acceleration 1. The curves of healthy m. rectus femoris, weakened m. rectus femoris (10% maximum controls) and weakened m. rectus femoris with spring support are compared.

M. rectus fem. contribution to fore-aft femur acceleration

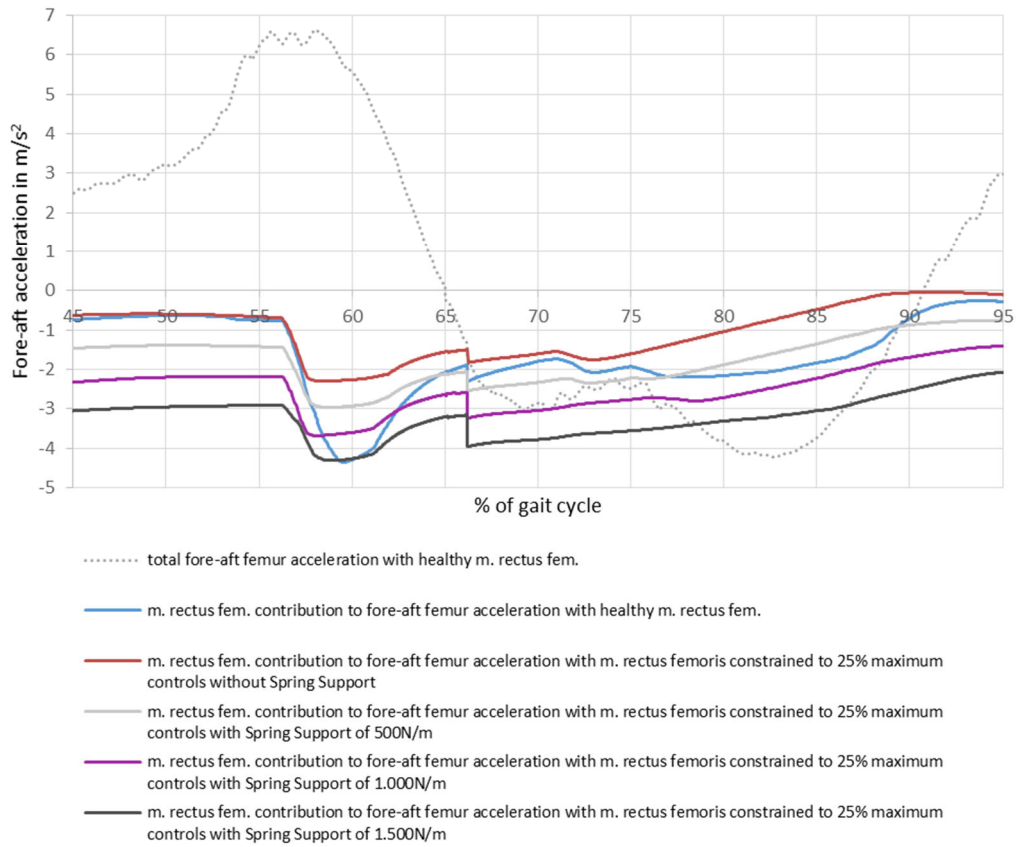


Figure 53: M. rectus femoris contribution to fore-aft femur acceleration 2. The curves of healthy m. rectus femoris, weakened m. rectus femoris (25% maximum controls) and weakened m. rectus femoris with spring support are compared.

M. rectus fem. contribution to vertical femur acceleration

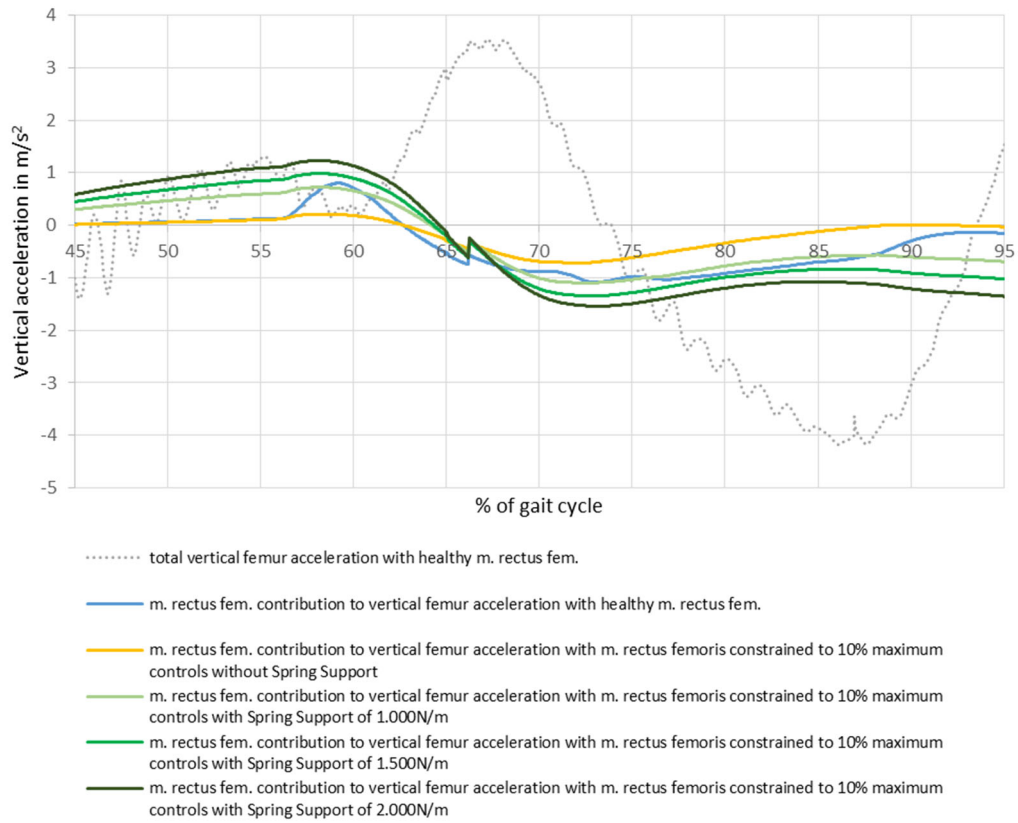


Figure 54: M. rectus femoris contribution to vertical femur acceleration 1. The curves of healthy m. rectus femoris, weakened m. rectus femoris (10% maximum controls) and weakened m. rectus femoris with spring support are compared.

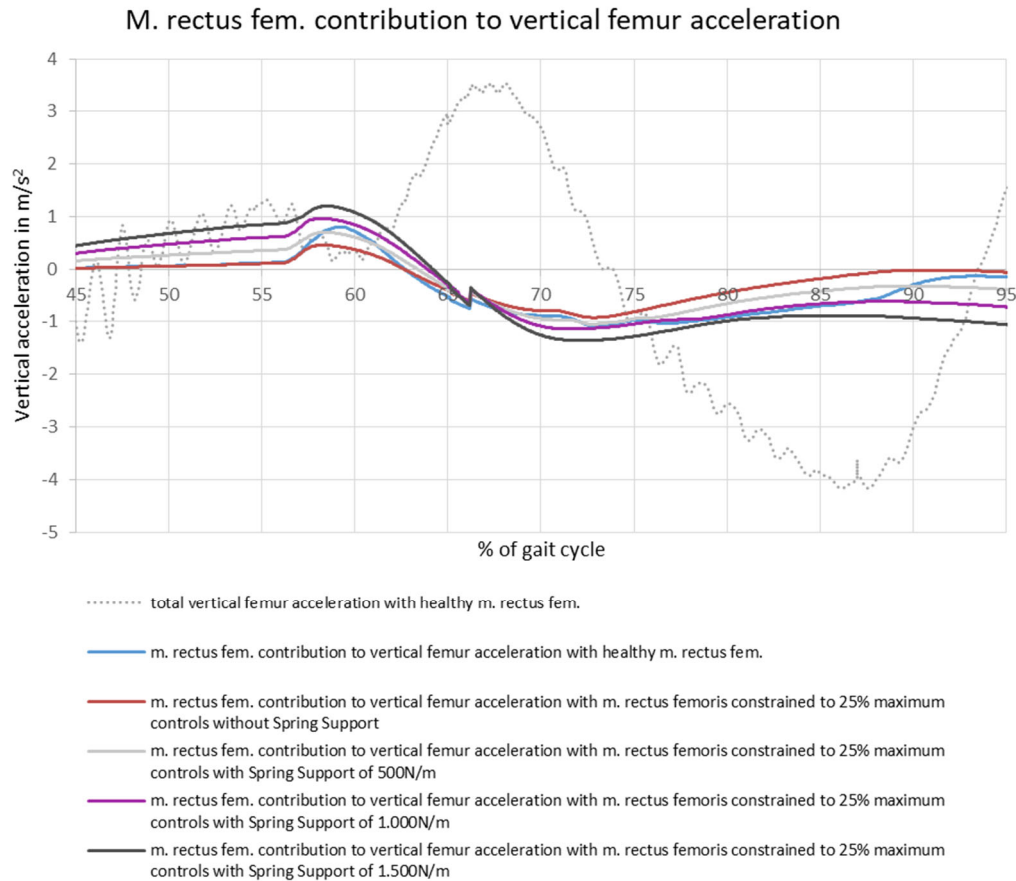


Figure 55: M. rectus femoris contribution to vertical femur acceleration 2. The curves of healthy m. rectus femoris, weakened m. rectus femoris (25% maximum controls) and weakened m. rectus femoris with spring support are compared.

4.5.2. M. vastus intermedius

a) Effects of weakening - Healthy m. rectus fem. (blue) vs. weakened m. rectus fem. (yellow & red)

At the beginning of the considered gait cycle period (from 45% to approximately 57%) both curves follow the same course. Then, weakness of m. rectus femoris increases the m. vastus intermedius contribution to femur acceleration nearly for the entire period from 57% to 95% of the gait cycle. Generally, it can be stated that a higher activation deficit leads to a higher difference between the reference curve and the curve describing the weakened m. rectus femoris case. The highest difference between these curves occurs at about 61% of the gait cycle. There is another peak visible at 87% for the curves describing fore-aft acceleration contribution.

b) Effects of the spring – Weakened m. rectus fem. (yellow & red) vs. weakened m. rectus fem. with spring (green & purple) & assimilation to reference curve (blue)

Fore-aft direction

Spring Support increases the contribution to fore-aft acceleration of m. vastus intermedius for the complete considered part of the gait cycle. The higher the stiffness value, the higher the difference to the reference curve.

Vertical direction

In vertical direction, it depends on the gait cycle time if the spring support curves increase or decrease the acceleration contribution of *m. vastus intermedius*. From 75% until the end of the gait cycle, the spring support curves contribute to negative vertical acceleration, while the reference curve contributes to positive acceleration.

One cannot say that spring implementation definitely leads to an assimilation to reference curve. Except the gait cycle period from 57% to 67%, the lowest stiffness value shows better assimilation to the reference curve than the higher stiffness values.

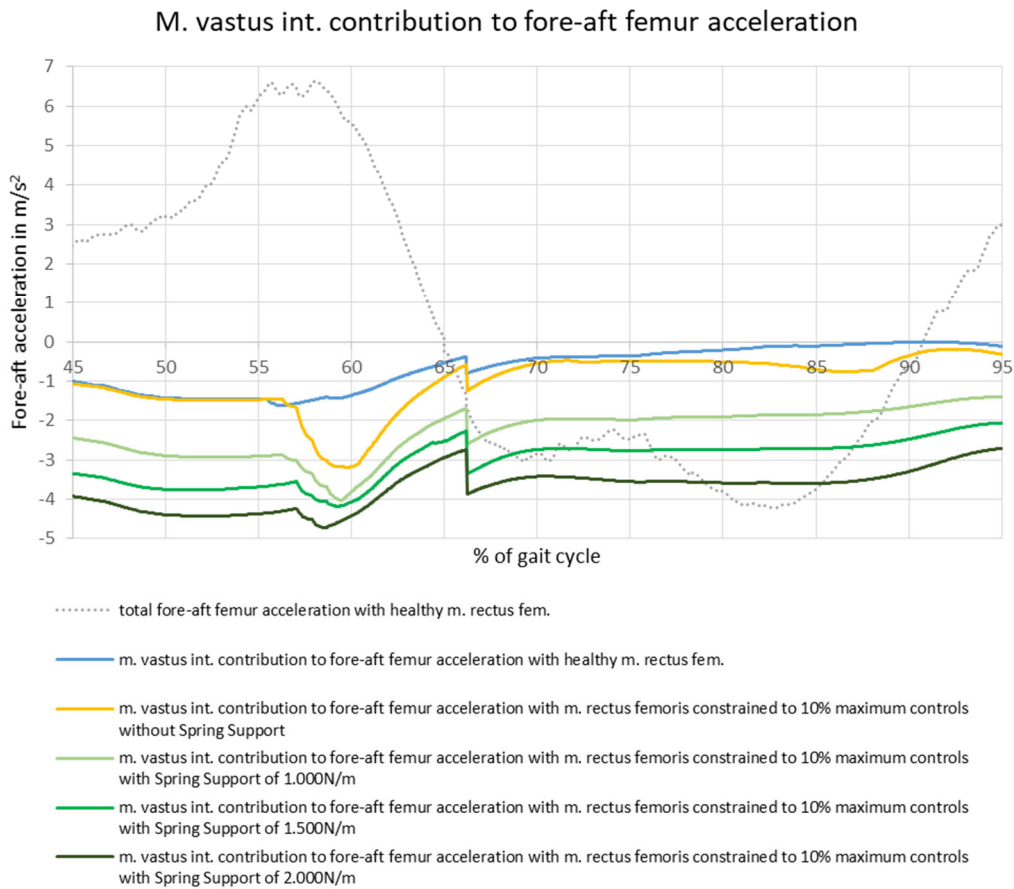


Figure 56: *M. vastus intermedius* contribution to fore-aft femur acceleration 1. The curves of *m. vastus intermedius* in healthy conditions, *m. vastus intermedius* with weakened *m. rectus femoris* (10% maximum controls) and *m. vastus intermedius* with weakened *m. rectus femoris* and spring support are compared.

M. vastus int. contribution to fore-aft femur acceleration

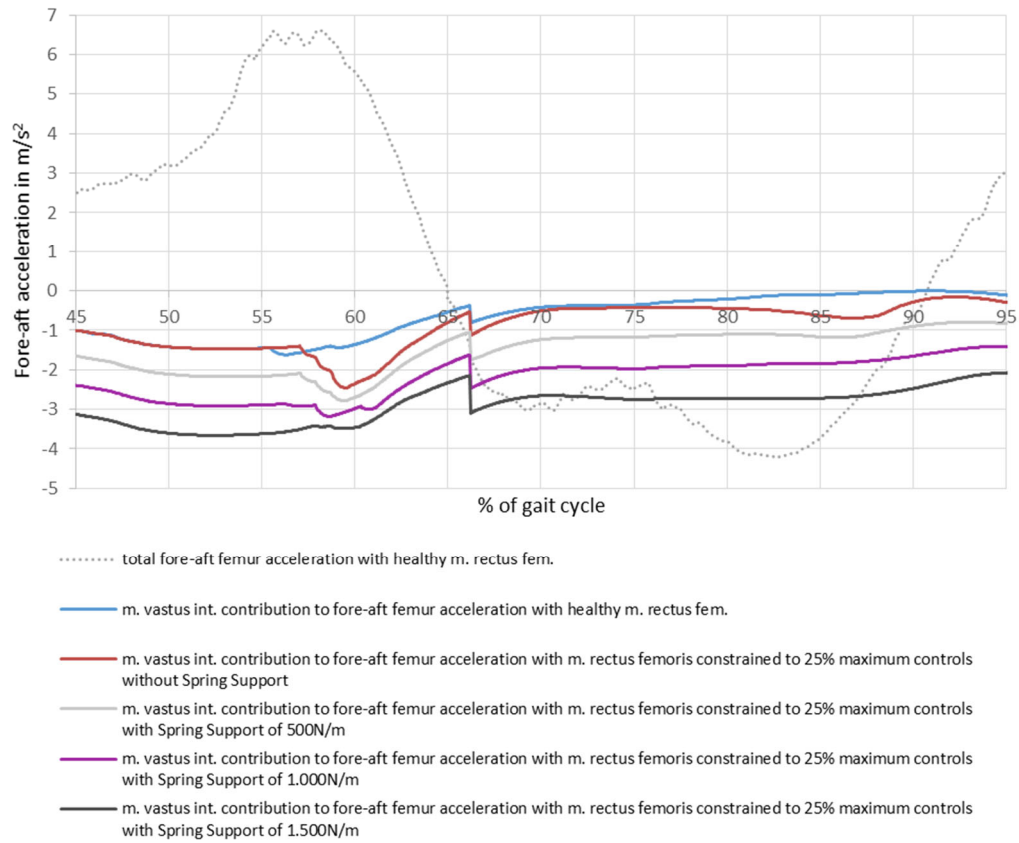


Figure 57: M. vastus intermedius contribution to fore-aft femur acceleration 2. The curves of m. vastus intermedius in healthy conditions, m. vastus intermedius with weakened m. rectus femoris (25% maximum controls) and m. vastus intermedius with weakened m. rectus femoris and spring support are compared.

M. vastus int. contribution to vertical femur acceleration

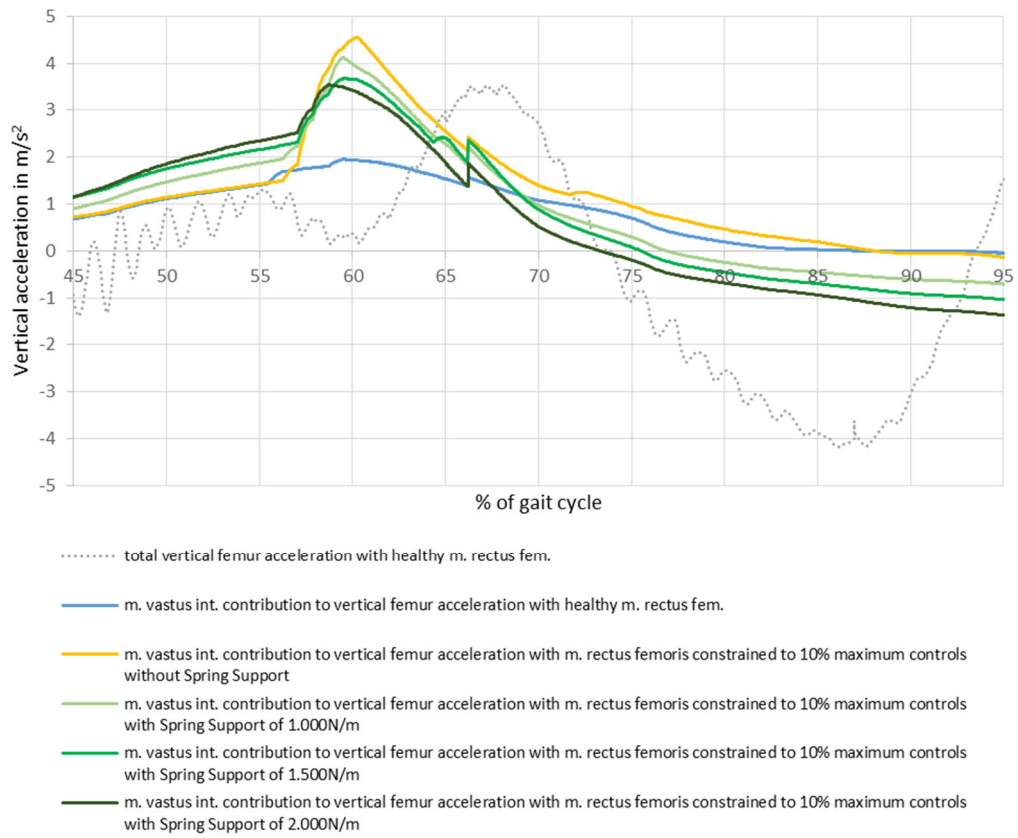


Figure 58: *M. vastus intermedius* contribution to vertical femur acceleration 1. The curves of *m. vastus intermedius* in healthy conditions, *m. vastus intermedius* with weakened *m. rectus femoris* (10% maximum controls) and *m. vastus intermedius* with weakened *m. rectus femoris* and spring support are compared.

M. vastus int. contribution to vertical femur acceleration

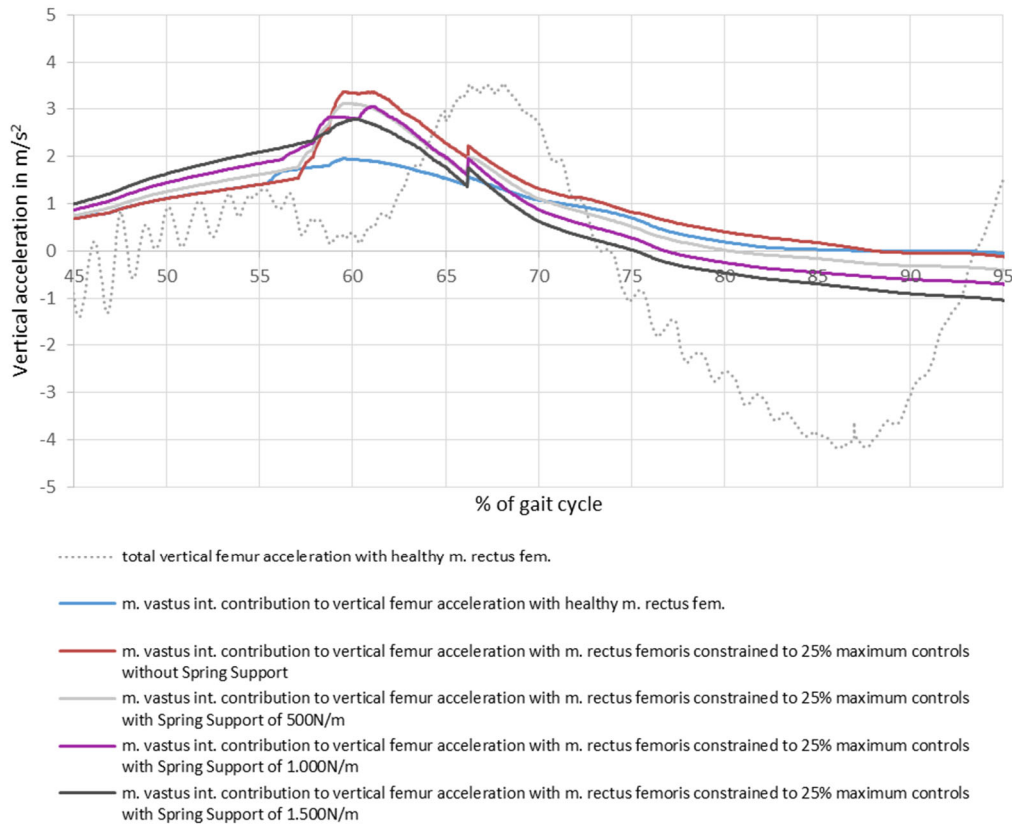


Figure 59: M. vastus intermedius contribution to vertical femur acceleration 2. The curves of m. vastus intermedius in healthy conditions, m. vastus intermedius with weakened m. rectus femoris (25% maximum controls) and m. vastus intermedius with weakened m. rectus femoris and spring support are compared.

4.5.3. M. biceps femoris caput longum

a) Effects of weakening - Healthy m. rectus fem. (blue) vs. weakened m. rectus fem. (yellow & red)

The acceleration contribution curves of m. biceps femoris caput longum in case of healthy and weakened m. rectus femoris do not show much difference. Only at the beginning of the considered gait cycle period (approximately at 47% of the gait cycle), differences are visible.

b) Effects of the spring – Weakened m. rectus fem. (yellow & red) vs. weakened m. rectus fem. with spring (green & purple) & assimilation to reference curve (blue)

Fore-aft direction

In fore-aft direction, the spring stiffness curves either exceed or fall below the reference curve for the entire considered gait cycle period. From 45% to 63% of the gait cycle they show negative contribution, while the reference curve shows positive contribution. For some stiffness values this incident is observed a second time during 80% and 87%.

Spring implementation leads to higher differences between the healthy and weakened m. rectus femoris case for the entire considered gait cycle period. Comparing the spring support curves, lower stiffness values lead to less difference to the reference curve.

Vertical direction

In vertical direction, the spring support curves exceed the curve describing the weakened m. rectus femoris case from 45% to 79% of the gait cycle. Then, they fall below the curve and start exceeding it again at 90%.

As in fore-aft direction, spring implementation leads to higher differences between the healthy and weakened m. rectus femoris case for the entire considered gait cycle period. Spring support curves with low stiffness values lead to less difference to reference curve.

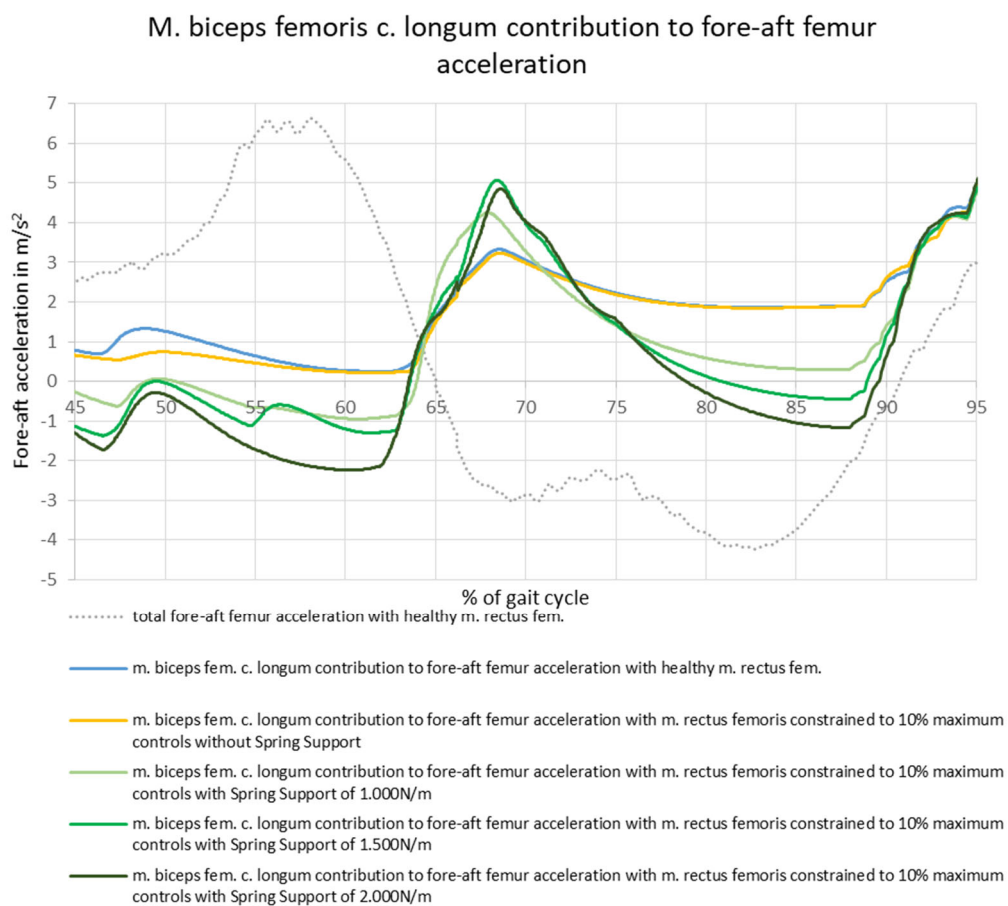


Figure 60: M. biceps femoris caput longum contribution to fore-aft femur acceleration 1. The curves of m. biceps femoris c. longum in healthy conditions, m. biceps femoris c. longum with weakened m. rectus femoris (10% maximum controls) and m. biceps femoris c. longum with weakened m. rectus femoris and spring support are compared.

M. biceps femoris c. longum contribution to fore-aft femur acceleration

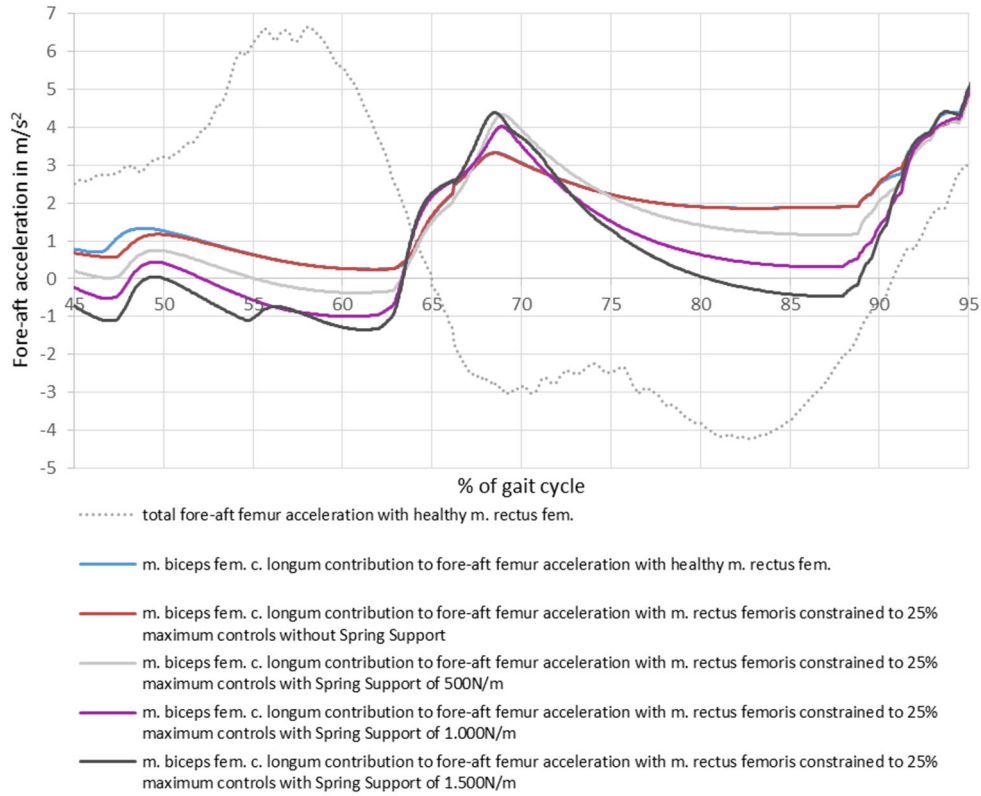


Figure 61: M. biceps femoris caput longum contribution to fore-aft femur acceleration 2. The curves of m. biceps femoris c. longum in healthy conditions, m. biceps femoris c. longum with weakened m. rectus femoris (25% maximum controls) and m. biceps femoris c. longum with weakened m. rectus femoris and spring support are compared.

M. biceps femoris c. longum contribution to vertical femur acceleration

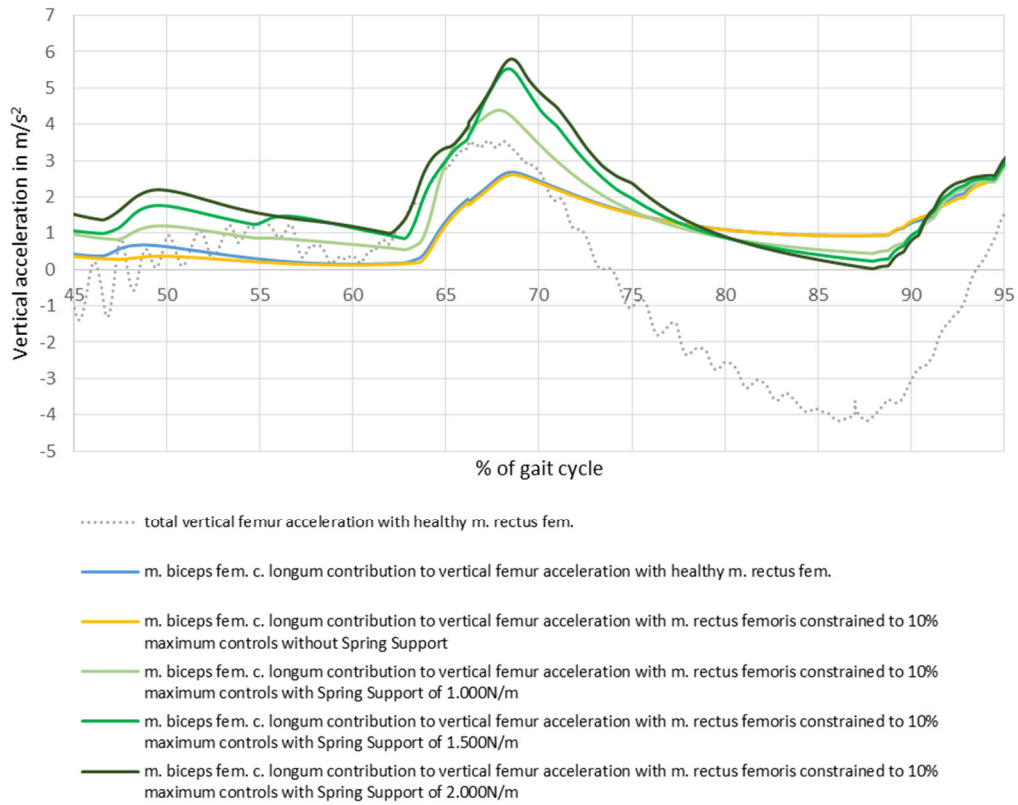


Figure 62: M. biceps femoris caput longum contribution to vertical femur acceleration 1. The curves of m. biceps femoris c. longum in healthy conditions, m. biceps femoris c. longum with weakened m. rectus femoris (10% maximum controls) and m. biceps femoris c. longum with weakened m. rectus femoris and spring support are compared.

M. biceps femoris c. longum contribution to vertical femur acceleration

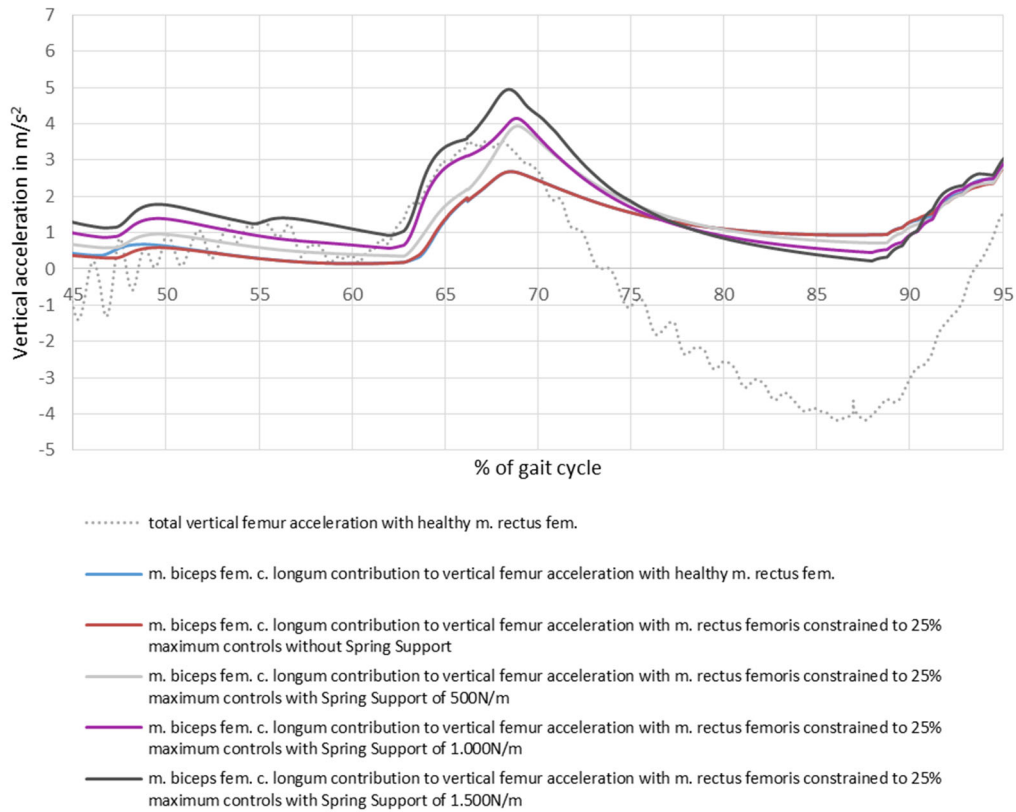


Figure 63: *M. biceps femoris caput longum* contribution to vertical femur acceleration 2. The curves of *m. biceps femoris c. longum* in healthy conditions, *m. biceps femoris c. longum* with weakened *m. rectus femoris* (25% maximum controls) and *m. biceps femoris c. longum* with weakened *m. rectus femoris* and spring support are compared.

4.6. Induced Accelerations of the Femur – Illustrations using Resultant Vectors

The following three pictures show the acceleration contribution of the selected muscles in a very demonstrative and comprehensible fashion. They are used for illustration reasons of the fore-aft and vertical acceleration contribution curves. Eighteen time points of the considered gait cycle are chosen and the resultant vector of the fore-aft and vertical acceleration contribution is calculated and pictured. Only the weakness degree to 10% maximum controls and the spring support curve with the stiffness value of 1.000N/m are taken into account.

M. rectus femoris contribution to fore-aft and vertical femur acceleration

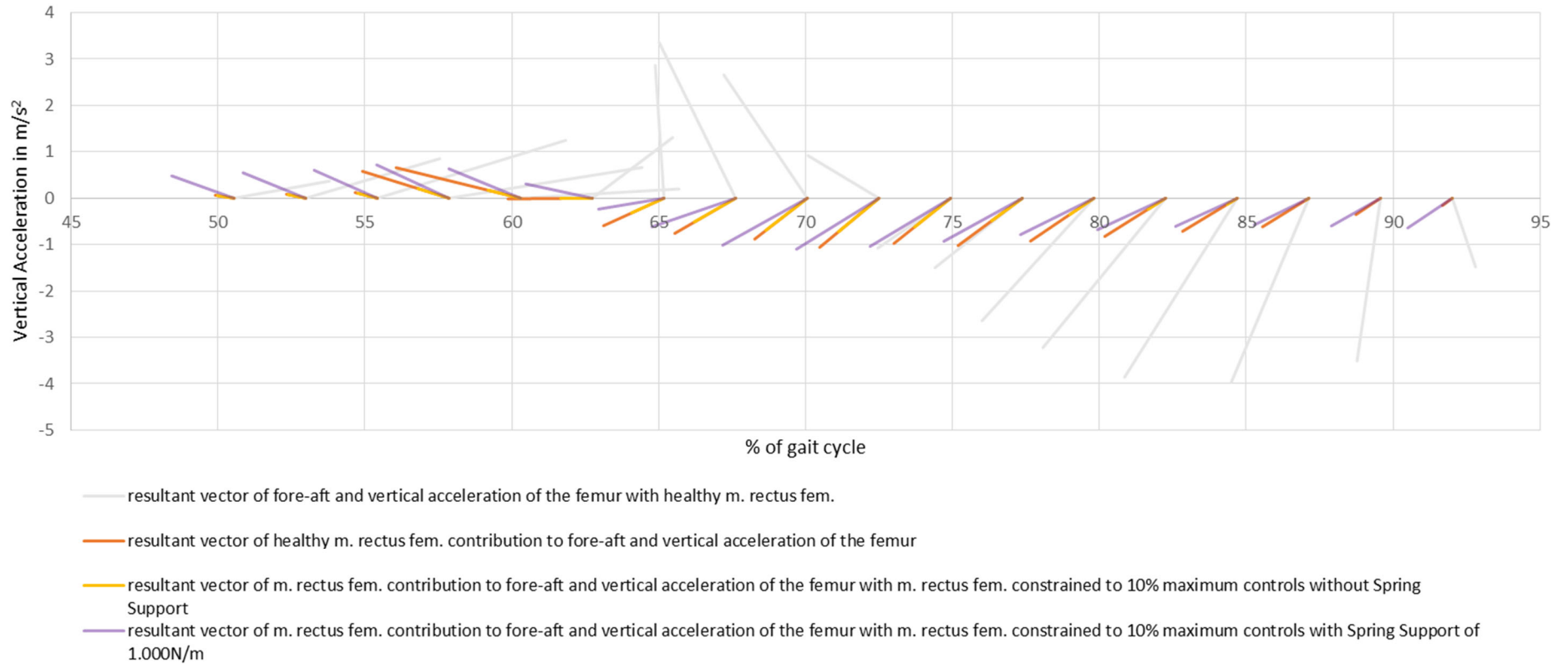


Figure 64: Resultant vectors describing m. rectus femoris contribution to fore-aft and vertical femur acceleration. Each ray expresses the vector of the fore-aft and vertical accelerations. The y-axis expresses the vertical acceleration and the x-axis shows the fore-aft acceleration. The length of the vector illustrates the total femur acceleration contribution. The vectors are plotted versus per cent gait cycle. The vectors of healthy m. rectus femoris, weakened m. rectus femoris (10% maximum controls) and weakened m. rectus femoris with spring support are compared.

M. vastus intermedius contribution to fore-aft and vertical femur acceleration

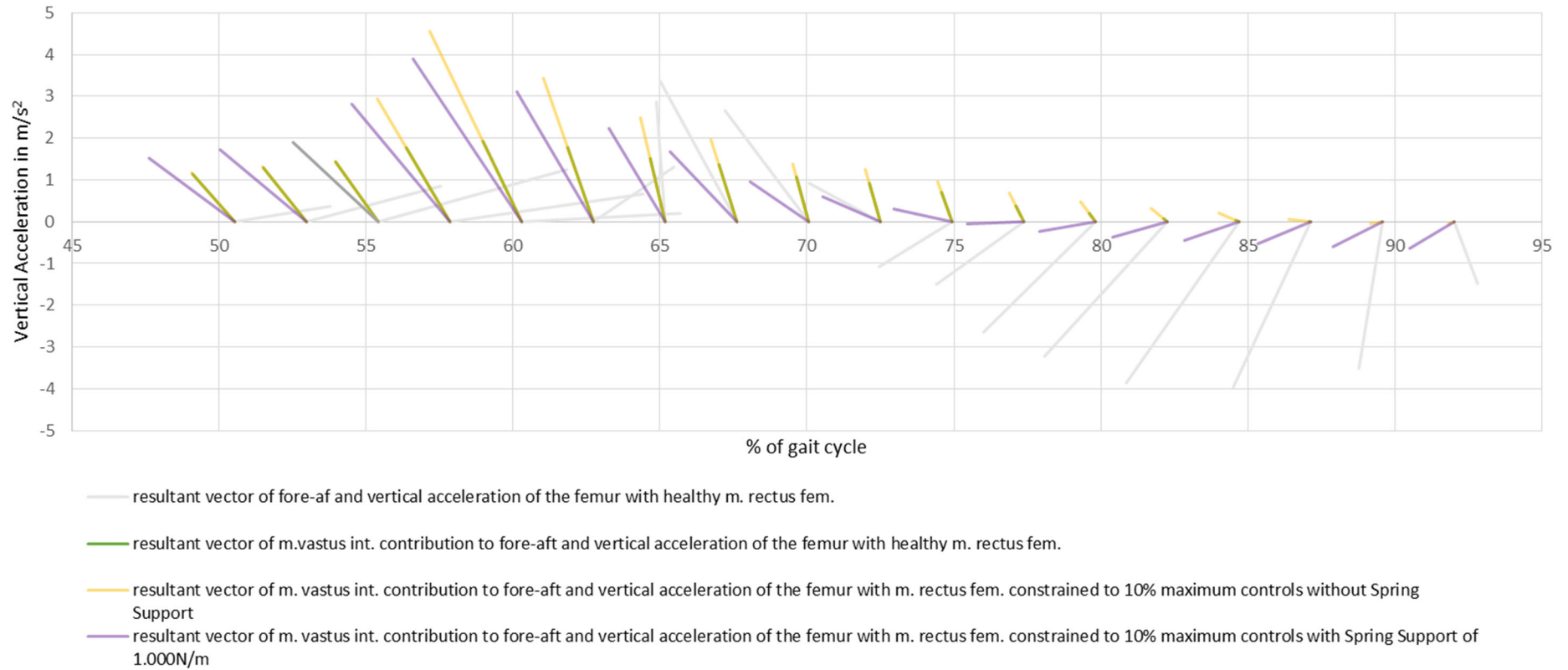


Figure 65: Resultant vectors describing m. vastus intermedius contribution to fore-aft and vertical femur acceleration. Each ray expresses the vector of the fore-aft and vertical accelerations. The y-axis expresses the vertical acceleration and the x-axis shows the fore-aft acceleration. The length of the vector illustrates the total femur acceleration contribution. The vectors are plotted versus per cent gait cycle. The vectors of m. vastus intermedius in healthy conditions, m. vastus intermedius with weakened m. rectus femoris (25% maximum controls) and m. vastus intermedius with weakened m. rectus femoris and spring support are compared.

M. biceps femoris caput longum contribution to fore-aft and vertical femur acceleration

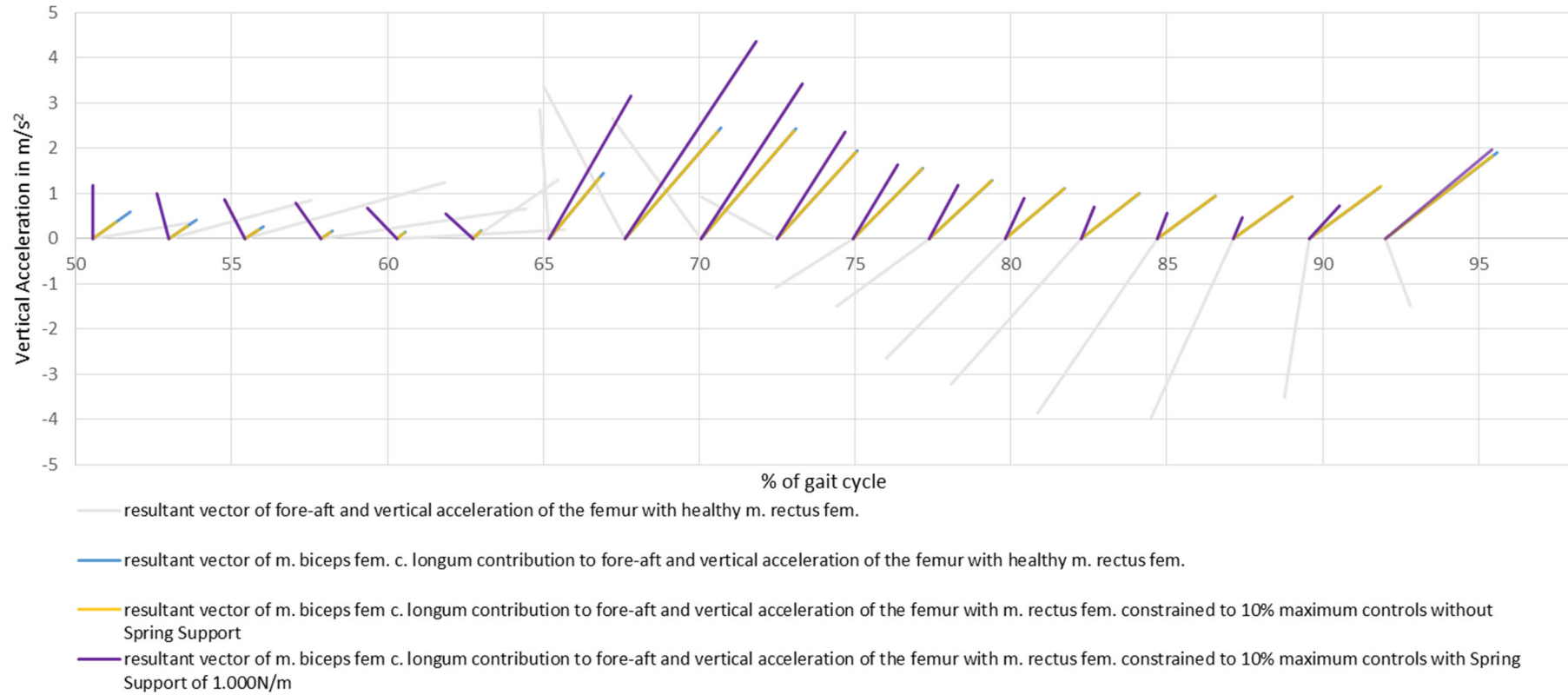


Figure 66: Resultant vectors describing m. biceps femoris caput longum contribution to fore-aft and vertical femur acceleration. Each ray expresses the vector of the fore-aft and vertical accelerations. The y-axis expresses the vertical acceleration and the x-axis shows the fore-aft acceleration. The length of the vector illustrates the total femur acceleration contribution. The vectors are plotted versus per cent gait cycle. The vectors of m. biceps femoris c. longum in healthy conditions, m. biceps femoris c. longum with weakened m. rectus femoris (10% maximum controls) and m. biceps femoris c. longum with weakened m. rectus femoris and spring support are compared.

5. Discussion

This chapter starts with the validation of the OpenSim tools CMC and IAA. Then, the OpenSim software is generally discussed and evaluated. As a next step, the simulation results are compared to other studies and study limitations are considered. The chapter ends with the discussion of the simulation results.

5.1. Validation

To prove accuracy and credibility, the simulation results are validated. The chapter is divided into two parts. First, the CMC results are evaluated. Then, the validation of the IAA results is performed.

5.1.1. CMC Validation

The OpenSim user documentation provides a checklist to evaluate CMC results (National Center for Simulation in Rehabilitation Research, n. d. 12).

1. Peak reserve actuator torque $< 10\%$ of peak joint torque
2. Peak residual forces $< 25\text{N}$
Peak residual moments $< 75\text{Nm}$
3. Matching of RRA and CMC kinematics
4. Comparison of simulated activations to experimental EMG data – similar timing and magnitude

The first four points of the validation procedure are performed with one of the musculoskeletal models used for simulation 3, with m. rectus femoris constrained to 10% maximum controls and spring implementation of 1.500N/m. For the activation comparison, the musculoskeletal model of simulation 1 is chosen, because its data are compared to a healthy subject. For all validations, the whole gait cycle and not only the considered gait cycle period from 45% to 95% is taken into account.

Since the other musculoskeletal models used for simulations all perform the same movement and exhibit comparable composition, they are supposed to be valid too. Furthermore, the results from scaling, IK and RRA are all used as CMC inputs and therefore are all supposed to be valid.

Ad 1)

Table 6 compares the peak reserve actuator torque with 10% of the peak joint torque. The values are rounded to two decimal places.

Table 6: CMC Validation - Peak reserve actuator torques vs. 10% of peak joint torque.

Coordinate	Peak reserve actuator torque		10% of peak joint torque
Hip flexion	0,02 Nm	<	8,74 Nm
Hip adduction	0,02 Nm	<	5,92 Nm
Hip rotation	0,26 Nm	<	1,69 Nm
Knee angle	0,04 Nm	<	6,3 Nm
Ankle angle	5,28 Nm	<	12,84 Nm
Subtalar angle	18,31Nm	>	2,28 Nm
MTP angle	0,12 Nm	>	0,01 Nm

The validation criterion is not fulfilled for the subtalar joint and for the MTP joint. To recheck this criterion failure, the musculoskeletal model from simulation 1 was used, providing CMC values calculated by the OpenSim community. The values from the OpenSim community had comparable dimensions as the results above. The criterion was not fulfilled either. Therefore, this criterion failure is accepted and not discussed further.

Ad 2)

The following diagram shows the residual forces and moments that occur during walking for the duration of one gait cycle. All forces stay below 25N. The moments reach peak values of about 20Nm, which is far below the accepted 75Nm.

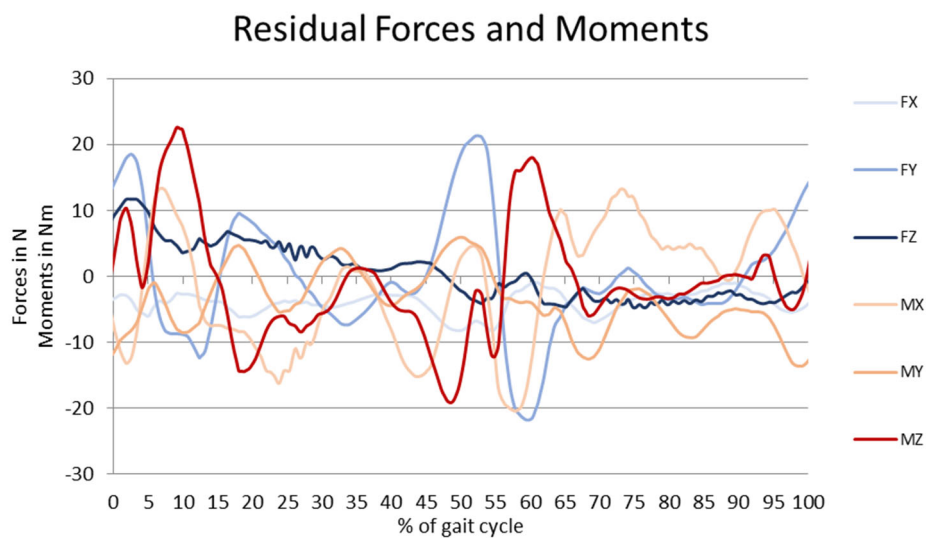


Figure 67: CMC Validation 1 - Residual forces and moments.

Ad 3)

The following diagrams illustrate the CMC and RRA kinematics for the flexion movement of hip and knee for one gait cycle. The first picture concerns joint angles, the second deals with angular velocity and the third shows angular acceleration. The compared kinematics show good matching.

CMC vs. RRA - Joint angles

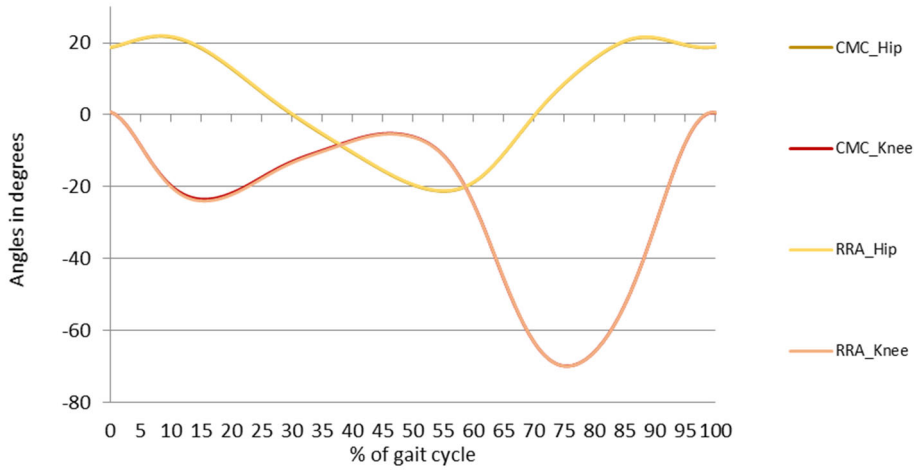


Figure 68: CMC Validation 2 - Joint angles of hip and knee.

CMC vs. RRA - Angular speed

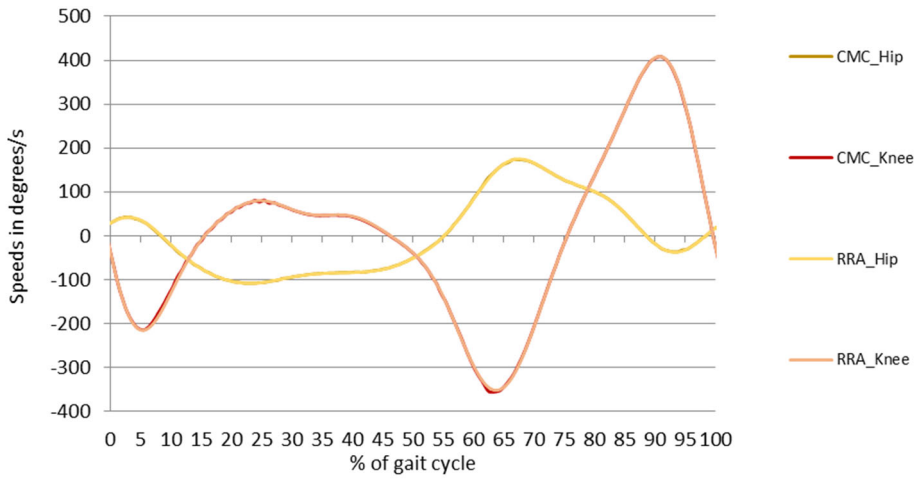


Figure 69: CMC Validation 3 - Angular velocity of hip and knee.

CMC vs. RRA - Angular acceleration

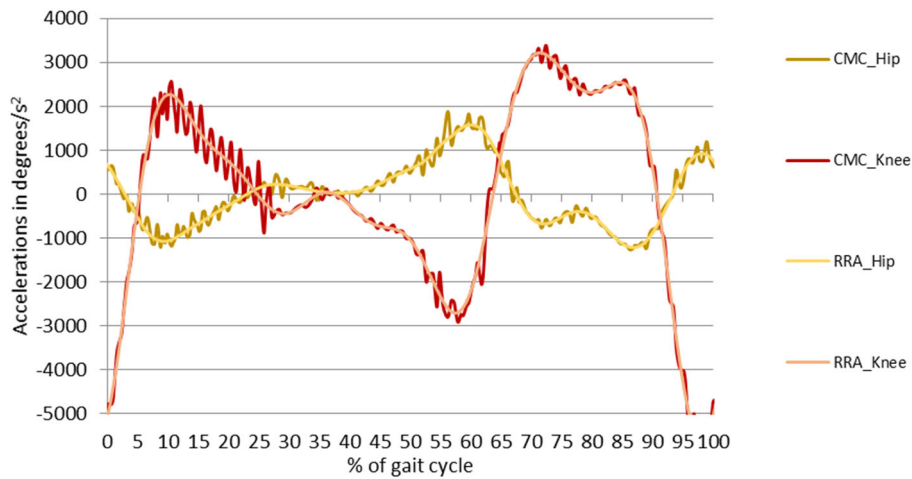


Figure 70: CMC Validation 4 - Angular Acceleration of hip and knee.

Ad 4)

The diagrams below show the activations of m. rectus femoris, m. vastus intermedius and m. biceps femoris caput longum computed with OpenSim and derived from literature.

The EMG of m. rectus femoris derived from literature (figure 71) shows activation of about 20% during the middle of pre-swing and the middle of initial swing corresponding to about 60% and 73% of the gait cycle. The OpenSim model shows a slightly higher activation occurring a little bit later in the gait cycle (figure 72).

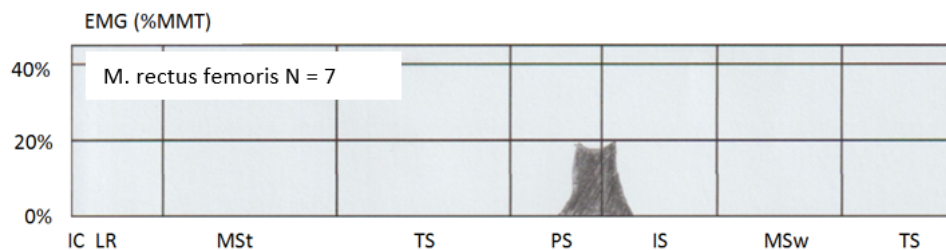


Figure 71: CMC Validation 5 - Activation of m. rectus femoris derived from literature (Perry, 2003).

Activation - M. rectus femoris

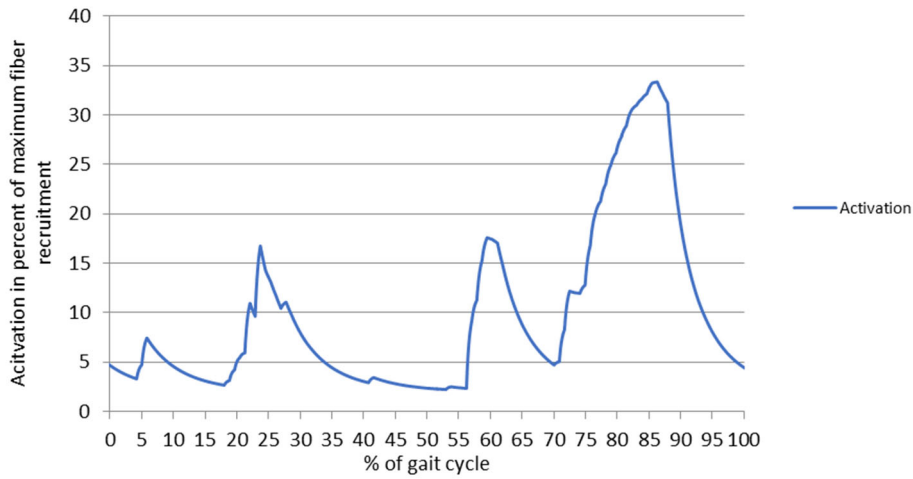


Figure 72: CMC Validation - Activation of *m. rectus femoris* derived from OpenSim.

The literature derived EMG of *m. vastus intermedius* (figure 73) shows activation from terminal stance to mid stance. Activation values of about 20% are reached. As with *m. rectus femoris*, the OpenSim model, whose activation is described by figure 74, reaches slightly higher activation values. Further, the activation occurs later in the gait cycle.

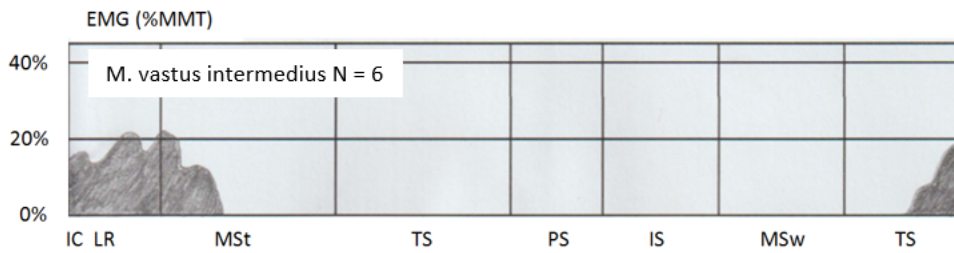


Figure 73: CMC Validation 7 - Activation of *m. vastus intermedius* derived from literature (Perry, 2003).

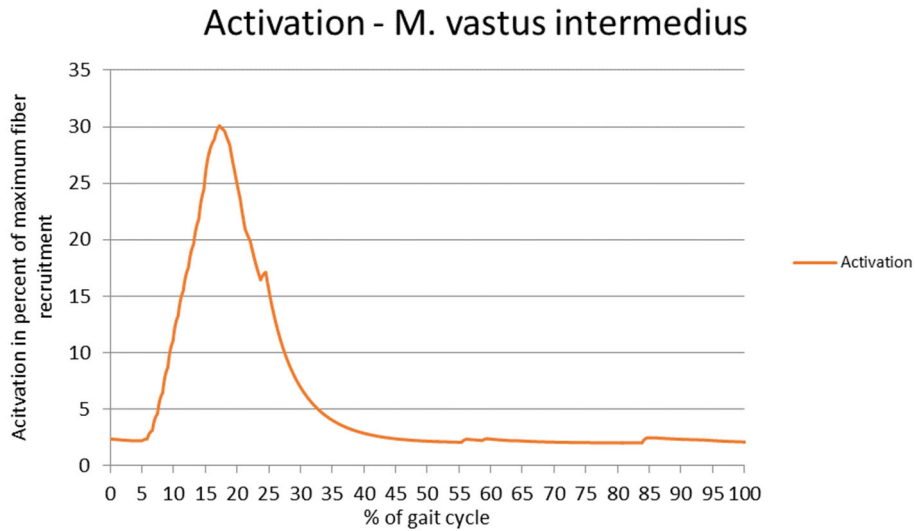


Figure 74: CMC Validation 8 - Activation of *m. vastus intermedius* derived from OpenSim.

M. biceps femoris caput longum shows much higher activation in the OpenSim model (figure 76), where values of about 60% are reached. The EMG taken from literature sources (figure 75) only achieves 20% as maximum activation level. Further, the activation documented in the OpenSim model from 40% to 70% of the gait cycle is not shown in the EMG from literature.

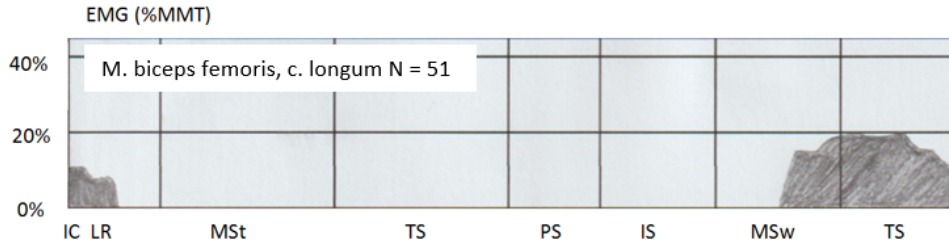


Figure 75: CMC Validation 9 - Activation of *m. biceps femoris caput longum* derived from literature (Perry, 2003).

Activation - M. biceps femoris caput longum

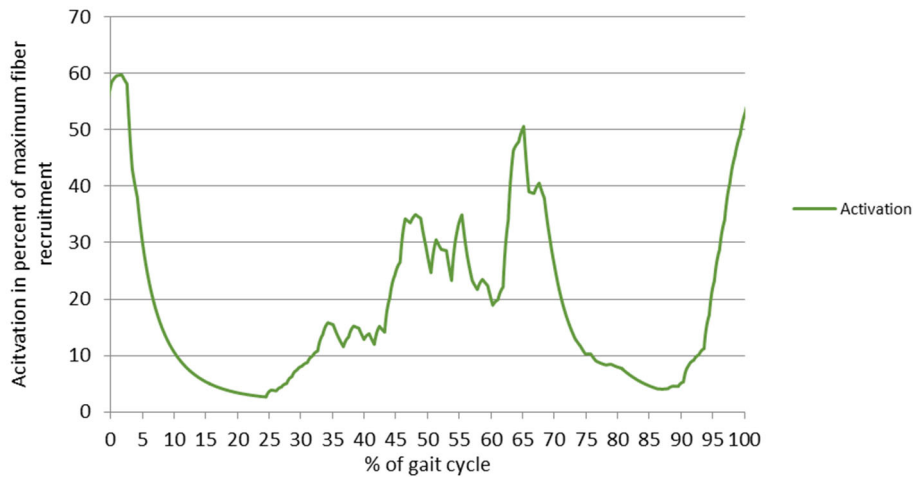


Figure 76: CMC Validation 10 - Activation of *m. biceps femoris caput longum* derived from OpenSim.

In the study of Alexander and Schwameder (2016) calculated and measured muscle activity data were compared during walking. The calculated data were obtained using a musculoskeletal model. They observed differences between calculated and measured data of about the same order as described in this thesis. Therefore it can be concluded that these differences are in an acceptable range.

5.1.2. IAA Validation

First, it is checked if the obtained results are in the same order of magnitude as the results from the study of Hamner and Delp (Hamner and Delp, 2013). This is proven to be the case.

Furthermore, accuracy of the applied rolling-on-surface constraint is tested. Therefore, the OpenSim user documentation advises to report the constraint reaction forces and compare them to the experimental reaction forces (National Center for Simulation in Rehabilitation Research, n. d. 9). The following diagrams (figures 77 and 78) show the experimental reaction forces derived from the OpenSim 'Gait2354' package and the reaction forces obtained with IAA from the musculoskeletal model of simulation 1.

The reaction forces and the reaction moment in y-direction show high coincidence. The reaction moments in x- and z- direction are almost zero in the experimental data and reach values of about 10Nm in the IAA computation. Nevertheless, moments of 10Nm are rather small and can therefore be neglected.

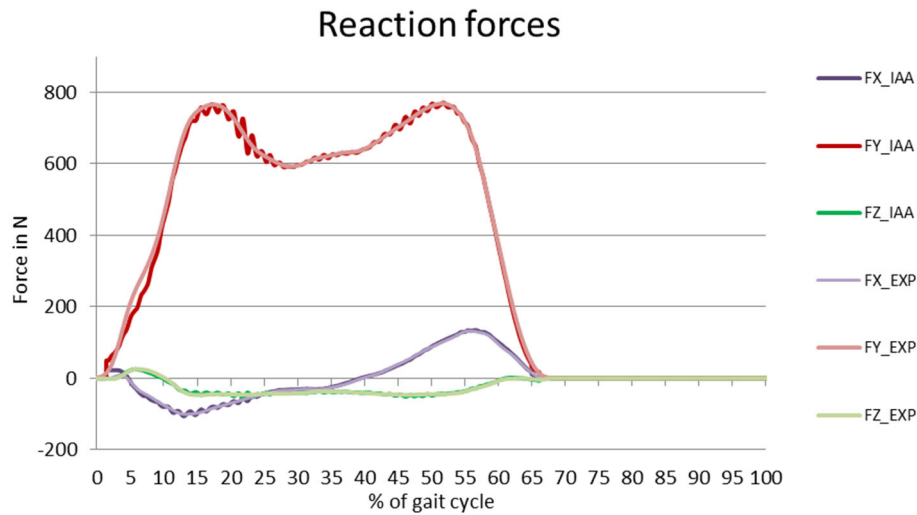


Figure 77: IAA Validation 1 – Comparison of the experimental and the constraint reaction forces.

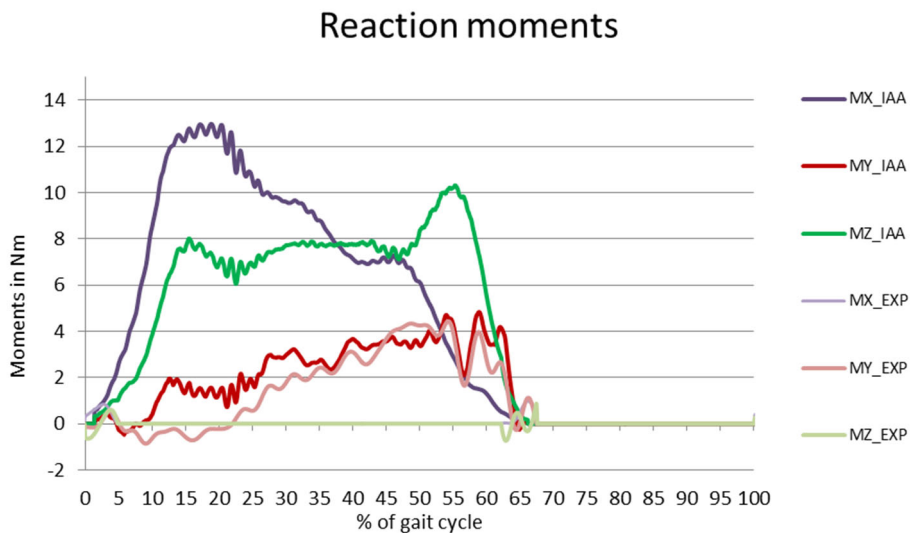


Figure 78: IAA Validation 2 - Comparison of the experimental and the constraint reaction moments.

5.2. Usability

Generally, the usage of the OpenSim software to perform simulations of motions is recommendable due to the high usability. The base functions e.g. IK and CMC are easy to apply and the user documentation is comprehensive. It contains tutorials that facilitate software introduction and show possible simulations and results. Furthermore, the software and all software packages are freely accessible.

Nevertheless, working with the software confronts the user with several problems. The user documentation is very helpful for unexperienced users, but for experienced users the information is not sufficient. To get further

information, the only possibility is to ask questions in the forum. The administrators are nice and try to reply to every post, but in most cases, their answers are short and not comprehensive enough. Searching in the web for further information is very difficult, since the majority of articles only describes simulation results and omits the simulation process. It is difficult to perform selection of decisive simulation parameters and create individual setup files with rare comparison possibilities. Due to these reasons, a deep understanding of the software application requires a lot of time.

5.3. Comparison to other studies

There was no other study found that examines the effects on muscle performance of a passive spring parallel to a weakened muscle. Most studies that investigated passive spring implementation were concerned with improving healthy muscle conditions as reducing the energy cost of walking.

Several studies as for example the one from Farris et al. (2013) documented the effects of a passive ankle exoskeleton on the soleus muscle force during hopping. They implemented a passive spring parallel to the plantar flexor muscles and reported lower soleus force production during exoskeleton assistance. In this thesis, the same effect is considered with m. rectus femoris muscle force, which decreases with spring implementation (compare with preliminary simulations). Farris et al. further reported in a follow-up study that the force of m. tibialis anterior, a counter muscle of the plantar flexors, increased slightly with the implementation of a passive ankle exoskeleton. This result is comparable to the increased force production of biceps femoris caput longum with spring implementation parallel to m. rectus femoris (Farris et al., 2014).

An OpenSim webinar examined the fore-aft and vertical accelerations of the centre of mass. Muscles that compensated for a m. quadriceps femoris activation deficit were tested. They showed increased contribution to COM acceleration during quadriceps weakness (Thompson et al., 2013). This result reinforces the findings of this thesis although not the COM acceleration contribution but the femur acceleration contribution is measured for m. vastus intermedius, representing a compensator muscle for the activation deficit of m. rectus femoris.

5.4. Limitations

The biggest limitation is represented by missing practicability. Nobody would ever insert a spring into a living person. The study just intends to theoretically examine how passive springs act on different muscles. The findings possibly help to construct passive assistive devices including springs.

There was no study found concerning sole m. rectus femoris weakness. Therefore, it can be concluded that in most cases patients exhibit activation deficits not only at one single muscle.

5.5. Simulation results

In the following section the simulation results are discussed. First, the two different activation deficits (10% and 25% maximum controls) are compared. Then, the results of the muscle parameters force and power are

discussed. The next part of this chapter deals with the muscle parameter results of normalized fiber length and normalized fiber velocity. Finally, the induced acceleration results are discussed.

5.5.1. Comparison of activation deficits

To compare the behaviour of the spring support curves in dependence of the two different activation deficits, one has to consider the spring support curves with the stiffness value of 1.000N/m and 1.500N/m. These two spring stiffness values are used for the support of weakened m. rectus femoris to 10% maximum controls, as well as for the m. rectus femoris weakening to 25% maximum controls.

The same stiffness value has the same effect in the force and power curves of m. vastus intermedius. This means for example that a stiffness value of 1.000N/m reduces the m. vastus intermedius curve with weakened m. rectus femoris for about 100N for both modelled activation deficits. Figures 79 and 80 illustrate this effect of force reduction for m. vastus intermedius for both activation deficits.

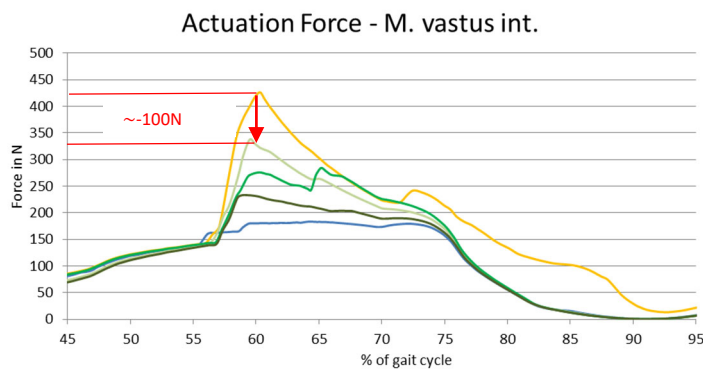


Figure 79: Discussion 1 - Actuation force of m. vastus intermedius with m. rectus femoris weakened to 10% maximum controls. A force reduction of approximately 100N can be considered with implementation of a spring with stiffness of 1.000N/m.

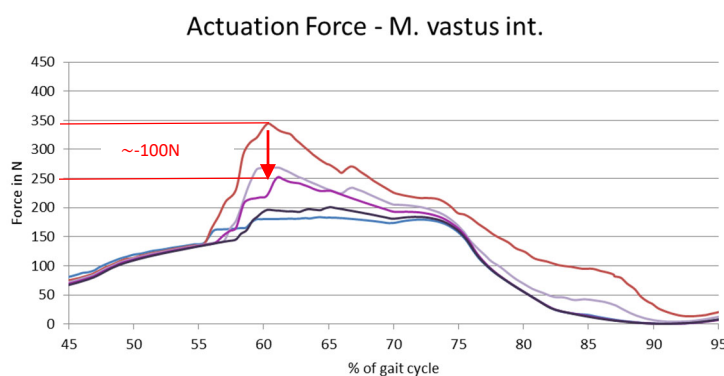


Figure 80: Discussion 2 - Actuation force of m. vastus intermedius with m. rectus femoris weakened to 25% maximum controls. A force reduction of approximately 100N can be considered with implementation of a spring with stiffness of 1.000N/m.

Consideration of m. biceps femoris shows that the same stiffness value leads to a higher increase of the force and power curves when the activation is constrained to 10% maximum controls. It follows that m. biceps femoris, as counter muscle of m. rectus femoris and m. vastus intermedius, has to work more with higher

activation deficit of m. rectus femoris. The IAA results show similar behaviour. A high activation deficit generally leads to a high reaction of the spring support curves in comparison to a low activation deficit. This observation can be explained by the fact that when the activation deficit is low, the performance of all muscles is closer to the healthy m. rectus femoris case. The higher the activation deficit, the more the muscles differ from their normal behaviour, leading to higher impacts on the parameter curves.

5.5.2. Force and Power

The following section discusses the simulation results of the muscle parameters force and power. First, the effects of m. rectus femoris weakening are discussed. Later, the effect of spring implementation to weakened m. rectus femoris is considered.

a) Effects of weakening

M. rectus femoris

Muscle weakening by constraining the maximum control level, leads to reductions in muscle activation. In consequence, force and power reduction of m. rectus femoris occur.

M. vastus intermedius

In the phases of high force loss of weakened m. rectus femoris, m. vastus intermedius shows a force and power increase. Even the peak differences are replicated. These findings lead to the conclusion that m. vastus intermedius compensates for m. rectus femoris weakness. This compensatory behaviour can be explained by the synergistic relationship of m. vastus intermedius and m. rectus femoris during knee extension movement. Furthermore, both muscles act as knee extensors, which facilitates force and power compensation. Figures 81 and 82 illustrate the phases of difference increase and decrease between the healthy and the weakened m. rectus femoris case for the force curves of m. rectus femoris and m. vastus intermedius.

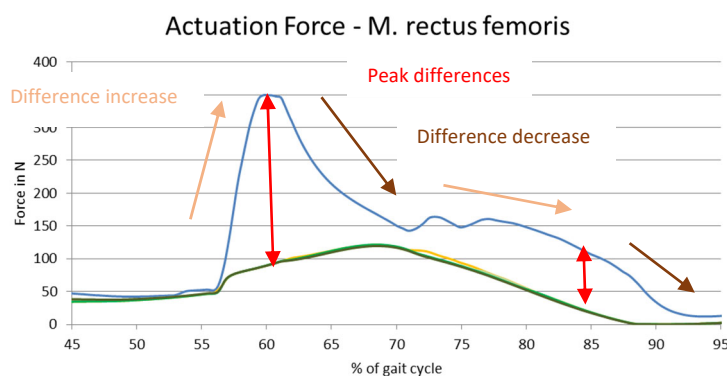


Figure 81: Discussion 3 - Actuation force of m. rectus femoris. Phases of difference increase and decrease between the healthy and the weakened m. rectus femoris force curve are illustrated.

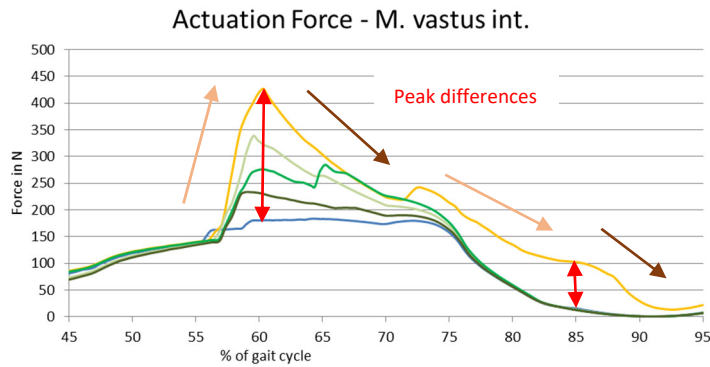


Figure 82: Discussion 4 - Actuation force of *m. vastus intermedius*. Phases of difference increase and decrease between the *m. vastus intermedius* force curve in healthy conditions and in case of weakened *m. rectus femoris* are illustrated.

M. biceps femoris caput longum

The *m. biceps femoris caput longum* force and power curves do not show much effect on *m. rectus femoris* weakness. An explanation for this fact provides the agonist – antagonist relationship of *m. biceps femoris caput longum* and *m. rectus femoris* during knee extension movement. This relationship results in alternate activation times of the muscles. *M. biceps femoris caput longum* is only active, when *m. rectus femoris* is not. Therefore, the weakness of *m. rectus femoris* does not affect the performance of *m. biceps femoris caput longum*.

The explanations in the section above prove the parts in hypothesis 1 concerning force and power to be confirmed.

b) Effects of the spring

M. rectus femoris

As supposed in hypothesis 2, spring implementation has no effect on the force and power curves of weakened *m. rectus femoris*. The modelled activation deficit prohibits higher force and power generation. Since stiffness values are set at a lower level not to risk insufficient muscle challenge, no further reduction of the force and power curves of weakened *m. rectus femoris* occurs with spring implementation.

M. vastus intermedius

In the gait cycle period from 57% to 75%, spring support approaches but not assimilates the force and power curves to the reference curves. The higher the stiffness value, the better the approach. If the stiffness value is set to a level that is too low, the spring is not able to produce enough force to take over the force loss of *m. rectus femoris* and so *m. vastus intermedius* still has to compensate. When the stiffness value is high enough, the spring is capable to take over *m. rectus femoris* force loss and *m. vastus intermedius* only shows low compensation. From 75% until the end of the gait cycle, the force and power curves of *m. vastus intermedius* with spring support follow the same course as the reference curves. The force loss of *m. rectus femoris* in this period is not so high and therefore the spring is able to take over complete force loss. Figure 83 illustrates the *m. vastus intermedius* force curve approach to reference curve with spring implementation.

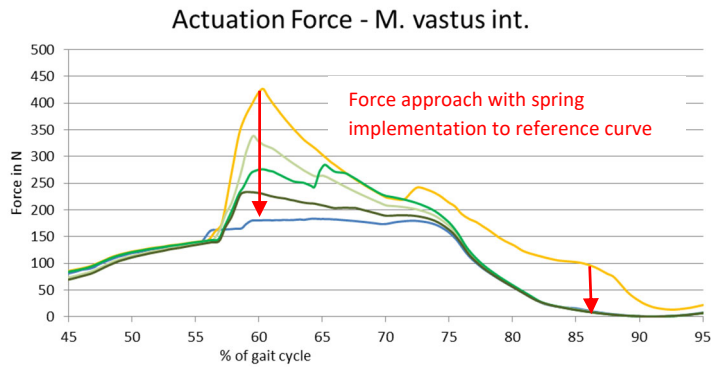


Figure 83: Discussion 5 - Actuation force of *m. vastus intermedius*. Spring implementation causes a decrease in the force curve.

Considering the force and power curves, spring implementation has a positive effect on the curves describing the weakened *m. rectus femoris* case. An approximation to reference curve is considered, as expected in hypothesis 3.

M. biceps femoris caput longum

The spring support curves of *m. biceps femoris caput longum* produce higher forces and higher power than in case of healthy *m. rectus femoris*. Comparison of the force curves of *m. rectus femoris* and *m. biceps femoris caput longum* shows that *m. biceps femoris caput longum* produces higher force precisely when *m. rectus femoris* does not need support of the spring. This is the case when the reference and weakened *m. rectus femoris* force curves are close to each other. *M. biceps femoris caput longum*, a counter muscle of *m. rectus femoris*, has to work against this spring force, which is not needed by *m. rectus femoris*. Figure 84 shows the phases of high and low force support need of *m. rectus femoris*. Figure 85 illustrates the phases of high and low difference between the *m. biceps c. longum* force curve of the healthy and the weakened *m. rectus femoris* case.

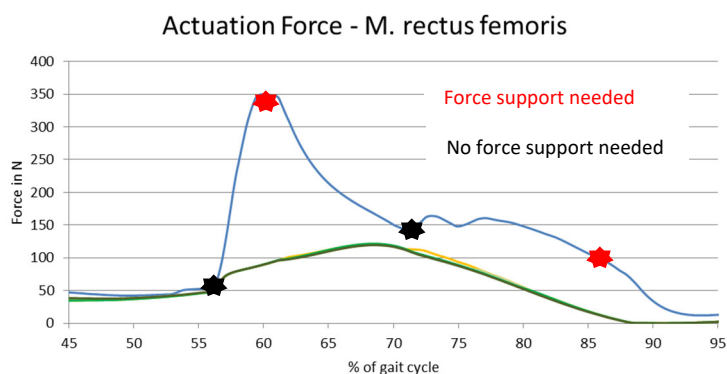


Figure 84: Discussion 6 - Actuation force of *m. rectus femoris*. The figure illustrates points of high and low force support needs of *m. rectus femoris*.

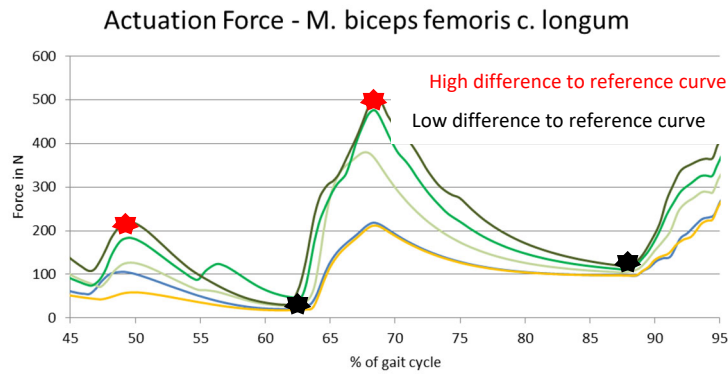


Figure 85: Discussion 7 - Actuation force of *m. biceps femoris caput longum*. Phases of high and low difference between the *m. biceps c. longum* force curve in the weakened *m. rectus femoris* case and the reference curve.

As supposed in hypothesis 4, spring implementation has a negative effect on the *m. biceps femoris caput longum* force and power curves with weakened *m. rectus femoris*.

The section above confirms the parts in hypothesis 2, 3 and 4 concerning force and power.

5.5.3. Normalized Fiber Length and Normalized Fiber Velocity

The curves documenting normalized fiber length and the normalized fiber velocity do not show considerable differences because the kinematics of the musculoskeletal model referring to a healthy human subject are maintained and used as inputs for all simulations.

The muscle parameters normalized fiber length and normalized fiber velocity are therefore excluded from hypotheses verification.

5.5.4. Induced Accelerations

The following section discusses the simulation results of IAA. As in the force and power chapter, the effects of *m. rectus femoris* weakening are discussed first. Then, the effect of spring implementation to weakened *m. rectus femoris* is considered.

a) Effects of weakening

Muscle force generates joint torques and thereby induces body segment acceleration. Consideration of the femur acceleration contribution curves of *m. rectus femoris* and *m. vastus intermedius* shows, that the behaviour of the force and power curves is reflected. Weakness of *m. rectus femoris* reduces its acceleration contribution and *m. vastus intermedius* compensates the acceleration loss with higher contribution. The points of highest difference between the healthy and weakened *m. rectus femoris* case are located almost at the same places as they did in the force and power curves. The only curve, which pattern slightly differs from those of the other contribution curves, represents the vertical acceleration contribution of *m. vastus intermedius*. Only the peak difference at 61% is visible. Figures 86 – 89 illustrate the phases of high and low difference between the femur acceleration curves between the healthy and weakened *m. rectus femoris* case for *m. rectus femoris* and *m. vastus intermedius*.

Equally to the force and power curves, the m. biceps femoris caput longum acceleration contribution curve does not show much effect on m. rectus femoris weakness.

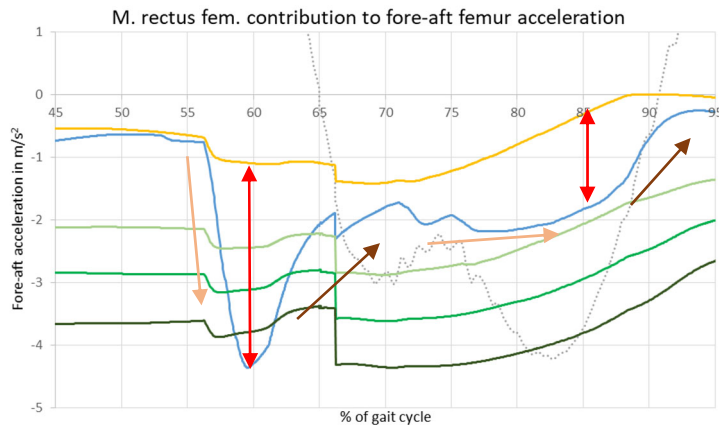


Figure 86: Discussion 8 - M. rectus femoris contribution to fore-aft femur acceleration. Phases of difference increase and decrease between the m. rectus femoris femur acceleration curve in healthy conditions and in case of weakened m. rectus femoris are illustrated.

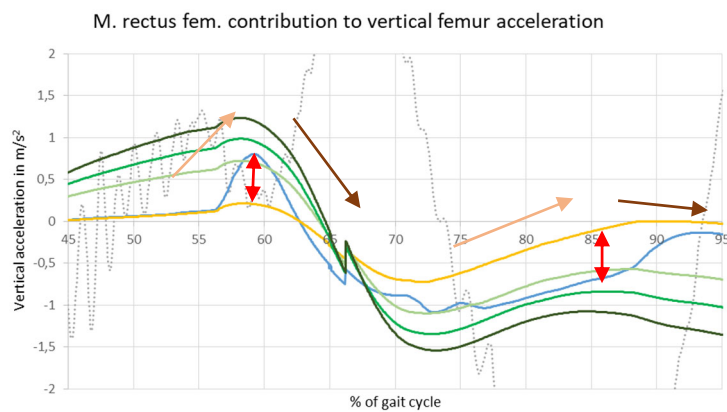


Figure 87: Discussion 9 - M. rectus femoris contribution to vertical femur acceleration. Phases of difference increase and decrease between the m. rectus femoris femur acceleration curve in healthy conditions and in case of weakened m. rectus femoris are illustrated.

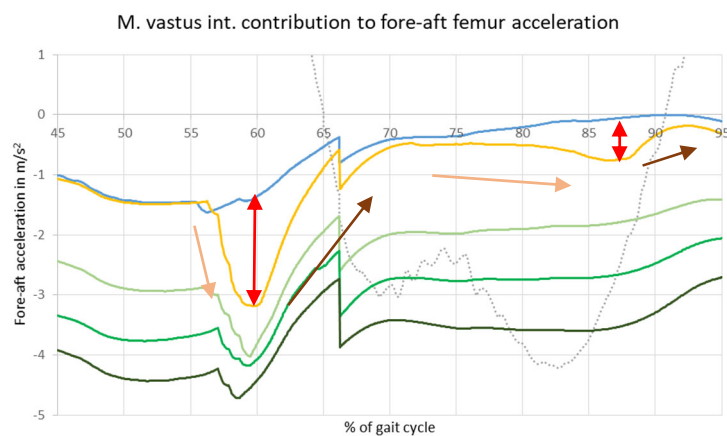


Figure 88: Discussion 10 - M. vastus intermedius contribution to fore-aft femur acceleration. Phases of difference increase and decrease between the m. vastus intermedius femur acceleration curve in healthy conditions and in case of weakened m. rectus femoris are illustrated.

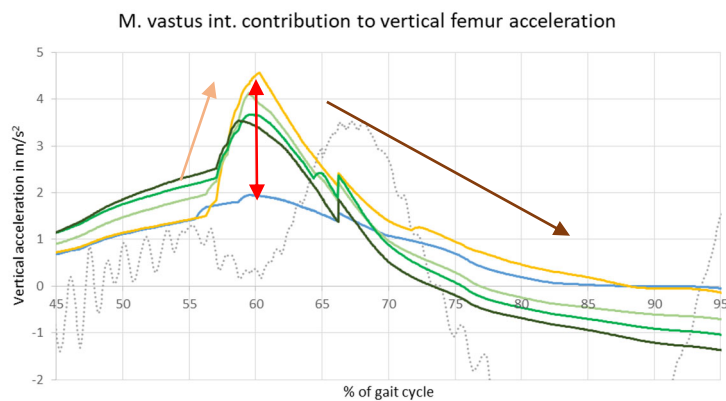


Figure 89: Discussion 11 - *M. vastus intermedius* contribution to vertical femur acceleration. Phases of difference increase and decrease between the *m. vastus intermedius* femur acceleration curve in healthy conditions and in case of weakened *m. rectus femoris* are illustrated.

Consideration of the effect of weakening in the induced acceleration results confirms hypothesis 1.

a) Effects of the spring

Although the force and power curves of weakened *m. rectus femoris* do not react to spring support, the acceleration contribution curves of *m. rectus femoris* show an effect. For most of the considered gait cycle period and for most of the stiffness values, they contribute more than in the healthy *m. rectus femoris* case and do not show better approximation to reference curve than the curves of weakened *m. rectus femoris* without support. The same phenomenon is considered with *m. vastus intermedius* and *m. biceps femoris caput longum*. In most cases, the curves describing the weakened *m. rectus femoris* case without spring support are even closer to the reference curve than the spring support curves. Only for *m. biceps femoris caput longum*, this behaviour of the spring support curves is already observed with the force and power curves.

For all selected muscles, the spring support curves generally show higher acceleration contributions. For example, if the reference curve is positive, the spring support curves show an even higher positive value. Since the kinematic and kinetic inputs are the same in all simulated cases, the total femur acceleration in both considered directions must be equal and cannot be the reason for the performance of the spring support curves. Equal total femur acceleration with increasing muscle contribution is only possible when all muscles contribute more. When the contribution increases within all muscles, negative and positive contribution increases and the overall acceleration stays the same. One explanation for this phenomenon of increased acceleration contribution of all considered muscles is based on the OpenSim software implementation. One has to expect that the software does not take the spring into account for IAA calculations, since there are no spring results computed. When the spring is able to produce force but does not contribute to femur acceleration, maybe some other muscles have to take over the contribution of the implemented spring and therefore increase their contribution. Then all the other muscles also have to increase their contribution to keep the total acceleration constant.

Only hypothesis 4, which supposes negative effects with spring implementation to m. biceps femoris caput longum can be confirmed considering the effects of the spring in the induced acceleration results. Hypothesis 2 and 3 have to be rejected.

6. Summary

Since muscle weakness possibly leads to devastating impact on the gait pattern, research on devices, capable to assist walking movement, is of major importance (Hislop et al., 2014 and Nacy et al., 2016). Due to energy efficiency and mass minimization reasons, research focusses on passive devices, which replace actuators with light springs (Farris et al., 2013).

The purpose of this thesis is to examine the effects of m. rectus femoris weakening on muscle performance during walking. Furthermore, the main goal is the answer the following research question: What are the effects of a passive path spring implementation parallel to weakened m. rectus femoris on the main muscle parameters during walking? Force, power, normalized fiber length, normalized fiber velocity and induced femur acceleration are selected as main muscle parameters and the walking movement is analysed during the pre-swing, initial swing and mid-swing phases of gait. The investigation is limited to the three muscles m. rectus femoris, m. vastus intermedius and m. biceps femoris caput longum.

This thesis is a simulation study, which uses the software OpenSim. All model and motion data are included in the 'Gait2354' package derived from the OpenSim library. Three different types of simulations are performed. The first one is based on healthy model conditions and aims at the achievement of reference data. For the second simulation, an activation deficit of m. rectus femoris is implemented in the model to illustrate weakening of m. rectus femoris. Additionally to m. rectus femoris weakening, the third simulation contains a passive path spring parallel to m. rectus femoris. Two different degrees of weakening and three different spring stiffness values are implemented.

Concerning the muscle parameters force, power and induced femur acceleration, m. rectus femoris weakening leads to reduced performance of m. rectus femoris, increased performance of m. vastus intermedius and has no effect on the performance of m. biceps femoris caput longum. M. vastus intermedius, which acts as knee extender just like m. rectus femoris, compensates for m. rectus femoris weakness. On the other hand, m. biceps femoris caput longum, a counter muscle to m. rectus femoris, is not affected by m. rectus femoris weakness.

With regard to answering the research question, the effects of the spring are considered. Since m. rectus femoris is weakened by implementation of an activation deficit, it cannot produce higher force or power. Therefore, spring implementation has no effect on the force and power curves of m. rectus femoris. For the m. vastus intermedius force and power curves, spring implementation has a positive effect, since the curves are approached to the reference curve. M. vastus intermedius can reduce its compensatory behaviour. In contrast, spring implementation has a negative effect on the force and power curves of m. biceps femoris caput longum. The force and power curves increase because m. biceps femoris has to work against the spring force. Concerning induced femur acceleration, spring implementation has a negative effect and increases the contribution for all muscles. The curves show more difference to the reference curves than the curve describing weakened m. rectus femoris case without spring implementation.

It can be stated that the spring's impact on force and power depends on the function that the specific muscle exhibits in relation to m. rectus femoris. Consideration of force and power performance of all three muscles

shows that the positive effect of the spring on m. vastus intermedius is destroyed by the negative effect that the spring has on m. biceps femoris caput longum. Concerning induced femur acceleration, spring implementation always shows a negative effect. In summary, the overall muscle performance cannot be improved by spring implementation parallel to weakened m. rectus femoris.

Since all induced femur acceleration results yield negative effects of spring implementation, further studies have to examine if the reasons of this bad performance can possibly be explained by limitations of IAA. Maybe the IAA implementation is not designed for musculoskeletal models including springs. Furthermore, this study has to be expanded and include more muscles. Only then it is possible gain insight into the overall muscle performance. It is also important to implement further springs on different locations and check their effects. For example, path spring implementation parallel to m. biceps femoris caput longum possibly can counteract the negative effect of the spring parallel to m. rectus femoris. Furthermore, future studies should take into account the maximum stresses and strains of the considered muscles, since the springs should assist and help the people's muscles and not harm them.

7. Bibliography

7.1. List of References

- Abernethy, Bruce; Kippers, Vaughan; Hanrahan, Stephanie J.; Pandy, Marcus G.; McManus, Alison M.; Mackinnon, Laurels (2013): Biophysical foundations of human movement. 3rd ed. Leeds: Human Kinetics.
- Alexander, Nathalie; Schwameder, Hermann (2016): Comparison of Estimated and Measured Muscle Activity During Inclined Walking. In *Journal of applied biomechanics* 32 (2), pp. 150–159.
- Andersen, F. C.; Pandy, M. G. (1999): A dynamic optimization solution for vertical jumping in three dimensions. In *Computer Methods in Biomechanics and Biomedical Engineering* 2 (3), pp. 201–231.
- Annaswamy, Thiru M.; Giddings, Candace J.; Della Croce, Ugo; Kerrigan, D. Casey (1999): Rectus femoris: Its role in normal gait. In *Archives of Physical Medicine and Rehabilitation* 80 (8), pp. 930–934.
- Arnold, Allison: Introduction to Muscle Analysis. OpenSim Workshop, checked on 12/31/2018.
- Bach, Bernard R.; Hasan, Samer S. (1999): Anatomy and Physiology of the Musculoskeletal System. In Robert C. Schenck (Ed.): *Athletic training and sports medicine*. 3rd ed. Rosemont: American Academy of Orthopaedic Surgeons, pp. 85–113.
- Bassile, Clare C.; Hayes, Sheila M. (2016): Gait Awareness. In Glen Gillen (Ed.): *Stroke rehabilitation. A function-based approach*. 4th ed. St. Louis: Elsevier, pp. 194–224.
- Beardsley, Chris (n. d.): Biomechanics definitions. Available online at <https://www.strengthandconditioningresearch.com/biomechanics/biomechanics-definitions/>, checked on 12/30/2018.
- Biller, José (Ed.) (2012): *Practical Neurology*. 4th ed. Philadelphia: Wolters Kluwer.
- Bonewit-West, Kathy; Hunt, Sue A.; Applegate, Edith (2016): *Today's medical assistant. Clinical & administrative procedures*. 3rd ed. St. Louis: Elsevier.
- Chaitow, Leon; DeLany, Judith (2011): *Clinical application of neuromuscular techniques. Volume 2 - The lower body*. 2nd ed. n. p.: Churchill Livingstone Elsevier. Available online at <http://site.ebrary.com/lib/alltitles/docDetail.action?docID=10594317>.
- Chen, Bing; Ma, Hao; Qin, Lai-Yin; Gao, Fei; Chan, Kai-Ming; Law, Sheung-Wai et al. (2016): Recent developments and challenges of lower extremity exoskeletons. In *Journal of orthopaedic translation* 5, pp. 26–37.
- Cianca, John; Mimbella, Paolo (2018): Hamstring Strain. In Walter R. Frontera, Silver Julie K., Thomas D. Rizzo (Eds.): *Essentials of Physical Medicine and Rehabilitation. Musculoskeletal disorders, pain, and rehabilitation*. 4th ed. Philadelphia: Elsevier, pp. 378–384.
- Cifu, David X. (Ed.) (2015): *Braddom's Physical Medicine and Rehabilitation*. 5th ed. Philadelphia: Elsevier. Available online at <http://gbv.ebib.com/patron/FullRecord.aspx?p=4187432>.
- Clippinger, Karen (2016): *Dance anatomy and kinesiology. Principles and exercises for improving technique and avoiding common injuries*. 2nd ed. Champaign: Human Kinetics.
- Collins, Steven H.; Wiggin, M. Bruce; Sawicki, Gregory S. (2015): Reducing the energy cost of human walking using an unpowered exoskeleton. In *Nature* 522 (7555), pp. 212–215.
- Cramer, Gregory D.; Darby, Susan A. (2014): *Clinical Anatomy of the Spine, Spinal Cord, and ANS*. 3rd ed. St. Louis: Elsevier. Available online at <http://gbv.ebib.com/patron/FullRecord.aspx?p=1431126>.
- Delp, S. L.; Loan, J. P.; Hoy, M. G.; Zajac, F. E.; Topp E.L.; Rosen, J. M. (1990): An interactive graphics-based model of the lower extremity to study orthopaedic surgical procedures. In *IEEE Transactions on Biomedical Engineering* 37 (8), pp. 757–767.
- Delp, Scott L.; Anderson, Frank C.; Arnold, Allison S.; Loan, Peter; Habib, Ayman; John, Chand T. et al. (2007): OpenSim: open-source software to create and analyze dynamic simulations of movement. In *IEEE Transactions on Biomedical Engineering* 54 (11), pp. 1940–1950.
- Delp, Scott L.; Arnold, Edith M. (2011): Fibre operating lengths of human lower limb muscles during walking. In *Philosophical Transactions of the Royal Society* 366 (1570), 1530–1539.
- Delp, Scott L.; Ku, Joy P.; Pande, Vijay S.; Sherman, Michael A.; Altman, Russ B. (2012): Simbios: an NIH national center for physics-based simulation of biological structures. In *Journal of the American Medical Informatics Association : JAMIA* 19 (2), pp. 186–189.
- Dicharry, Jay (2010): Kinematics and Kinetics of Gait: From Lab to Clinic. In Mark D. Miller, Robert P. Wilder (Eds.): *The Runner*. 1st ed. 29 volumes. Philadelphia: Saunders (Clinics in sports medicine, 3), pp. 347–365.

- Disselhorst-Klug, Catherine; Besdo, Silke; Oehler, Simone (2015): Biomechanik des muskuloskelettalen Systems. In Marc Kraft, Catherine Disselhorst-Klug (Eds.): *Rehabilitationstechnik*. Berlin/Boston: De Gruyter (Biomedizinische Technik, 10), pp. 53–88.
- Farris, Dominic James; Hicks, Jennifer L.; Delp, Scott L.; Sawicki, Gregory S. (2014): Musculoskeletal modelling deconstructs the paradoxical effects of elastic ankle exoskeletons on plantar-flexor mechanics and energetics during hopping. In *The Journal of experimental biology* 217 (22), pp. 4018–4028.
- Farris, Dominic James; Robertson, Benjamin D.; Sawicki, Gregory S. (2013): Elastic ankle exoskeletons reduce soleus muscle force but not work in human hopping. In *Journal of applied physiology* 115 (5), pp. 579–585.
- Farris, Dominic James; Sawicki, Gregory S. (2012): Linking the mechanics and energetics of hopping with elastic ankle exoskeletons. In *Journal of applied physiology* 113 (12), pp. 1862–1872.
- Fleming, Jerome (n. d.): What causes a limb to rotate - force or torque? Available online at <https://slideplayer.com/slide/4645528/>, checked on 12/31/2018.
- Friederich, J. A.; Brand, R. A. (1990): Muscle fiber architecture in the human lower limb. In *Journal of Biomechanics* 23 (1), pp. 91–95.
- Fritz, Sandy; Chaitow, Leon; Hymel, Glenn M. (2008): *Clinical massage in the healthcare setting*. 1st ed. St. Louis: Mosby/Elsevier (Mosby's massage career development series).
- Frontera, Walter R.; Silver Julie K.; Rizzo, Thomas D. (Eds.) (2018): *Essentials of Physical Medicine and Rehabilitation. Musculoskeletal disorders, pain, and rehabilitation*. 4th ed. Philadelphia: Elsevier.
- Gillen, Glen (Ed.) (2016): *Stroke rehabilitation. A function-based approach*. 4th ed. St. Louis: Elsevier. Available online at <http://search.ebscohost.com/login.aspx?direct=true&scope=site&db=nlebk&db=nlabk&AN=1151798>.
- Götz-Neumann, Kirsten (2003): *Gehen verstehen. Ganganalyse in der Physiotherapie*. 1st ed. Stuttgart: Thieme.
- Grabowski, Alena M.; Herr, Hugh M. (2009): Leg exoskeleton reduces the metabolic cost of human hopping. In *Journal of applied physiology* 107 (3), pp. 670–678.
- Gray, Richard (2016): The real reasons why we walk on two legs and, not four. BBC. Available online at <http://www.bbc.com/earth/story/20161209-the-real-reasons-why-we-walk-on-two-legs-and-not-four>, checked on 12/29/2018.
- Halaki, Mark; Gi, Karen (2012): Normalization of EMG Signals: To Normalize or Not to Normalize and What to Normalize to? In Ganesh R. Naik (Ed.): *Computational Intelligence in Electromyography Analysis - A Perspective on Current Applications and Future Challenges*: InTech.
- Hamner, Samuel R.; Delp, Scott L. (2013): Muscle contributions to fore-aft and vertical body mass center accelerations over a range of running speeds. In *Journal of Biomechanics* 46 (4), pp. 780–787.
- Hamner, Samuel R.; Seth, Ajay; Steele, Katherine M.; Delp, Scott L. (2013): A rolling constraint reproduces ground reaction forces and moments in dynamic simulations of walking, running, and crouch gait. In *Journal of Biomechanics* 46 (10), pp. 1772–1776.
- Hansen, John T. (2014): *Netter's anatomy flash cards*. 4th ed. Philadelphia: Saunders Elsevier.
- Hazen, Kirk (2015): *An introduction to language*. 1st ed. Malden: Wiley-Blackwell (Linguistics in the world).
- Hislop, Helen J.; Avers, Dale; Brown, Marybeth; Daniels, Lucille (2014): *Daniels and Worthingham's muscle testing. Techniques of manual examination and performance testing*. 9th ed. St. Louis: Elsevier/Saunders.
- Horak, Holli A. (2012): Approach to the Patient with Acute Muscle Weakness. In José Biller (Ed.): *Practical Neurology*. 4th ed. Philadelphia: Wolters Kluwer, pp. 304–310.
- John, Chand T. (n. d.): Complete Description of the Thelen2003Muscle Model. National Center for Simulation in Rehabilitation Research.
- John, Chand T.; Andersen, F. C.; Higginson Jill S.; Delp, S. L. (2012): Stabilisation of walking by intrinsic muscle properties revealed in a three-dimensional muscle-driven simulation. In *Computer Methods in Biomechanics and Biomedical Engineering* 16 (4), pp. 451–462.
- King of the gym (2012): *Leg Anatomy: All about the Leg Muscles*. Available online at <http://www.kingofthegym.com/leg-anatomy/>, checked on 12/31/2018.
- Knudson, Duane (2003): *Fundamentals of Biomechanics*. New York: SPRINGER.
- Koca, Kenan; Verim, Samet (2016): The Radiographic Evaluation of the Musculoskeletal System and Spine. In Feza Korkusuz (Ed.): *Musculoskeletal Research and Basic Science*. 1st ed. Cham: Springer International Publishing, pp. 109–139.
- Korkusuz, Feza (Ed.) (2016): *Musculoskeletal Research and Basic Science*. 1st ed. Cham: Springer International Publishing. Available online at <http://gbv.eblib.com/patron/FullRecord.aspx?p=4179367>.

- Kraft, Marc; Disselhorst-Klug, Catherine (Eds.) (2015): *Rehabilitationstechnik*. Berlin/Boston: De Gruyter (Biomedizinische Technik, 10).
- Lisa, Joel A. de; Shalala, Donna E. (Eds.) (1998): *Gait Analysis in the Science of Rehabilitation // Gait analysis in the science of rehabilitation*. n. p.: Diane Publishing Co.
- Lovegreen, William; Murphy, Douglas P.; Smith, William K.; Stevens, Phillip; Webster, Joseph (2015): *Lower Limb Amputation and Gait*. In David X. Cifu (Ed.): *Braddom's Physical Medicine and Rehabilitation*. 5th ed. Philadelphia: Elsevier, pp. 191–225.
- MacLester, John; St. Pierre, Peter (2008): *Applied biomechanics. Concepts and connections*. Belmont: Thomson Wadsworth.
- Mansfield, Paul Jackson; Neumann, Donald A. (2014): *Essentials of kinesiology for the physical therapist assistant*. 2nd ed. St. Louis: Elsevier.
- Mason, Peggy (2017): *Medical neurobiology*. 2nd ed. New York: Oxford University Press. Available online at <http://dx.doi.org/10.1093/med/9780190237493.001.0001>.
- McGowan, Blake (2018): *Industrial Exoskeletons: What you're not hearing*. In *Occupational Health & Safety* 2018, 10/1/2018. Available online at <https://ohsonline.com/articles/2018/10/01/industrial-exoskeletons-what-youre-not-hearing.aspx>, checked on 12/29/2018.
- Millard, Matthew; Uchida, Thomas; Seth, Ajay; Delp, Scott L. (2013): *Flexing Computational Muscle: Modeling and Simulation of Musculotendon Dynamic*. In *Journal of Biomechanical Engineering* 135.
- Miller, Mark D.; Wilder, Robert P. (Eds.) (2010): *The Runner*. 1st ed. 29 volumes. Philadelphia: Saunders (Clinics in sports medicine, 3).
- Nacy, Somer M.; Ghaeb, Nebras H.; Abdallah, Mays M. M. (2016): *A Review of Lower Limb Exoskeletons*. In *Innovative Systems Design and Engineering* 7 (11), pp. 2222–2871.
- Naik, Ganesh R. (Ed.) (2012): *Computational Intelligence in Electromyography Analysis - A Perspective on Current Applications and Future Challenges*: InTech.
- National Center for Simulation in Rehabilitation Research (n. d. 8): *Analyses*. Available online at <https://simtk-confluence.stanford.edu/display/OpenSim/Analyses>, checked on 12/30/2018.
- National Center for Simulation in Rehabilitation Research (n. d. 1): *Gait 2392 and 2354 Models*. National Center for Simulation in Rehabilitation Research.
- National Center for Simulation in Rehabilitation Research (n. d. 6): *How CMC Works*. Available online at <https://simtk-confluence.stanford.edu:8443/display/OpenSim/How+CMC+Works>, checked on 12/30/2018.
- National Center for Simulation in Rehabilitation Research (n. d. 9): *How IAA Works*. Available online at <https://simtk-confluence.stanford.edu/display/OpenSim/How+IAA+Works>, checked on 12/30/2018.
- National Center for Simulation in Rehabilitation Research (n. d. 4): *How Inverse Kinematics Works*. Available online at <https://simtk-confluence.stanford.edu:8443/display/OpenSim/How+Inverse+Kinematics+Works>, checked on 12/30/2018.
- National Center for Simulation in Rehabilitation Research (n. d. 5): *How RRA Works*. Available online at <https://simtk-confluence.stanford.edu:8443/display/OpenSim/How+RRA+Works>, checked on 12/30/2018.
- National Center for Simulation in Rehabilitation Research (n. d. 3): *How Scaling Works*. National Center for Simulation in Rehabilitation Research. Available online at <https://simtk-confluence.stanford.edu:8443/display/OpenSim/How+Scaling+Works>, checked on 12/30/2018.
- National Center for Simulation in Rehabilitation Research (n. d. 10): *OpenSim::PathSpring Class Reference*. Available online at https://simtk.org/api_docs/opensim/api_docs32/classOpenSim_1_1PathSpring.html, checked on 12/30/2018.
- National Center for Simulation in Rehabilitation Research (n.d. 12): *Simulation with OpenSim - Best Practices*. Available online at <https://simtk-confluence.stanford.edu/display/OpenSim/Simulation+with+OpenSim+-+Best+Practices>, checked on 12/31/2018.
- National Center for Simulation in Rehabilitation Research (n. d. 11): *Simulation-Based Design to Reduce Metabolic Cost*. Available online at <https://simtk-confluence.stanford.edu/display/OpenSim/Simulation-Based+Design+to+Reduce+Metabolic+Cost>, checked on 12/30/2018.
- National Center for Simulation in Rehabilitation Research (n. d. 2): *Thelen 2003 Muscle Model*. Available online at <https://simtk-confluence.stanford.edu:8443/display/OpenSim/Thelen+2003+Muscle+Model>, checked on 12/30/2018.
- National Center for Simulation in Rehabilitation Research (n. d. 7): *Working with Static Optimization*. Available online at <https://simtk-confluence.stanford.edu/display/OpenSim/Working+with+Static+Optimization>, checked on 12/30/2018.
- National Institutes of Health (n. d.): *NIH Roadmap National Centers for Biomedical Computing*. National Institutes of Health. Available online at <http://www.ncbcs.org/summary.html>, checked on 12/30/2018.

- Nene, A.; Byrne, C.; Hermens, H. (2003): Is rectus femoris really a part of quadriceps? Assessment of rectus femoris function during gait in able-bodied adults. In *Gait & Posture* 20 (1), pp. 1–13.
- Noyes, Frank R. (Ed.) (2017): *Noyes' knee disorders. Surgery, rehabilitation, clinical outcomes*. 2nd ed. Philadelphia: Elsevier. Available online at <https://www.clinicalkey.com/dura/browse/bookChapter/3-s2.0-C20130186734>.
- Palastanga, Nigel; Soames, Roger (2012): *Anatomy and human movement. Structure and function*. 6th ed. Edinburgh: Churchill Livingstone.
- Perry, Jacquelin (2003): *Ganganalyse. Norm und Pathologie des Gehens*. 1st ed. München: Urban & Fischer.
- Plowman, Sharon A.; Smith, Denise L. (2014): *Exercise physiology for health, fitness, and performance*. 4th ed. Philadelphia: Wolters Kluwer/Lippincott Williams & Wilkins Health.
- Romero, F.; Alonso, F. J. (2016): A comparison among different Hill-type contraction dynamics formulations for muscle force estimation. In *Mechanical Sciences* 7 (1), pp. 19–29.
- Schenck, Robert C. (Ed.) (1999): *Athletic training and sports medicine*. American Academy of Orthopaedic Surgeons. 3rd ed. Rosemont: American Academy of Orthopaedic Surgeons.
- Schmidt, Jeanette P.; Delp, Scott L.; Sherman, Michael A.; Taylor, Charles A.; Pande, Vijay S.; Altman, Russ B. (2008): The Simbios National Center: Systems Biology in Motion. In *Proceedings of the IEEE Institute of Electrical and Electronics Engineers* 96 (8), p. 1266.
- Sisto, Sue (1998): An Overview of the Value of Information Resulting from Instrumented Gait Analysis for the Physical Therapist. In Joel A. de Lisa, Donna E. Shalala (Eds.): *Gait Analysis in the Science of Rehabilitation // Gait analysis in the science of rehabilitation*. n. p.: Diane Publishing Co., pp. 76–85.
- Sreekumar, S. (2010): *Basic physiology*. New Delhi: PHI Learning Private Limited.
- Steckel, Hanno (2018): *Genial beweglich! Alles über Rücken, Schulter, Hüfte, Knie - und was hilft, wenn's zwickt*. München: Droemer.
- Strickland, Justin P.; Fester, Erik W.; Noyes, Frank R. (2017): Lateral and Posterior Knee Anatomy. In Frank R. Noyes (Ed.): *Noyes' knee disorders. Surgery, rehabilitation, clinical outcomes*. 2nd ed. Philadelphia: Elsevier, pp. 23–37.
- Tehrani, Arman; Vermeire, Maxime (2007): *Design of a Below-Knee Prosthesis Powered by Electric Drives*. Master thesis, Brussels.
- The Ohio State University (2018): *Musculoskeletal Modeling and Simulation of Human Movement. The Value of Modeling and Simulations*. Available online at <https://nmb1.engineering.osu.edu/research/modeling>, checked on 12/31/2018.
- Thelen, Darryl G. (2003): Adjustment of Muscle Mechanics Model Parameters to Simulate Dynamic Contractions in Older Adults. In *Journal of Biomechanical Engineering* 125 (1), p. 70.
- Thelen, Darryl G.; Anderson, Frank C. (2006): Using computed muscle control to generate forward dynamic simulations of human walking from experimental data. In *Journal of Biomechanics* 39 (6), pp. 1107–1115.
- Thelen, Darryl G.; Anderson, Frank C.; Delp, Scott L. (2003): Generating dynamic simulations of movement using computed muscle control. In *Journal of Biomechanics* 36 (3), pp. 321–328.
- Thompson, Julie; Chaudhari, Ajit M. W.; Schmitt, Laura C.; Best, Thomas M.; Siston, Robert A. (2013): Gluteus maximus and soleus compensate for simulated quadriceps atrophy and activation failure during walking 46 (13), pp. 2165–2172.
- van den Berg, Frans; Cabri, Jan (2003): *Das Bindegewebe des Bewegungsapparates verstehen und beeinflussen*. 2nd ed. Stuttgart: Thieme (Angewandte Physiologie, 1).
- Van den Bogert, Antonie J. (2003): Exotendons for assistance of human locomotion. In *BioMedical Engineering Online* 2, pp. 1–8. Available online at <http://www.biomedical-engineering-online.com/content/2/1/17>, checked on 12/29/2018.
- Watkins, James (2018): *Laboratory and field exercises in sport and exercise biomechanics*. London, New York: Routledge.
- Wickiewicz, T. L.; Roy, R. R.; Powell, P. L.; Edgerton, V. R. (1983): Muscle architecture of the human lower limb. In *Clinical Orthopaedics and Related Research* (179), pp. 275–283.
- Willson, Andrea (2017): *A Quasi-Passive Biarticular Prosthesis and Novel Musculoskeletal Model for Transtibial Amputees*. Thesis. University of Washington, Washington. Available online at <https://digital.lib.washington.edu/researchworks/handle/1773/40644>.
- Winter, David A. (2009): *Biomechanics and motor control of human movement*. 4th ed. Hoboken, N.J.: Wiley. Available online at <http://dx.doi.org/10.1002/9780470549148>.
- Woodford, Chris (2018): *Springs*. Available online at <https://www.explainthatstuff.com/how-springs-work.html>, checked on 12/30/2018.

7.2. List of Figures

Figure 1: Illustration of the gait cycle	5
Figure 2: Start and end positions of pre-swing.....	7
Figure 3: Start and end positions of initial swing.....	8
Figure 4: Start and end positions of mid-swing	9
Figure 5: Gait kinematics	10
Figure 6: Ground reaction forces.....	11
Figure 7: Coordinate system of the ground reaction forces	11
Figure 8: Illustration of muscle force and moment arm	12
Figure 9: Activation pattern of m. rectus femoris during gait	13
Figure 10: Activation pattern of m. vastus intermedius during gait	14
Figure 11: Activation pattern of m. biceps femoris caput longum during gait.....	14
Figure 12: Red marked m. rectus femoris	15
Figure 13: Red marked m. vastus intermedius.	15
Figure 14: Red marked m. biceps femoris long head.....	15
Figure 15: Graphical User Interface of OpenSim.....	17
Figure 16: Hill-type muscle model.....	19
Figure 17: Illustration of musculotendon mechanics modeling.....	21
Figure 18: Thelen muscle model – muscle properties	22
Figure 19: Schematic of a muscle-driven simulation in OpenSim	23
Figure 20: Schematic of CMC applied to gait.....	27
Figure 21: Illustration of the Rolling on surface constraint.....	29
Figure 22: Unpowered exoskeleton design from Grabowski and Herr	29
Figure 23: Unpowered exoskeleton design from Collins et al.....	29
Figure 24: Tendon-force length relationship	33
Figure 25: Normalized active and passive force-length curves	33
Figure 26: Replacement of m. rectus femoris by a path spring	34
Figure 27: Effects on force production of m. rectus femoris, when a path spring is implemented in parallel to healthy m. rectus femoris.	35
Figure 28: Controls (muscle excitations) of m. rectus femoris with different maximum limitations.....	36
Figure 29: Force curves of healthy weakened m. rectus femoris. Muscle weakening is performed using control constraints.	36
Figure 30: M. biceps femoris caput longum.	38
Figure 31: M. vastus intermedius, M. rectus femoris & passive path spring.....	38
Figure 32: Simulation process.	40
Figure 33: Actuation force of m. rectus femoris 1.....	42
Figure 34: Actuation force of m. rectus femoris 2.....	42
Figure 35: Actuation force of m. vastus intermedius 1.....	43
Figure 36: Actuation force of m. vastus intermedius 2.....	44
Figure 37: Actuation force of m. biceps femoris c. longum 1	45
Figure 38: Actuation force of m. biceps femoris caput longum 2.	45
Figure 39: Actuation power of m. rectus femoris 1	46
Figure 40: Actuation power of m. rectus femoris 2.....	46
Figure 41: Actuation power of m. vastus intermedius 1.....	47
Figure 42: Actuation power of m. vastus intermedius 2.....	47
Figure 43: Actuation power of m. biceps femoris caput longum 1	48
Figure 44: Actuation power of m. biceps femoris caput longum 2	49
Figure 45: Normalized fiber length of m. rectus femoris	49
Figure 46: Normalized fiber length of m. vastus intermedius	50
Figure 47: Normalized fiber length of m. biceps femoris caput longum.	50
Figure 48: Normalized fiber velocity of m. rectus femoris	51

Figure 49: Normalized fiber velocity of m. vastus intermedius.....	51
Figure 50: Normalized fiber velocity of m. biceps femoris caput longum.....	52
Figure 51: IAA – coordinate system.	52
Figure 52: M. rectus femoris contribution to fore-aft femur acceleration 1	53
Figure 53: M. rectus femoris contribution to fore-aft femur acceleration 2	54
Figure 54: M. rectus femoris contribution to vertical femur acceleration 1	55
Figure 55: M. rectus femoris contribution to vertical femur acceleration 2.....	56
Figure 56: M. vastus intermedius contribution to fore-aft femur acceleration 1	57
Figure 57: M. vastus intermedius contribution to fore-aft femur acceleration 2.....	58
Figure 58: M. vastus intermedius contribution to vertical femur acceleration 1	59
Figure 59: M. vastus intermedius contribution to vertical femur acceleration 2.....	60
Figure 60: M. biceps femoris caput longum contribution to fore-aft femur acceleration 1.....	61
Figure 61: M. biceps femoris caput longum contribution to fore-aft femur acceleration 2.....	62
Figure 62: M. biceps femoris caput longum contribution to vertical femur acceleration 1.....	63
Figure 63: M. biceps femoris caput longum contribution to vertical femur acceleration 2.....	64
Figure 64: Resultant vectors describing m. rectus femoris contribution to fore-aft and vertical femur acceleration.	65
Figure 65: Resultant vectors describing m. vastus intermedius contribution to fore-aft and vertical femur acceleration	66
Figure 66: Resultant vectors describing m. biceps femoris caput longum contribution to fore-aft and vertical femur acceleration.....	67
Figure 67: CMC Validation 1 - Residual forces and moments	69
Figure 68: CMC Validation 2 - Joint angles of hip and knee.....	70
Figure 69: CMC Validation 3 - Angular velocity of hip and knee.....	70
Figure 70: CMC Validation 4 - Angular Acceleration of hip and knee	71
Figure 71: CMC Validation 5 - Activation of m. rectus femoris derived from literature	71
Figure 72: CMC Validation - Activation of m. rectus femoris derived from OpenSim.....	72
Figure 73: CMC Validation 7 - Activation of m. vastus intermedius derived from literature	72
Figure 74: CMC Validation 8 - Activation of m. vastus intermedius derived from OpenSim.....	73
Figure 75: CMC Validation 9 - Activation of m. biceps femoris caput longum derived from literature	73
Figure 76: CMC Validation 10 - Activation of m. biceps femoris caput longum derived from OpenSim.....	74
Figure 77: IAA Validation 1 – Comparison of the experimental and the constraint reaction forces.	75
Figure 78: IAA Validation 2 - Comparison of the experimental and the constraint reaction moments.	75
Figure 79: Discussion 1 - Actuation force of m. vastus intermedius with m. rectus femoris weakend to 10% maximum controls.....	77
Figure 80: Discussion 2 - Actuation force of m. vastus intermedius with m. rectus femoris weakened to 25% maximum controls.....	77
Figure 81: Discussion 3 - Actuation force of m. rectus femoris.....	78
Figure 82: Discussion 4 - Actuation force of m. vastus intermedius	79
Figure 83: Discussion 5 - Actuation force of m. vastus intermedius	80
Figure 84: Discussion 6 - Actuation force of m. rectus femoris.....	80
Figure 85: Discussion 7 - Actuation force of m. biceps femoris caput longum	81
Figure 86: Discussion 8 - M. rectus femoris contribution to fore-aft femur acceleration	82
Figure 87: Discussion 9 - M. rectus femoris contribution to vertical femur acceleration	82
Figure 88: Discussion 10 - M. vastus intermedius contribution to fore-aft femur acceleration	82
Figure 89: Discussion 11 - M. vastus intermedius contribution to vertical femur acceleration	83

7.3. List of Tables

Table 1: Overview of the gait sub-phases	6
Table 2: Overview of muscle activity and tasks of m. biceps femoris caput longum, m. rectus femoris and m. vastus intermedius during pre-swing, mid-swing and initial swing	9
Table 3: Start and end times of the relevant gait sub-phases	32
Table 4: Sought values from the ‘Gait 2354‘ musculoskeletal model	33
Table 5: Overview of all performed simulations.....	39

Table 6: CMC Validation - Peak reserve actuator torques vs. 10% of peak joint torque 69